DANMARKS OG GRØNLANDS GEOLOGISKE UNDERSØGELSE RAPPORT 2006/30

Alteration patterns in Au-mineralised zones of Storø, Nuuk region – West Greenland

Pasi Eilu, Paolo Garofalo, Peter W. U. Appel & Wouter Heijlen

GEOLOGICAL SURVEY OF DENMARK AND GREENLAND
MINISTRY OF THE ENVIRONMENT

GEUS

DANMARKS OG GRØNLANDS GEOLOGISKE UNDERSØGELSE RAPPORT 2006/30

Alteration patterns in Au-mineralised zones of Storø, Nuuk region – West Greenland

Pasi Eilu, Paolo Garofalo, Peter W. U. Appel & Wouter Heijlen

GEOLOGICAL SURVEY OF DENMARK AND GREENLAND
MINISTRY OF THE ENVIRONMENT

G E U S

Contents

Abstract

A Mesoarchaean greenstone belt on the Storø island, close to Nuuk, the capital of Greenland, contains gold occurrences in amphibolite-facies host rocks. The greenstone belt, cut by a regional shear zone, comprises two supracrustal units of slightly different age. Regional deformation and metamorphism in the area took place repeatedly during the Archaean, and peaked under upper-amphibolite facies conditions at ~2850 Ma. The belt has been intruded by syn- and late-orogenic pegmatites some of which are related to a nearby, ca. 2550 Ma old, granite, and the pegmatites have been variably deformed within the shear zone.

Gold at Storø is mainly found in laminated quartz veins. The best-mineralised zones, named Main Zone and New Main Zone by the company NunaMinerals A/S holding the concession, extend for up to several hundred metres along strike and have widths from 2 to 60 m. These two zones occur in amphibolites of volcanic and garnet-mica-rich rocks of doubtful origin. The mineralised zones are relatively early, as they are deformed by the local D2 and D3 stages deformation.

The present study, which is carried out on drill core samples and surface mapping and sampling, focuses on alteration features in the gold mineralised rocks and attempts to establish the precursors of the amphibolites, sillimanite schists and a peculiar rock type comprising garnetites, garnet-mica-rich rocks with bands of magnetite.

The first alteration event in the area produced calc-silicate rocks dominated by epidote and diopside. This event took place prior to metamorphism at or immediately below the sea floor under spilitic conditions. This alteration is unrelated to and predates the gold mineralization. Next alteration stage produced biotite-garnet alteration domains in the amphibolites and appears to be related to gold mineralization. Alteration haloes formed in this stage display a progressive increase of modal abundance of biotite, garnet, sulphides (pyrrhotite and arsenopyrite), and quartz towards the gold zones and quartz veins in amphibolite. Biotite-garnet alteration has several features typical for orogenic gold mineralization formed under amphibolite-facies conditions.

Critical to our understanding of alteration and mineralization at Storø is the interpretation of when these took place with respect to metamorphism and the stages of deformation. The relative timing sequence provides constraints on structural environment of gold precipitation, and can be used for the construction of a genetic model. Our work suggests that calc-silicate alteration predated all regional metamorphism and deformation, and formation of what now are biotite-garnet altered domains was syn-early metamorphic (syn-D1), that gold was precipitated within biotite-garnet altered domains, and that mineralization and what now is biotite-garnet alteration are genetically related. Further, fluid inclusion and garnet-biotite geothermometry data enable us to quantify the peak-metamorphic P-T conditions at around 530-630°C and 4 to 6 kbar.

Introduction

GEUS and Bureau Minerals and Petroleum started in 2004 a project, entitled: *Is there a gold province in the Nuuk region?* (Appel et al., 2005), which is a follow-up project of a project initiated in 2003 entitled: *Preliminary evaluation of the economic potential of the greenstone belts in the Nuuk region* (Appel et al., 2003). In 2005 GEUS carried out detailed studies on the Storø area where the best gold occurrences occur. This study was carried out in close co-operation with the Greenlandic company NunaMinerals A/S, which holds the concession on the Storø gold occurrences. Part of the sample material for this study was collected from drill core in close co-operation with Tom Robyn from NunaMinerals A/S.

The aim of the present study was to carry out a petrographic and geochemical study of the gold zones at Qingaaq, Storø. The samples used here were selected from five locations in and close to the gold zones at Qingaaq, and from the core drilled by NunaMinerals on July 2005 on the N slope of Qingaaq. With this material, we (1) give a preliminary description of the petrography and geochemical characteristics of the amphibolites (both the least altered and the more intensely altered), Al-rich rocks, and magnetite-garnet rocks close to the Au-mineralised zones, (2) attempt to identify the early calc-silicate alteration and its relation with the gold zones, and (3) evaluate mass transfer related to biotite-garnet alteration. In addition, we (4) present some fluid inclusion and mineral composition data which can be used to estimate pressure and temperature conditions of the garnet-biotite alteration.

The gold occurrences at Storø near Nuuk, West Greenland, are zones comprising quartz veins and sulphide dissemination in altered amphibolites, garnet-rich rocks and sillimanite schists. The mineralised zones extending for up to several hundred metres, have widths of 2-60 m and occur within ductile shear zones (Appel et al. 2003, Appel et al. 2005, Coller & Coller 2005). They all seem to occur within the domain of the NE-trending regional Storø Shear Zone which is interpreted as a major terrane boundary in the Archaean Nuuk Fjord region (Appel et al. 2005) (Fig. 1).

The gold prospect on Storø has been sampled and drilled extensively over the years and yielded promising results: 11.1 ppm Au over 10 meters, 37 ppm Au over 1.5 meters, 2.7 ppm Au over 11.3 meters and 4.5 ppm Au over 4.45 meters (Trepka-Bloch, 1995, Skyseth, 1997).

The gold-enriched zones crop out at Storø, mainly along the contact zones between amphibolites (mafic volcanic rocks) and pale-grey Al-rich gneisses which previously have been called metasediments (Fig. 2). New Main zone (named by NunaMinerals) on the mountain of Qingaaq consists of sheeted quartz veins (Fig. 3) and disseminated sulphides mainly pyrrhotite, chalcopyrite and arsenopyrite locally with visible gold (Appel et al. 2005, Coller & Coller 2005). The mineralised zones are broadly sub parallel with the lithological units and with the planar mineral fabric of the host rocks. However, in detail, the auriferous quartz veins are at a small angle to lithological contacts, and at the northern slopes of Qingaaq the New Main Zone clearly transects the layering of the amphibolite (Appel et al. 2005, Coller & Coller 2005). Some mineralised zones (e.g., the New Main Zone) are folded and displaced by the D2-D3 stages of the development of the Storø Shear Zone (Appel et al. 2005). This feature and other structural and geological data suggest that the Au zones at Storø were formed during or soon after the D1 stage of the regional deformation, and that the following folding, thrusting, and shearing events deformed the gold-mineralised zones (Appel et al. 2005, Coller & Coller 2005). Thus, the present shape and site of the gold zones at Storø reflects, at least to a certain extent, the control from the latest deformation stages of the area, and many primary features of mineralization and hydrothermal alteration may have been obliterated beyond recognition.

One important feature of the Storø gold zones is the occurrence of biotite-garnet alteration. This alteration is reflected in a progressive increase of modal abundance of biotite, garnet, sulphides (pyrrhotite and arsenopyrite), and quartz towards the gold zones and quartz veins in amphibolite (Era Maptec 1995, Pedersen 1998, Skyseth 1998). A diopside-epidote (calc-silicate) type of alteration is also reported from the region, both at Storø and Ivisaartoq, but is shown to pre-date the gold mineralization (e.g., Appel et al. 2005, Polat 2005, and references therein). Critical to our understanding of the gold zones of Storø is the interpretation of when the biotite-garnet alteration occurred with respect to metamorphism. Indeed, evidence for formation of these alteration haloes before, during, or after the peak metamorphic conditions provides constraints on both timing and structural environment of gold precipitation, and can be used for the construction of a genetic model.

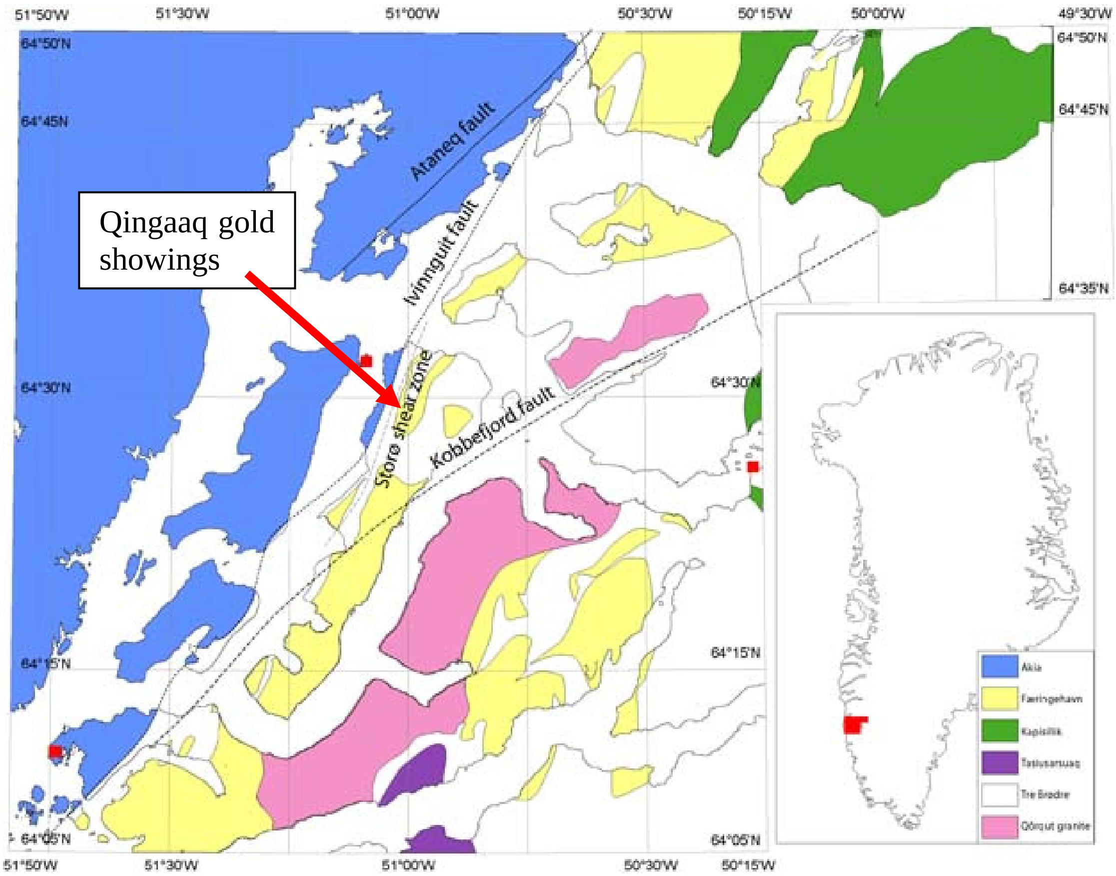

Figure 1. *Schematic map showing the approximate boundaries of the known geological terranes in the central Godthåbsfjord region, after Friend & Nutman (2005), from Hollis et al. (2004).*

Figure 2. *New Main zone at Qingaaq. The auriferous zone is slightly discordant to the contact between amphibolite to the right and "metasediment" to the left. Hammer about 50 cm long.*

Figure 3. *Auriferous sheeted quartz vein in the amphibolite shown on Fig. 2. Qingaaq, Storø. 64°24'32.1"E, 051°05'09.6"W. Scale 10 cm.*

Geological setting

The Nuuk region of West Greenland comprise Archaean gneisses, tonalites and greenstone belts with ages ranging from >3.8 Ga to ~2.5 Ga. The region has been investigated in great detail over a number of years and been subdivided into a varying number of terranes (Friend and Nutman and references therein) (Fig. 1). Several major shear zones occur in the region. Of particular significance in the present context is the regional Storø Shear Zone. This shear zone cuts through a package of supracrustal rocks on central Storø where promising gold showings have been discovered. The package consists of massive to banded amphibolites, sillimanite schists or gneisses, fuchsite quartzites and a peculiar rock type consisting of garnet, quartz, feldspars and micas with up to half a meter thick bands of near massive magnetite. The garnet content may locally be more than 75 percent. Adjacent to the supracrustal rocks are thin (500 to 1000 m thick) units of anorthosites and gabbroanorthosites. The rocks have been repeatedly deformed and metamorphosed under amphibolite facies conditions. Also various types of alteration have affected the rocks, as described below.

Preliminary age work indicates that the greenstone belt on Storø can be subdivided into two packages of supracrustal rocks with a different age (~3050 Ma and ~2850 Ma) (Hollis pers. comm.). Age work on garnets from amphibolites and garnetite indicates a metamorphic age of ~2530 Ma for the schists (Hollis and Persson pers. comm.). The nearby Qôrqut granite yields a radiometric age of 2550 Ma. Numerous pegmatites intrude the greenstone belt. They have been dated at ~2600 Ma (Hollis pers. comm.).

Visible gold occurs in sheeted quartz veins and in a loellingite-arsenopyrite-pyrrhotite association. Textural relationships indicate that gold was precipitated together with the first generation of arsenopyrite. During metamorphism, the arsenopyrite broke down to loellingite and pyrrhotite with liberation of gold as visible gold. During retrograde metamorphic conditions pyrrhotite and loellingite reacted and formed a second generation of arsenopyrite. The second generation of arsenopyrite was later replaced by garnet. Pb isotope work on second generation arsenopyrite yielded an age of 2858 Ma (Juul-Pedersen, 2005). This obviously is a minimum age of the gold mineralization at Storø. Garnets replacing the late arsenopyrite have been dated to 2748±62 Ma by Pb step leaching (Juul-Pedersen, 2005).

Field and analytical methods

Detailed mapping at Qingaaq took place at five sites (Figs. 4–11). This work concentrated on rock type and alteration identification, geometry of the structures and visible domains of altered rocks. This consideration of both geological and topological features of the altered rocks commonly provides useful constraints on the relations between Au zones and alteration patterns and guide sampling (e.g. Garofalo 2004a, 2004b). Sampling was intended for the petrographic and geochemical study of the lithologies and alteration (Figs. 7–11). At site 5 and in core DDH 05-06 it was carried out along profiles that explicitly consider the spatial extent of the alteration haloes (Figs. 6 and 11). This was done to get a control on mineralogical and chemical changes related to alteration, on both large scale and in detail, and is similar to what has been used for alteration mapping in greenschist-facies orogenic gold deposits (e.g., Eilu & Mikucki 1998, Garofalo 2004b). Thus, for example, sample 6 of site 5 (*i.e.*, no. 493266 in Fig. 11) represents the least-altered amphibolite of that specific section, and the other neighbouring samples represent contiguous aliquots of apparently progressively altered amphibolite. The same sampling method has been applied also for drill core DDH05-06 (Fig. 6), although the intense deformation and the lithological heterogeneity make this profile less homogeneous. These two sets of samples also provide some insight on the spatial variability of the biotite-garnet alteration at Storø.

In all, 97 polished thin sections and 30 whole-rock geochemical analyses were done, including all samples from site 5 and DDH05-06 (App. 1 and 2). The whole-rock geochemical analyses were carried out with fusion ICP (Si, Ti, Al, Fe, Mn, Mg, Ca, Na, K, P, LOI, Ba, Sr, Y, Sc, Zr, Be, and V), neutron activation (INAA: Au, As, Br, Cr, Cs, Co, Ce, Eu, Hf, Ir, La, Lu, Mo, Nd, Rb, Sb, Se, Sm, Ta, Th, Tb, U, W, and Yb), total acid digestion-ICP (TD-ICP: S, Ag, Bi, Cd, Cu, Ni, Pb, and Zn) and infrared (C, S) at Activation Laboratories ltd. (App. 2). From the Actlabs quality control data, one can derive that the relative precision in SiO_2 analyses was ±1 %, in $Fe_2O_3^{tot}$ ±2 %, in Al_2O_3, MnO, MgO, CaO, Na_2O and La ±5 %, in K_2O ±10 % below 1 % and ±5 % above 1 % concentration, in TiO_2 ±10 % below 0.5 % and ±5 % above 0.5 % concentration, in P_2O_5, Co, Cr, Eu, Sm, Sr, and V ±10 %, in CO_2, Ba, Lu, Sc, and Zr ±15 %, in Cu, Ni, Y, Yb, and Zn ±20 %, in S ±25 % below 0.5 % and ±5 % above 0.5 % concentration, in Ce ±25 %, in Au variable at ±5 - ± 30 % (no obvious correlation with concentration), in Pb up to ±50 % for the values <20 ppm detected in this study, and for Nb and Th ±50 % throughout the data. In addition, all or nearly all of the concentrations measured were below the detection limit for Be, Br, Hf, Ir, Se, Ta, Tb, U, W, Ag, Bi, and Cd (App. 2): these elements are hence not included in the geochemical discussion of this report.

Semi-quantitative SEM EDS analyses of individual minerals were done on site 5 and DDH05-06 samples. The SEM analyses were carried out with a Philips 515 equipped with an EDAX DX4 by using 2 nA/ 15 kV. In the SEM work, analytical precision is in most cases better than 5% for the major elements and better than 10% for the minor elements. In addition, garnet, biotite and chlorite from a variety of samples were analysed quantitatively by microprobe at the University of Copenhagen, on a GEOL Superprobe 8200 at 15kV/15 nA with natural and synthetic standards. SEM EDS and microprobe data are summarised in Tables 1 to 5.

Fluid inclusions measurements were done at the University of Leeds using a Linkam MDS600 heating-freezing stage mounted on an Olympus BX-50 microscope. The stage was calibrated with synthetic inclusions. Investigated samples came from garnet-biotite-quartz segregations, both from drillcore and outcrop samples (site 3).

Rock types

Assessment of primary mineral and chemical composition for each rock type present in an area is essential for establishing alteration zoning sequences and for modelling metasomatism. The general trends in mineralogical and chemical composition of the least altered rocks investigated and sampled by us at Qingaaq in 2005 are therefore described first, in this section, prior to an evaluation of the possible mineralogical and chemical changes which took place. We also briefly discuss here the possible genetic relationships between the amphibolites and other rock types at Qingaaq. This is important because of the uncertainties in the primary identity of the garnet-magnetite rocks, felsic gneisses, and sillimanite-garnet gneisses.

Amphibolite

The least-altered amphibolites are relatively homogeneous, foliated and dark green in colour (Fig. 14). Textures are metamorphic, granoblastic, with very little, if any, of primary features preserved. The mineral assemblage is dominated by hornblende and plagioclase with minor to trace volumes of quartz, ilmenite, magnetite, titanite, apatite, pyrrhotite and chalcopyrite (Figs. 12A, C, and Appendix 1). Also this rock may have experienced some alteration. The samples that fulfil the criteria of the least-altered amphibolite at Qingaaq are: 493263, 493265, 493266, and 491136 (Appendix 2). They contain <0.30 % K_2O suggesting that all the four samples contain a maximum of 1–2 mass-% of biotite. There also is local, minor, retrograde replacement of plagioclase by epidote, but no indications of calc-alkaline alteration, no pervasive biotitisation, and no or very rare garnet. At this point, it is also interesting to note that one of the samples originally mapped as 'unaltered' (491136) does contain nearly twice more K than one of the samples (493265) mapped as biotitised, showing how difficult it can be at field to correctly map alteration.

Whole-rock analyses on amphibolites are presented in Appendix 2. All amphibolite samples are also plotted in Jensen cation plot (Jensen 1976) in Plot 1, in a TiO_2 vs. Zr Plot 2a, and in REE plots (Plot 3 and 4). These plots indicate that there is just one, Fe-tholeiitic, precursor for all amphibolite types mapped at Qingaaq.

Garnet-magnetite rock sequence

Garnet-magnetite-rich rocks form 0.5-2 m wide bands close to the amphibolite unit at Qingaaq (Figs. 7-9). The rock has a mineral assemblage of magnetite - garnet - quartz - cummingtonite-grunerite - biotite (Fig. 15, Tables 1–4, App. 1) and grades into magnetite-free, more biotite- and quartz-rich varieties, both away from the magnetite-dominated bands and where quartz veins or synkinematic pegmatites are abundant (Figs. 9, 16–21, App. 1). Some lithological units are mafic and resemble totally biotitised amphibolite (Figs. 22–23), but their Zr-Ti and other immobile-element ratios and siting in the Jensen plot (Plot 5) show that they are not derived from the typical amphibolite at Qingaaq.

The unit is so tightly isoclinally folded (Figs. 8, 9, 16–18) that the garnet-magnetite rock bands may even represent a single primary layer. The magnetite-poor units shown in Figures 7–11 and Appendices 1 and 2 have depending on their apparently dominant minerals and chemical compositions, been called leucocratic gneiss, biotite-garnet-quartz-plagioclase amphibolite, felsic garnet-mica gneiss, felsic mica gneiss, mica gneiss, etc. Note however, that no amphibole has been detected in these gneisses (App. 1).

Due to intense multi-stage deformation and high-grade regional metamorphism, it is hard to say, by using petrographic evidence only, if these rocks really define a narrow unit of iron formation (BIF *sensu stricto*), are products of other sorts of chemical sedimentation at sea floor, or are intensely metasomatised amphibolites. In any case, the narrow sequence appears as having been inhomogeneous already before metamorphism, especially when viewed in places like site 3 (Figs. 9 and 18).

The chemical compositions of the garnet-magnetite and associated rocks show a large range of variation (App. 2). The Ti-Zr plot allows them all having at least some common origin, clearly different from the amphibolites (Plot 2c), if Ti and Zr were immobile also in this context. The REE plot (Plot 6) furthermore shows that one cannot make the felsic gneisses and magnetite-rich rocks by just one-stage alteration from the amphibolite, unless a strong LREE enrichment is associated with a large net mass gain. The net mass gain would however be strongly against what is suggested by the REE trends of the sillimanite-garnet gneiss occurring next to the garnet-magnetite rocks and felsic gneisses. Hence, at this stage of the investigations, it is better not to strongly consider the garnet-magnetite and associated felsic rocks as simple alteration derivates of the Qingaaq amphibolites.

Drill hole no.	Depth (m)	GEUS nr.	Rock type	Mineral assemblage (accessory minerals after '+')	Texture	Alteration
DDH - 05-01	6.30	491101	Amphibolite	biot-gar-hbl-plag-po-act/di + py, chl, cpy, ilm, GOLD	Granoblastic host rock + massive quartz vein containing minor hbl and slivers of host rock comprising hbl+gar±act/di. Detected two gold grains both a few microns in diameter as inclusions in garnet in the amphibolite.	Hbl selvage on the quartz vein. Biot-Gar alteration beyond the hbl selvage.
DDH - 05-01	12.35	491102	Amphibolite	plag-hbl-biot-gar-po + qz, tit, cpy	Granoblastic host rock + massive quartz vein containing minor po, di, plag and hbl.	Hbl-selvage, biot+gar alteration on the other side of the vein. Abundant sulphides on both sides of the vein.
DDH - 05-01	13.00	491103	Qz vein + mica gneiss?	plag-biot-hbl + po, tit, ilm, cpy, apy	Granoblastic host rock + massive qz veins containing minor po, di, and hbl.	Hbl±tit selvages consistently on the quartz veins. All the two grains of apy in these selvages, too.
DDH - 05-01	14.50	491104	Amphibolite	biot-gar-plag-po + hbl, ilm, tit, graph, carb, zir	Granoblastic. All minerals appear as in equilibrium with each other.	Biot-Gar alteration.
DDH - 05-01	14.60	491105	Amphibolite + qz-hbl veins	biot-plag-gar-hbl-po + ilm, apy, tit, epid, apa, zir	Granoblastic. Deformed qz veins with hbl (or hbl-rich pieces of wallrock) + po, gar, cpy, apa. Epid only as inclusions in garnet.	Hbl selvage on the quartz veins. Biot-Gar alteration beyond the hbl selvage.
DDH - 05-01	16.85	491106	Albite rock + quartz veins	ab-qz-po + biot, ilm, apa, tit, cpy, GOLD	Massive, granoblastic; biot-rich bands 2-4 mm wide. One apa-rich band along a qz vein: all gold grains in this band, surrounded by qz.	Unknown primary rock type, alteration not possible to define
DDH - 05-01	18.70	491107	Amphibolite	plag-hbl-gar-biot + po, ilm, tit, epid, cpy, zir, apa	Granoblastic. Hbl + po in the vein: these probably are pieces of altered amphibolite in the vein. Epid only as inclusions in gar.	Hbl selvage on the quartz veins. Biot-Gar alteration beyond the hbl selvage.
DDH - 05-01	21.40	491108	Amphibolite: tuffite?	biot-plag-qz(?)-hbl + po, py, ilm, graph,cpy, sphal, apa	Granoblastic, foliated, homogeneous.	Biotitised. Po is replaced by supergene py (or marc) by a variable degree.
DDH - 05-01	24.50	491109	Amphibolite	Gar-biot-qz-plag + hbl, po, ilm, chl, cpy	Porphyroblastic garnet. Chlorite only as inclusions in garnet.	Biot-Gar alteration.
DDH - 05-01	31.30	491110	Amphibolite	gar-hbl-biot + ilm, po, apy, apa, cpy	Porphyroblastic garnet.	Biot-Gar alteration.
DDH - 05-01	39.65	491111	Amphibolite	plag-act(?)-gar-hbl + ilm, po, cpy	Grano- and porphyroblastic.	Metamorphosed spilite?
DDH - 05-01	43.30	491112	Amphibolite	gar-qz-hbl + ilm, chl, po, biot, cpy	Porphyroblastic gar with a grain size >1 cm. Chl only as inclusions (alteration?) in gar.	Garnet alteration.
DDH - 05-01	44.05	491113	Amphibolite	gar-qz-hbl + biot, plag, act, ilm, chl, po	Porphyroblastic gar with a grain size >1 cm. Chl mostly as inclusions (alteration?) in gar.	Biot-Gar alteration.
DDH - 05-01	45.80	491114	Amphibolite	biot-gar-hbl-plag + act, qz, ilm	Grano- and porphyroblastic.	Biot-Gar alteration. Act selvages along qz veins
DDH - 05-01	47.50	491115	Intermediate gneiss	plag-act + gar, biot, hbl, ilm, po, cpy, pentl	Granoblastic. A few gar porphyroblasts. No sill but very pale clinoamphibole in the rock	Metamorphosed spilitic stuff? originally albite + calcite + chlorite ??

Drill hole no.	Depth (m)	GEUS nr.	Rock type	Mineral assemblage (accessory minerals after '+')	Texture	Alteration
DDH - 05-01	50.50	491116	Amphibolite	hbl-plag + qz, po, biot, apa, cpy, ilm	Granoblastic.	Chiefly hbl-selvage matter. Plagioclase is partially sericitised.
DDH - 05-01	51.00	491117	Amphibolite	biot-hbl-gar-plag + ilm, po, cpy, graph	Grano- and porphyroblastic.	Biot-Gar alteration.
DDH - 05-01	52.50	491118	Intermediate gneiss	plag-biot-act-gar + po, ilm, cpy	Granoblastic. Porphyroblastic gar Act-qz and biot-gar-ilm -rich bands. No sill but very pale clinoamphibole in the rock	Metamorphosed spilitic stuff? Act-rich bands: originally albite + calcite + chlorite ??
DDH - 05-01	60.15	491119	Amphibolite	hbl-po-plag-gar + cpy, sphal, apa, epid, allanite?	Mostly hbl-selvage matter + deformed qz veins. Po-Cpy-Sp vein network throughout the sample.	Hbl selvage zone + early(?) sulphidation. Gar alteration. Abundant retrograde sericitisation in plag
DDH - 05-01	62.40	491120	Amphibolite	hbl-gar + chl, ilm, po, sphal	Mostly qz (-ilm) vein, some altered amphibolite (= hbl+gar).	Gar alteration. Chl partially replced by hbl.
DDH - 05-01	63.00	491121	Amphibolite	gar-hbl-qz + plag, ilm, chl, po, biot, cpy, zir	Porphyroblastic; the thin section represents material form quartz vein margins only? Chl mostly as inclusions (alteration?) in gar.	Biot-Gar alteration.
DDH - 05-01	64.05	491122	Amphibolite	hbl-plag-qz-gar-biot + ilm, cpy, apy	Grano- and porphyroblastic. Very rare sulphides in the thin section.	Biot-Gar alteration.
DDH - 05-01	70.25	491123	Amphibolite	gar-qz-hbl + biot, plag, ilm, po, chl, cpy	Porphyroblastic; a lot of gar Chl in fractures and as inclusions (alteration?) in gar.	Biot-Gar alteration.
DDH - 05-02	125.12	491124	Garnet-sillimanite rock	qz-ser-gar-sill-chl + ilm, po, cpy, biot, tourm	Porphyroblastic garnet.	Most of sill -> ser, nearly all biot -> chl + ser, some po replaced by lim: retrog. replaments common
DDH - 05-05	21.45	491125	Amphibolite	qz-hbl-biot-gar-plag + po, cpy, ilm	Grano- and porphyroblastic. Gar-biot intergrowth exceptionally common.	Biot-Gar alteration.
DDH - 05-05	46.75	491126	Amphibolite	hbl-biot-plag-gar + po, tit, cpy, rut	Granoblastic. Hbl-sulphide-rich selvage, containing all the titanite, along the quartz vein. No gold detected in thin section.	Hbl selvage on the quartz veins. Biot-Gar alteration beyond the hbl selvage.
DDH - 05-05	48.75	491127	Amphibolite	hbl-plag-po-biot + ilm, tit, cpy	Granoblastic. Sulphides look like partially remobilised ± melted, just as in many other samples, too.	Biotitised
DDH - 05-05	60.10	491128	Amphibolite	plag-act-biot-hbl + po, ilm, py, cpy	Granoblastic. Hbl- and act-rich domains along the quartz veins.	Hbl- and act-rich selvages on qz veins. Py replaces po locally in po grain margins.
DDH - 05-06	44.05	491129	Amphibolite	gar-biot-qz-hbl-plag-cum + po, ilm, apy, cpy, sphal, apa	Grano- and porphyroblastic.	Biot-Gar alteration.
DDH - 05-06	45.00	491130	Amphibolite	hbl-plag-biot-gar + cum, po, ilm, cpy	Granoblastic. Gar-biot intergrowth common.	Biot-Gar alteration.
DDH - 05-06	45.0a	491131	Mica gneiss	plag-biot-qz + po, cpy, tourm, apa	Granoblastic, foliated, homogeneous.	No hbl, no gar, no ilm, no tit: does not look like an altered amphibolite
DDH - 05-06	52.00	491132	Amphibolite	plag-hbl-gar-biot-qz + cum, ilm, po, apy, cpy, apa	Grano- and porphyroblastic.	Biot-Gar alteration.

Drill hole no.	Depth (m)	GEUS nr.	Rock type	Mineral assemblage (accessory minerals after '+')	Texture	Alteration
DDH - 05-06	54.00	491133	Amphibolite	plag-biot-hbl-cum-gar-qz + ilm, po, apy, cpy	Grano- and porphyroblastic. Gar-Biot-Qz intergrowth common.	Biot-Gar alteration.
DDH - 05-06	79.00	491134	Amphibolite	plag-hbl + cum, tit, ilm, po, cpy, pentl	Granoblastic, homogeneous. Pentlandite as tiny flames in pyrrhotite.	NO ALTERATION detected

Appendix 2. Chemical composition of a selection of the collected samples (continued).

			Site 5						Other				DDH05-06						
			2	3	4	5	6	1					1	2	3	4	5	6	7
GEUS no.			493262	493263	493264	493265	493266	493267	493268	493269	493270	493271	491129	491130	491132	491133	491134	491135	491136
dhd													44 m	45 m	52 m	54 m	79 m	84 m	90 m
Rock type			Amphibolite	Amphibolite	Amphibolite	Amphibolite	Amphibolite	Amphibolite	Amphibolite	Amphibolite	Amphibolite	Amphibolite	Amphibolite	Mica gneiss	Amphibolite	Amphibolite	Amphibolite	Amphibolite	Amphibolite
Alteration			Spilite + Biotite	Unaltered	Biotite	Unaltered	Unaltered	Garnet-biotite	Garnet-biotite	Spilite	Spilite	Spilite	Garnet-biotite	?	Garnet-biotite	Garnet-biotite	Unaltered	Biotite	Unaltered
	LOD	Method																	
wt%																			
SiO_2	0.01	FUS-ICP	50.38	50.1	47.49	49.54	49.65	50.91	52.39	49.13	45.56	49.67	45.6	56.72	52.21	49.86	46.79	48.08	49.35
Al_2O_3	0.01	FUS-ICP	13.7	13.66	15.18	13.54	13.8	14.15	18.77	15.79	13.56	17.45	14.2	12.72	13.43	15.12	14.96	14.29	14.31
Fe_2O_{3tot}	0.01	FUS-ICP	16.18	14.23	15.48	15.07	14.56	17.71	11.82	9.65	11.11	9.43	26.41	18.58	20.55	19.91	15.27	15.7	14.95
MnO	0.001	FUS-ICP	0.244	0.199	0.213	0.202	0.203	0.255	0.21	0.395	0.509	0.51	0.645	0.082	0.334	0.275	0.218	0.213	0.218
MgO	0.01	FUS-ICP	5.23	7.09	7.52	6.81	6.24	6.13	2.61	3.34	2.72	2.88	2.88	2.55	1.8	3.18	6.16	6.61	6.72
CaO	0.01	FUS-ICP	9.15	9.33	8.09	10.01	10.64	5.58	4.92	17.47	21.37	14.25	4.2	1.53	6.07	6.02	10.73	8.2	9.23
Na_2O	0.01	FUS-ICP	2.03	2.47	2.8	2.59	2.49	2.1	4.95	1.87	1.06	3.1	1.04	3.06	2.82	2.51	2.84	3.15	3.08
K_2O	0.01	FUS-ICP	0.42	0.27	0.79	0.1	0.11	0.9	1.72	0.18	0.04	0.21	2.3	2.69	0.99	1.31	0.51	0.46	0.29
TiO_2	0.001	FUS-ICP	1.769	1.452	1.482	1.617	1.452	1.949	1.352	1.024	0.959	1.201	1.692	0.556	1.899	1.689	1.604	1.726	1.515
P_2O_5	0.01	FUS-ICP	0.19	0.22	0.17	0.24	0.18	0.24	0.12	0.1	0.08	0.11	0.21	0.02	0.16	0.17	0.22	0.29	0.16
LOI	0.01	FUS-ICP	0.01	0.27	0.65	0.11	0.3	0.3	0.38	0.24	2.18	0.14	< 0.01	1.47	< 0.01	< 0.01	0.34	< 0.01	< 0.01
Total	0.01	FUS-ICP	99.3	99.29	99.87	99.81	99.61	100.2	99.25	99.17	99.14	98.95	98.65	99.98	99.82	99.53	99.64	98.19	99.71
S	0.001	TD-ICP	0.032	0.002	0.005	0.009	0.01	0.128	0.249	0.032	0.011	0.056	1.34	2.95	0.461	0.277	0.062	0.046	0.166
C	0.01	IR	0.04	0.03	0.05	0.03	0.03	0.04	0.02	0.06	0.55	0.03	0.04	0.03	0.03	0.04	0.03	0.03	0.03
S	0.01	IR	0.03	0.01	0.01	0.02	0.01	0.11	0.23	0.02	0.01	0.05	2.31	4.35	0.64	0.44	0.07	0.05	0.05
ppm (unless stated otherwise)																			
Ba	2	FUS-ICP	161	52	85	14	15	166	488	103	27	80	195	159	63	386	37	44	14
Sr	2	FUS-ICP	86	72	69	88	118	52	96	93	82	128	55	52	149	111	138	81	154
Y	1	FUS-ICP	40	31	30	35	31	36	24	27	29	28	49	22	38	33	34	38	30
Sc	1	FUS-ICP	39	34	36	36	33	43	47	36	37	45	42	16	22	25	35	38	35

Zr	2	FUS-ICP	116	80	82	91	80	125	64	53	46	67	125	123	143	124	113	108	86
Be	1	FUS-ICP	1	< 1	< 1	1	< 1	1	1	< 1	1	1	1	1	2	2	1	< 1	1
V	5	FUS-ICP	330	288	309	294	276	355	347	256	254	324	340	103	262	270	291	321	287
Au (ppb)	2	INAA	< 2	45	24	< 2	< 2	< 2	< 2	< 2	< 2	< 2	1610	47	315	484	11	55	< 2
As	0.5	INAA	2.8	< 0.5	3.3	4.1	3.9	4.2	3	10.9	9	13.5	293	16.8	1860	739	5	3.2	4.2
Br	0.5	INAA	< 0.5	< 0.5	< 0.5	< 0.5	< 0.5	< 0.5	< 0.5	< 0.5	< 0.5	< 0.5	< 0.5	< 0.5	< 0.5	< 0.5	< 0.5	< 0.5	< 0.5
Cr	5	INAA	146	158	190	169	185	170	166	126	118	156	162	123	8	12	198	162	232
Cs	1	INAA	2	< 1	6	< 1	< 1	6	7	1	< 1	< 1	9	7	2	5	< 1	3	< 1
Co	1	INAA	36	43	48	44	45	41	62	51	50	55	45	23	62	45	50	42	55
Ce	3	INAA	17	11	11	11	13	9	6	8	8	11	20	33	34	34	15	14	18
Eu	0.2	INAA	1.1	0.8	0.8	0.8	0.8	0.8	0.7	0.7	0.6	0.6	1	0.6	1.5	1.2	0.8	1.4	0.9
Hf	1	INAA	2	2	1	2	2	2	2	1	1	1	2	2	2	3	2	2	2
Ir (ppb)	5	INAA	< 5	< 5	< 5	< 5	< 5	< 5	< 5	< 5	< 5	< 5	< 5	< 5	< 5	< 5	< 5	< 5	< 5
La	0.5	INAA	8	5.7	5	3.3	5.1	3.4	2.4	3.5	3.3	4.4	10	18.2	18	16.3	6.9	7.3	6.4
Lu	0.05	INAA	0.57	0.43	0.41	0.49	0.45	0.47	0.34	0.38	0.41	0.42	0.74	0.29	0.48	0.38	0.54	0.63	0.55
Mo	5	INAA	< 5	< 5	< 5	< 5	< 5	< 5	< 5	< 5	< 5	< 5	< 5	< 5	< 5	< 5	< 5	< 5	< 5
Nd	5	INAA	8	8	7	< 5	8	7	< 5	< 5	6	7	8	11	19	9	< 5	< 5	11
Rb	20	INAA	< 20	< 20	50	< 20	< 20	< 20	60	< 20	< 20	< 20	80	130	< 20	70	< 20	< 20	< 20
Sb	0.2	INAA	< 0.2	< 0.2	0.3	< 0.2	< 0.2	< 0.2	0.3	< 0.2	< 0.2	< 0.2	< 0.2	0.3	< 0.2	< 0.2	< 0.2	< 0.2	< 0.2
Se	3	INAA	< 3	< 3	< 3	< 3	< 3	< 3	< 3	< 3	< 3	< 3	< 3	< 3	< 3	< 3	< 3	< 3	< 3
Sm	0.1	INAA	2.9	2.2	2.3	2.4	2.3	2.3	2	1.8	2	2.1	3.8	3.2	4.7	3.9	2.9	3.2	2.8
Ta	0.5	INAA	< 0.5	< 0.5	< 0.5	< 0.5	< 0.5	< 0.5	< 0.5	< 0.5	< 0.5	< 0.5	0.5	< 0.5	< 0.5	< 0.5	< 0.5	1.3	< 0.5
Th	0.2	INAA	1	0.8	0.8	0.9	0.6	0.9	< 0.2	0.7	< 0.2	0.4	1.4	2.8	1.5	1.2	< 0.2	1	0.6
Tb	0.5	INAA	0.6	< 0.5	0.5	< 0.5	< 0.5	0.9	< 0.5	< 0.5	0.6	< 0.5	< 0.5	< 0.5	0.8	0.7	< 0.5	< 0.5	0.9
U	0.5	INAA	< 0.5	< 0.5	< 0.5	< 0.5	< 0.5	4	< 0.5	< 0.5	< 0.5	< 0.5	< 0.5	< 0.5	< 0.5	< 0.5	< 0.5	< 0.5	< 0.5
W	1	INAA	< 1	< 1	< 1	< 1	3	< 1	< 1	< 1	< 1	< 1	< 1	< 1	< 1	< 1	< 1	< 1	< 1
Yb	0.2	INAA	3.9	2.9	2.9	3.2	3.3	3.2	2.6	2.7	2.7	2.6	5	2	3	2.7	3.6	3.9	3.7
Ag	0.5	TD-ICP	< 0.5	< 0.5	< 0.5	< 0.5	< 0.5	< 0.5	< 0.5	< 0.5	< 0.5	< 0.5	< 0.5	0.8	< 0.5	< 0.5	< 0.5	< 0.5	< 0.5
Cd	0.5	TD-ICP	< 0.5	< 0.5	< 0.5	< 0.5	< 0.5	< 0.5	< 0.5	< 0.5	< 0.5	< 0.5	0.6	< 0.5	< 0.5	< 0.5	< 0.5	< 0.5	< 0.5
Cu	1	TD-ICP	29	8	25	22	27	182	373	63	20	61	148	307	171	49	52	46	130
Ni	1	TD-ICP	84	123	159	127	147	58	173	148	125	144	97	102	30	38	155	73	124
Pb	5	TD-ICP	8	6	10	7	5	9	< 5	9	6	7	13	28	12	12	10	10	6

Zn	1	TD-ICP	147	111	102	105	111	146	136	130	264	103	157	190	163	152	104	99	89
Bi	10	TD-ICP	< 10	< 10	< 10	< 10	< 10	< 10	< 10	< 10	< 10	< 10	< 10	< 10	< 10	< 10	< 10	< 10	< 10

Abbreviations: Gar = garnet, hbl = hornblende, mag = magnetite, sill = sillimanite. LOD = detection limit; FUS-ICP = fusion ICP; TD-ICP = total digestion (by acids) ICP; INAA = neutron activation; IR = infra red (Leco). Spilite = pre-metamorphic spilitisation, now 'calc-silicate' alteration.

Sillimanite gneisses

Rocks that have commonly (e.g. Appel et al. 2003, Appel et al. 2005, Coller & Coller 2005) been called 'metasediments' at Qingaaq and Aappalaartoq, are second in volume, after amphibolite, in the detail mapping areas of 2005 at Qingaaq (Figs. 7, 8 and 10). These rocks have a yellowish weathering surface, grano-, nemato-, and porphyroblastic texture, normally a distinct foliation, and a mineral assemblage of plagioclase - quartz - sillimanite - garnet - biotite ± tourmaline, rutile, ilmenite, titanite, graphite (Figs. 24–27). Locally, the sillimanite is intensely sericitised. Due to variation in texture and mineral assemblage, samples from this unit have in Figs. 7, 8 and 11, and in Appendices 1 and 2 been called sillimanite-garnet mica gneiss (or schist), or quartz-sillimanite rock (unfoliated type).

So far, it remains unclear whether the sillimanite-garnet gneisses really are metasedimentary rocks or, possibly, products of pre-metamorphic advanced argillic alteration of the local amphibolite (or of something else). The chemical compositions of these Al-rich rocks suggest some similarity with strongly altered amphibolite (App. 2, Plot 5). For example, the Ti-Zr ratio of the sample 493256 (TiO_2 2.22 %, Zr 210 ppm) is similar to those of the amphibolites (Plot 2c), and the REE trends of all three sillimanite-rich samples analysed suggest LREE enrichment during alteration, if these were derived from the amphibolites (Plot 6).

Calc-silicate alteration

Locally in the amphibolites, there are 10 cm to 2 m wide, 1-30 m long, inhomogeneous domains which have previously been called 'calc-silicate alteration' (Figs. 28–29). These domains do not have any spatial relationship to quartz veining, gold mineralisation or biotite-garnet alteration.

Calc-silicate alteration in amphibolite is revealed by various amounts of diopside, epidote, hornblende, plagioclase, actinolite, and garnet as major to minor minerals, and titanite, quartz, pyrrhotite, chalcopyrite, apatite and carbonate as minor minerals (Figs. 30–32). The colour of the domains varies from pale grey (diopside-rich) to dark green (hornblende-rich) in centimetre scale. In places, the calc-silicate altered areas resemble pillow lavas, or flow top or flow bottom breccias, with diopside-epidote rich bands possibly defining pillow and breccia fragment margins and inter-pillow and breccia matrices. However, as also these domains are deformed, foliated and folded, one cannot be sure whether or not pillow and/or volcanic breccia structures really are present. In any case, deformation structures and cross-cutting veining indicate that the calc-silicate altered domains are early, just as suggested before by, for example, Polat (2005, and references therein). As the 'calc-silicate altered' zones so much resemble the above-mentioned primary structural features, it may be argued that they are product of an early synvolcanic, submarine, spilitic stage in the evolution of the local volcanic sequence (cf. Reed 1983, Barley et al. 1990), and that their present mineral assemblages are product of regional-metamorphic recrystallisation of the original chlorite-, epidote-, and albite-rich assemblages. The siting of the samples in Plots 1, 2a & 3, with respect to the least-altered amphibolite, support the idea that the spilites are derived from the surrounding amphibolite.

Petrographic and compositional characteristics of biotite-garnet alteration

Biotite-garnet alteration occurs in amphibolite as sheared zones from 0.5 m to >60 m wide. These altered domains comprise distal biotite and proximal biotite-garnet zones (Fig. 33–35), the latter with minor sulphidation (dominated by pyrrhotite). The biotite-garnet zones are replaced by the nearly monomineralic hornblende selvages next to the laminated quartz veins (Figs. 36-38). The change from biotite-only to biotite-garnet zone is gradual and difficult to recognise in outcrop or drill core in the dark greenish brown rock. This style of alteration has a close spatial relationship with gold mineralisation at Qingaaq and Aappalaartoq (Figs. 39–40). Although there are gold-mineralised zones also in other rock types at Qingaaq, we did not detect any clearly gold-related alteration in these rocks during field work in 2005. Therefore, we below concentrate on alteration in amphibolite. Below, we describe this style of alteration from site 5 and the drill core DDH05-06.

Biotite-garnet alteration at site 5

At site 5 (Figs. 11 and 41), the least-altered amphibolite (sample 493266 in Figs. 12 and 42) has the mineral assemblage hornblende-quartz-plagioclase with minor to trace volumes of rutile, titanite, and ilmenite. Amphibole makes about 55-60 vol% of the rock (visual estimate), and its composition is identified as Fe-hornblende or Fe-tschermakitic hornblende (Table 2, analyses 6a and 6b). The plagioclase is labradorite at An_{65} (Table 4). The decussate texture of the rock shows a clear equilibrium between these phases, the only exception being represented by the incipient replacement of rutile by ilmenite (Figure 12B). Even this rock shows minor, localised alteration by the presence of rare garnets (Fig. 42).

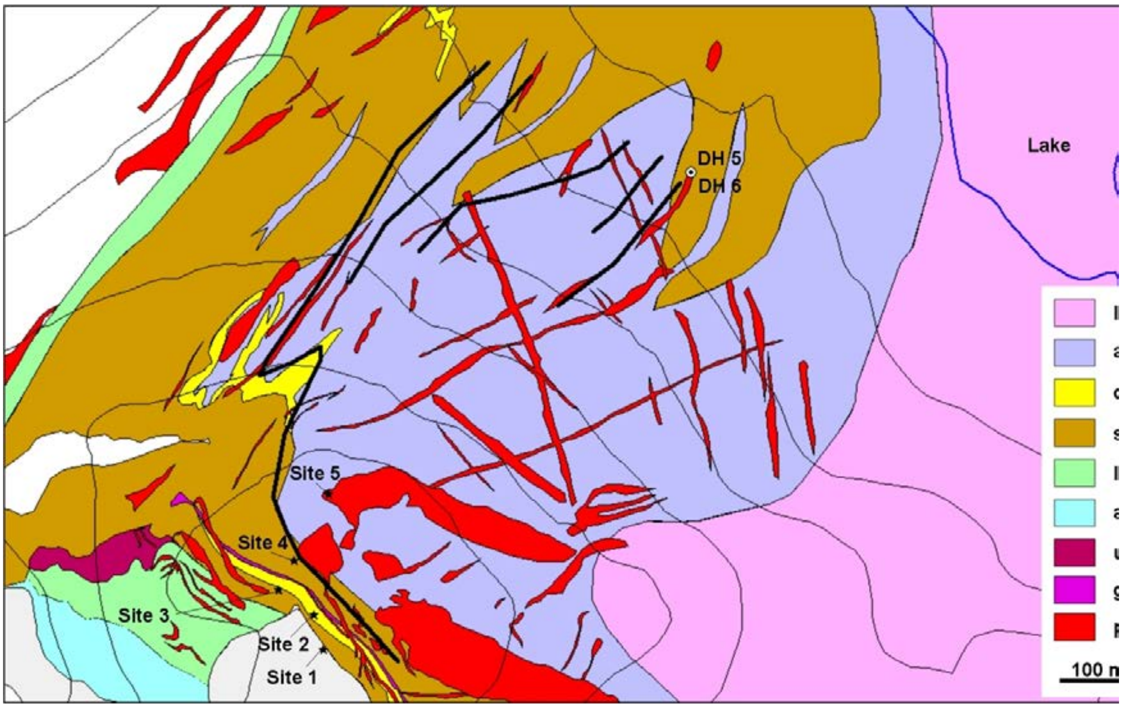

Figure 4. *Qingaaq: location of mapping sites and drill holes DDH05-05 and DDH05-06. North up. Black lines are known gold-rich zones at the present surface. White areas are unmapped, chiefly covered by snow. Explanations for the legend: quartzitic rock = felsic gneisses associated with garnet magnetite rock; sill-gn-mica gneiss = sillimanite-garnet gneiss; gn-mg unit = garnet-magnetite rock dominated unit. (Map from Coller & coller 2005).*

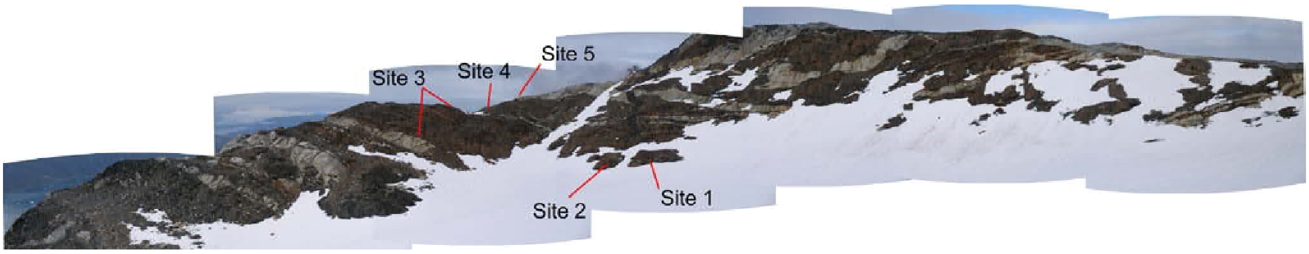

Figure 5. *Panorama of the SW slope of the mapping area at Qingaaq, in 28. July 2005.*

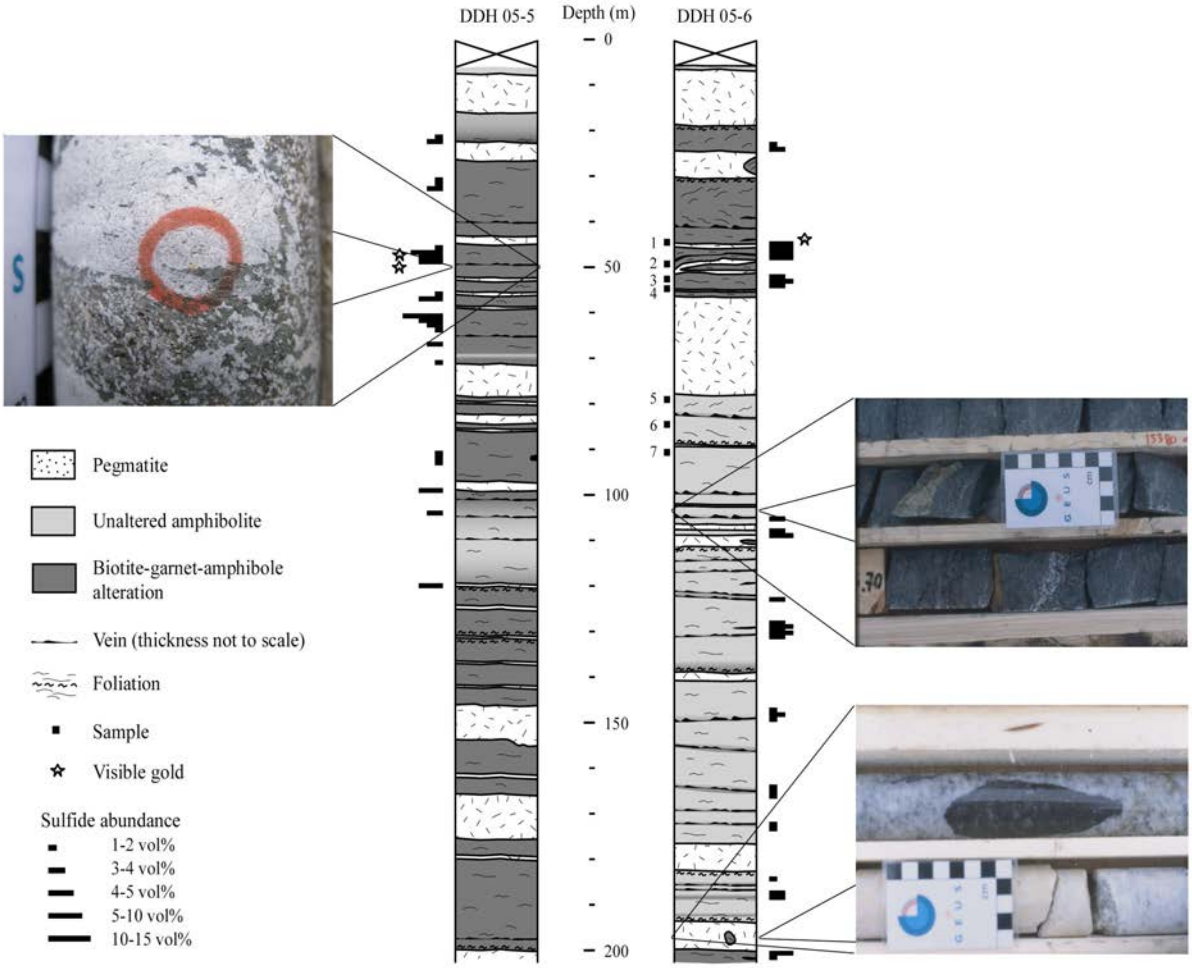

Figure 6. *Rock types, alteration, veining in drill cores DDH05-05 and DDH05-06, Storø. Note the contrast between the extent of alteration in the two drill cores. In the core DDH05-06, alteration mainly occurs in the uppermost 55 m, although fragments of intensely altered amphibolite also occur as inclusions in the late pegmatites.*

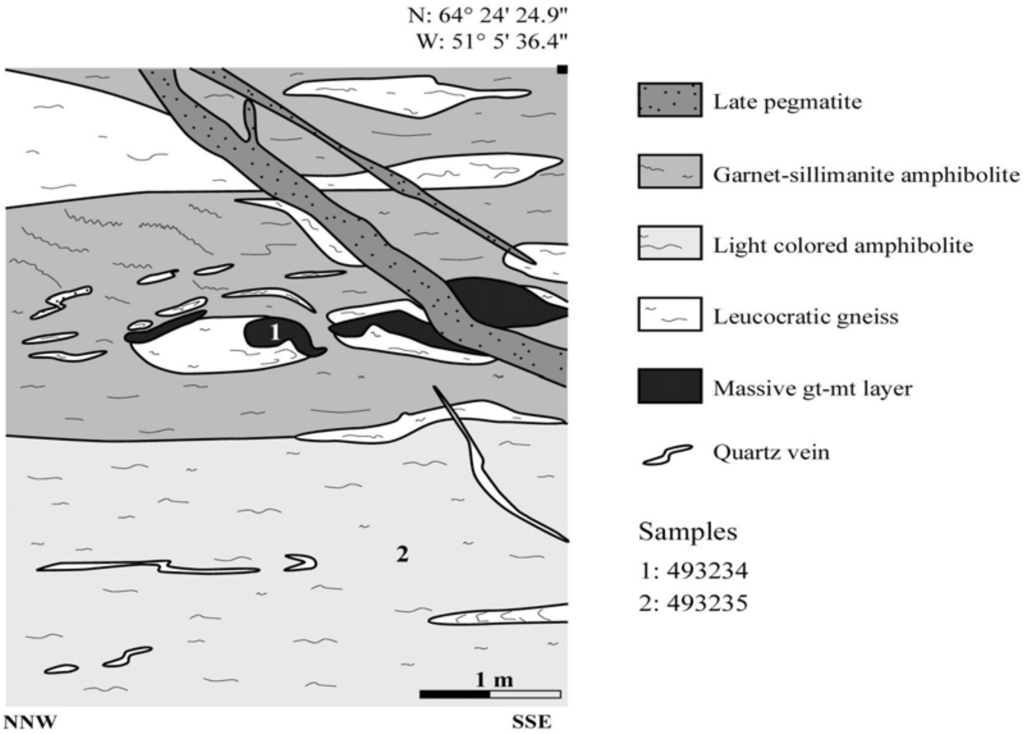

Figure 7. *Rock types, alteration, veining at site 1 at Qingaaq, Storø. Note, that what is in the legend called 'Light coloured amphibolite' is, in fact, sillimanite-garnet mica gneiss with a mineral assemblage of plagioclase - biotite - sillimanite - quartz - garnet - tourmaline - rutile - ilmenite.*

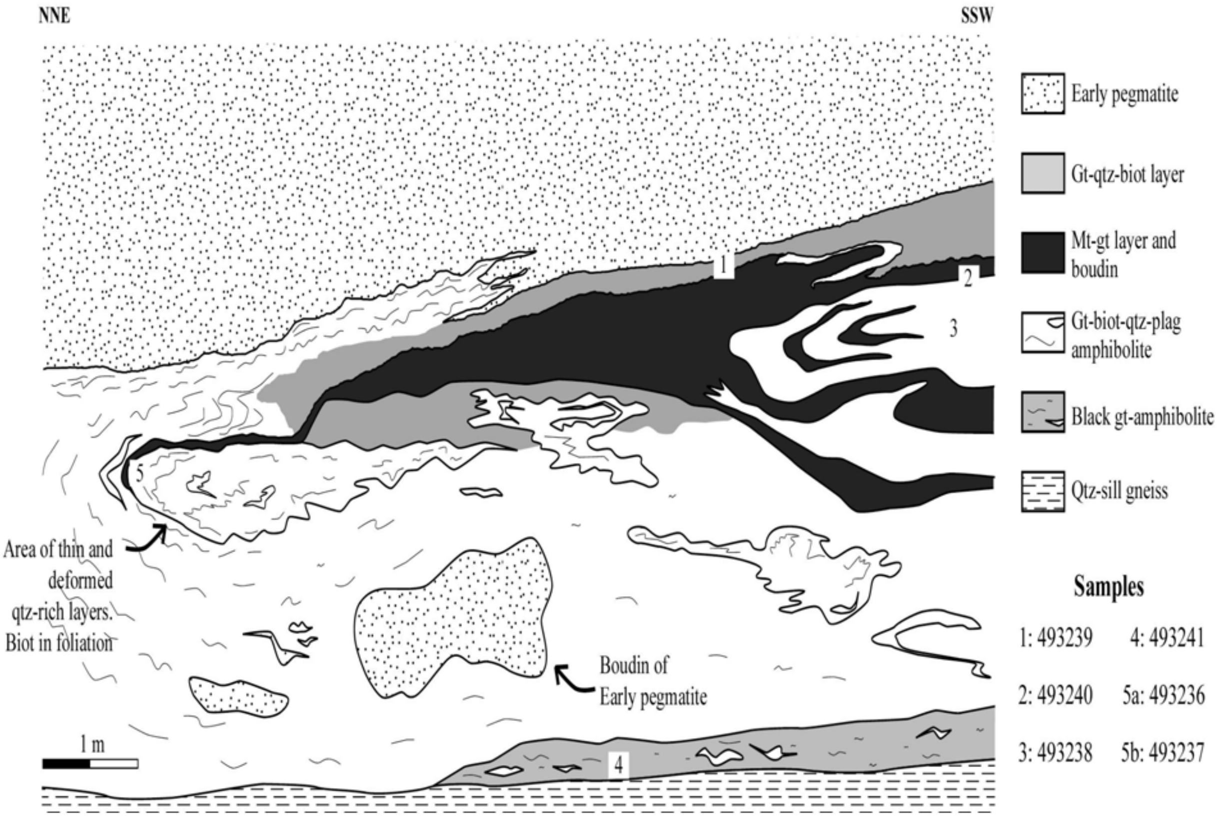

Figure 8. *Rock types, alteration, veining at site 2 at Qingaaq, Storø.*

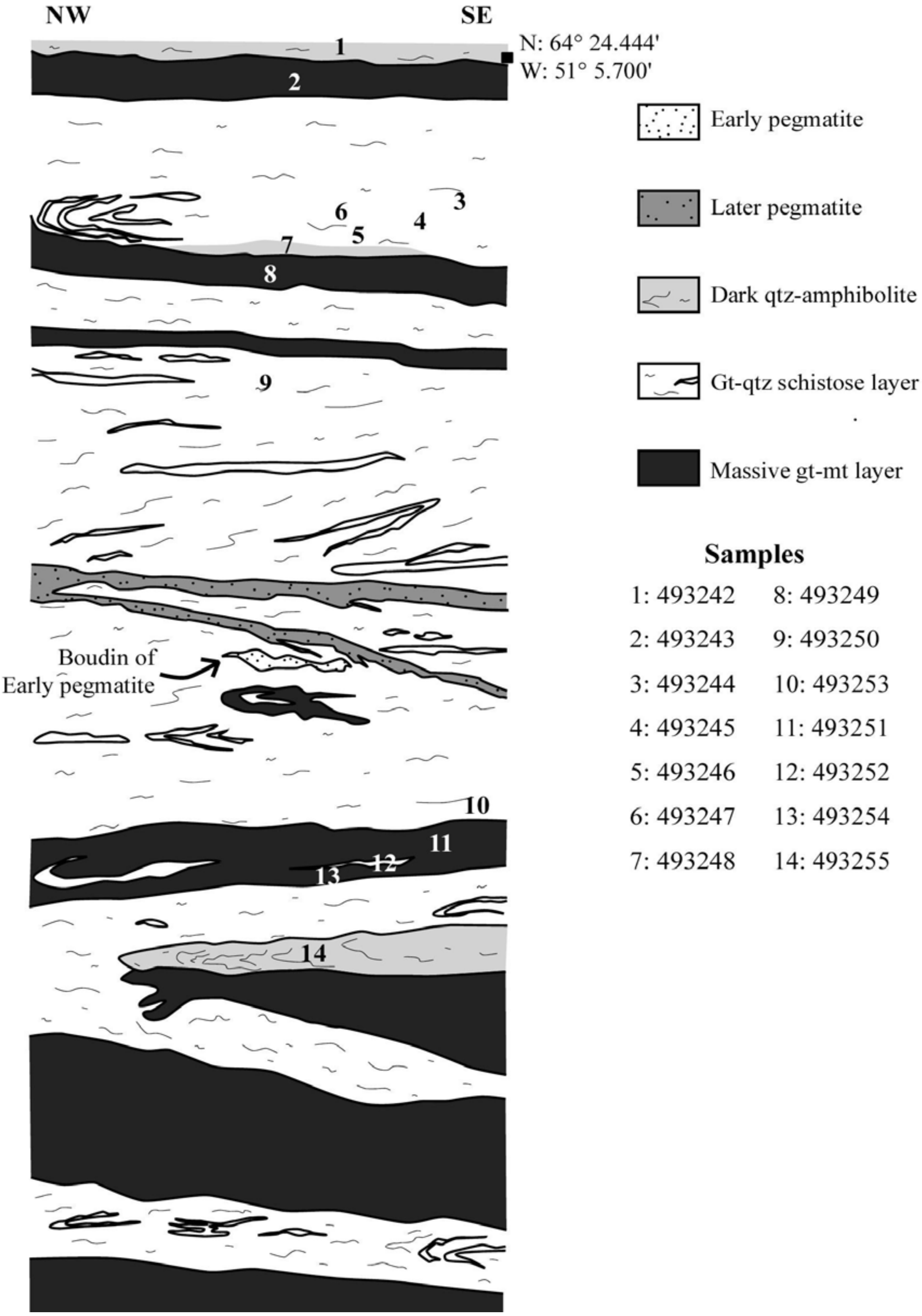

Figure 9. *Rock types, alteration, veining at site 3 at Qingaaq, Storø. Note that no amphibole has been detected in thin section in the rock type here called 'dark quartz-amphibolite' whose dark colour is essentially due to the presence of abundant biotite.*

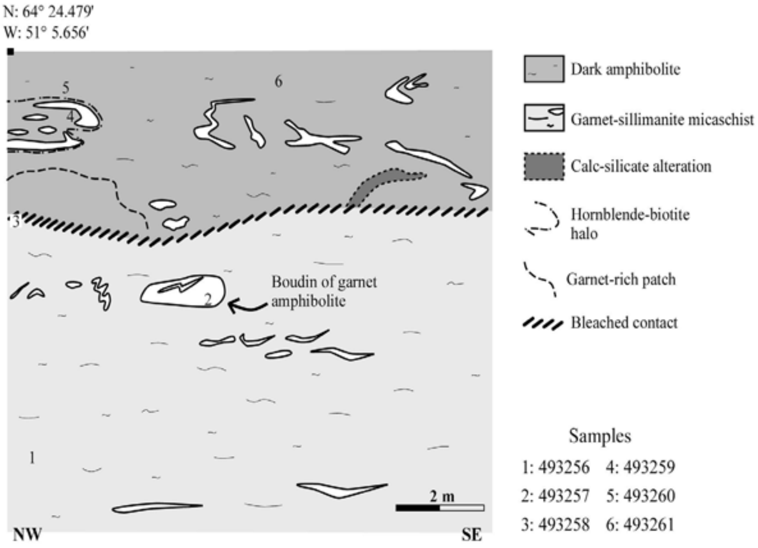

Figure 10. *Rock types, alteration, veining at site 4 at Qingaaq, Storø.*

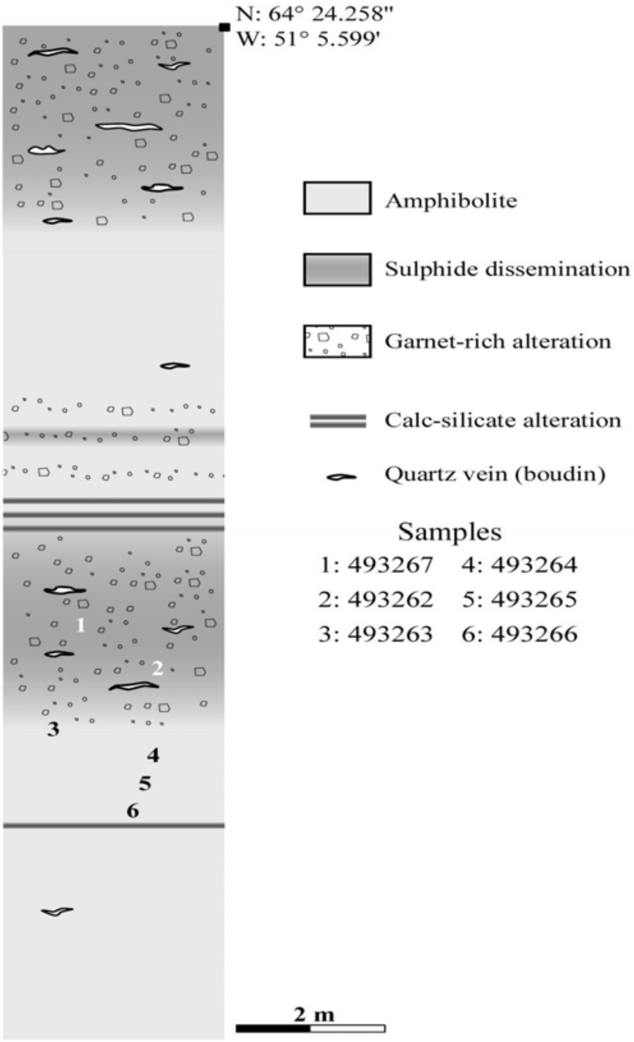

Figure 11. *Rock types, alteration, veining at site 5 at Qingaaq, Storø.*

Figure 12. *Typical unaltered (least-altered) amphibolite: distinct foliation, main minerals hornblende and plagioclase. Sample 493281. Location: 051°04'46.4''W, 64°25'14.6''N. Scale in cm.*

Table 1. *Composition of biotite (wt%)*

	SEM EDS analyses			Microprobe analyses*							
sample nr.	3-13_3 Site 3	3-13_4 Site 3	5a Site 5	472867 micro-area 1	472867 micro-area 2	472873	472895	472898 micro-area 2	472898 micro-area 3	472899 light variety	472899 dark variety
nr. of analyses				11	11	29	21	21	21	22	11
SiO_2	32.51	35.06	37.37	39.59/0.15	35.55/0.17	33.89/0.24	35.30/0.24	35.50/0.31	35.43/0.16	35.40/0.17	34.55/0.20
TiO_2	1.35	1.54	1.67	1.73/0.04	1.80/0.08	0.54/0.53	1.92/0.06	1.68/0.10	1.65/0.07	1.67/0.05	1.61/0.06
Al_2O_3	18.18	17.47	17.83	17.76/0.16	17.56/0.10	17.35/0.13	17.27/0.10	16.73/0.14	16.33/0.10	16.39/0.16	16.07/0.12
FeO	24.77	23.99	22.30	22.56/0.40	22.51/0.36	30.18/0.39	23.73/0.38	25.99/0.51	26.31/0.33	25.53/0.48	24.97/0.36
MnO	0.00	0.00	0.11	0.02/0.02	0.00/0.00	0.04/0.04	0.07/0.04	0.02/0.02	0.03/0.03	0.04/0.04	0.02/0.03
MgO	6.67	7.05	9.96	8.99/0.08	8.96/0.13	4.47/0.07	8.18/0.08	7.97/0.13	7.85/0.08	7.88/0.07	7.63/0.08
CaO	0.10	0.00	0.00	0.01/0.01	0.00/0.00	0.00/0.00	0.00/0.00	0.13/0.03	0.03/0.02	0.01/0.01	0.05/0.03
Na_2O	0.27	0.23	0.30	0.28/0.03	0.03/0.17	0.17/0.02	0.18/0.02	0.23/0.03	0.29/0.03	0.27/0.02	0.30/0.03
K_2O	5.02	8.73	9.42	9.11/0.12	0.14/9.14	9.14/0.11	9.41/0.09	8.60/0.30	8.96/0.14	9.05/0.08	8.71/0.13
Cr_2O_3	0.00	0.00	0.22	0.10/0.03	0.09/0.03	0.02/0.02	0.05/0.03	0.08/0.03	0.09/0.03	0.08/0.03	0.10/0.04
Total	88.87	94.07	99.18	96.15	95.80	95.81	96.12	96.93	96.96	96.33	94.01
Cations based on 11 O											
Si	2.680	2.761	2.760	2.724	2.731	2.717	2.728	2.737	2.743	2.748	2.750
Al^{IV}	1.320	1.239	1.240	1.276	1.269	1.283	1.272	1.263	1.257	1.252	1.250
Al^{VI}	0.447	0.382	0.312	0.327	0.321	0.356	0.301	0.257	0.233	0.257	0.257
Fe	1.708	1.580	1.378	1.444	1.446	2.023	1.533	1.676	1.703	1.652	1.662
Mg	0.820	0.828	1.097	1.026	1.026	0.534	0.942	0.917	0.907	0.912	0.905
Mn	0.000	0.000	0.007	0.001	0.000	0.003	0.004	0.001	0.002	0.002	0.001
Ca	0.009	0.000	0.000	0.001	0.000	0.000	0.000	0.011	0.002	0.001	0.004
Ti	0.084	0.091	0.093	0.100	0.104	0.032	0.112	0.097	0.096	0.098	0.096
Cr	0.000	0.000	0.013	0.006	0.005	0.001	0.003	0.005	0.006	0.005	0.006
K	0.528	0.877	0.888	0.890	0.886	0.935	0.928	0.846	0.885	0.891	0.884
Na	0.043	0.035	0.043	0.041	0.043	0.027	0.028	0.035	0.044	0.043	0.046
Fe/Fe+Mg	0.676	0.656	0.557	0.585	0.585	0.791	0.620	0.646	0.653	0.644	0.647

* analyses given as: mean composition/standard deviation
*

Table 2: Composition of amphiboles (SEM-EDS analyses; in wt%)

	3a Site 3	3b Site 3	5a Site 5	5b Site 5	6a Site 5	6b Site 5
SiO_2	51.60	50.11	55.11	45.75	44.19	44.29
TiO_2	0.00	0.00	0.00	0.97	0.86	0.61
Al_2O_3	1.26	0.93	1.17	13.39	13.20	13.40
FeO	32.62	31.78	25.54	16.75	17.99	17.89
MnO	0.00	0.00	0.32	0.11	0.20	0.18
MgO	10.94	10.90	16.27	10.14	8.86	8.71
CaO	0.45	0.22	0.43	11.22	11.54	11.52
Na_2O	0.30	0.35	0.38	1.46	1.71	1.50
K_2O	0.00	0.00	0.00	0.00	0.37	0.29
No. of oxygens	23	23	23	23	23	23
Struct. formulae						
Si	7.923	7.934	7.972	6.502	6.227	6.259
Al^{IV}	0.077	0.066	0.028	1.498	1.773	1.741
Al^{VI}	0.151	0.107	0.171	0.744	0.420	0.491
Ti	0.000	0.000	0.000	0.104	0.091	0.065
Fe^{3+}	0.000	0.000	0.000	0.728	2.120	2.114
Fe^{2+}	4.189	4.208	3.090	1.263	0.000	0.000
Mn	0.000	0.000	0.039	0.013	0.024	0.022
Mg	2.504	2.573	3.508	2.148	1.861	1.835
Ca	0.074	0.037	0.067	1.708	1.742	1.744
Na	0.089	0.107	0.107	0.402	0.467	0.411
K	0.000	0.000	0.000	0.000	0.067	0.052
OH^-	2.000	2.000	2.000	2.000	2.000	2.000
Total	17.008	17.033	16.982	17.111	16.792	16.734
Amphibole group	Fe-Mg-Mn	Fe-Mg-Mn	Fe-Mg-Mn	Ca	Ca	Ca
(Ca+Na) (B)	0.163	0.121	0.173	2.000	2.000	2.000
Na (B)	0.089	0.083	0.107	0.292	0.258	0.256
(Na+K) (A)	0.000	0.024	0.000	0.111	0.276	0.208
$Mg/(Mg + Fe^{2+})$	0.374	0.379	0.532	0.630	1.000	1.000
$Fe^{3+}/(Fe^{3+} + Al^{VI})$	0.000	0.000	0.000	0.494	0.835	0.812
Sum of S2	14.844	14.888	14.809	13.000	12.516	12.527
Amphibole names	Anthoph.	Anthoph.	Anthoph.	Mg-horn	Fe-tscher	Fe-hornbl

Notes: calculations based on 23 oxygens, with Fe^{2+}/Fe^{3+} estimations carried out assuming 13 cations - except for Fe-Mg-Mn amphiboles where 15 cations are assumed. No distinction is given between orthorhombic and monoclinic Fe-Mg-Mn amphiboles.

Table 3. *Composition of garnets (wt%)*

	SEM EDS analyses						Microprobe analyses*							
sample nr.	3-13_6	3-13_7	3-13_8	3-13_9	5-1_4	5-1_5	472867	472867	472873	472895	472895	472898	472898	472899
	Site 3	Site 3	Site 3	Site 3	Site 5	Site 5	micro-area 1	micro-area 2		centre	rim	micro-area 2	micro-area3, rim	rim
nr. of anal.							11	11	18	21	20	21	21	21
SiO_2	37.27	37.33	37.36	36.59	38.20	37.92	38.05/0.23	38.23/0.17	37.19/0.16	38.19/0.18	38.27/0.15	38.02/0.16	37.99/0.25	37.64/0.27
TiO_2	0.00	0.00	0.00	0.06	0.00	0.00	0.00/0.00	0.00/0.00	0.00/0.00	0.00/0.00	0.00/0.00	0.00/0.00	0.00/0.00	0.00/0.00
Al_2O_3	20.75	20.89	20.75	20.41	21.64	21.45	21.53/0.17	21.32/0.23	20.87/0.15	21.37/0.18	21.36/0.12	21.15/0.21	21.18/0.23	20.97/0.22
FeO	33.66	34.52	33.89	33.60	29.66	30.51	35.94/0.56	34.35/0.55	40.39/0.38	30.38/0.46	30.01/0.37	35.28/0.71	36.19/0.53	35.46/0.34
MnO	0.00	0.13	0.21	0.23	2.19	1.59	0.00/0.00	0.00/0.00	0.83/0.54	1.58/0.26	2.41/0.16	1.43/0.11	1.49/0.12	1.83/0.37
MgO	2.15	2.06	1.75	1.62	4.62	4.15	2.96/0.15	3.31/0.26	0.71/0.34	2.02/0.09	2.26/0.11	2.38/0.11	1.50/0.31	2.23/0.08
CaO	5.36	4.36	5.54	5.29	3.70	3.88	3.75/0.23	4.31/0.18	1.67/0.15	8.53/0.16	7.82/0.18	4.30/0.51	4.46/0.12	3.59/0.21
Na_2O	0.00	0.00	0.00	0.00	0.12	0.20	0.01/0.01	0.01/0.01	0.01/0.01	0.01/0.01	0.01/0.01	0.01/0.01	0.03/0.03	0.01/0.01
K_2O	0.00	0.00	0.00	0.00	0.04	0.00	0.00/0.00	0.00/0.00	0.00/0.00	0.00/0.00	0.00/0.00	0.00/0.00	0.02/0.02	0.01/0.01
Cr_2O_3	0.12	0.00	0.00	0.00	0.00	0.10	0.05/0.02	0.01/0.01	0.01/0.01	0.13/0.05	0.03/0.03	0.06/0.07	0.04/0.05	0.02/0.02
Total	99.31	99.29	99.50	97.80	100.17	99.80	102.30	101.59	101.68	102.21	102.17	102.63	102.91	101.75
$X_{almandine}$	0.76	0.79	0.76	0.77	0.66	0.69	0.78	0.75	0.90	0.65	0.65	0.76	0.79	0.77
$X_{grossular}$	0.15	0.13	0.16	0.16	0.11	0.11	0.10	0.12	0.05	0.23	0.22	0.12	0.12	0.10
X_{pyrope}	0.09	0.08	0.07	0.07	0.18	0.17	0.11	0.13	0.03	0.08	0.09	0.09	0.06	0.09
$X_{spessartine}$	0.00	0.00	0.00	0.01	0.05	0.04	0.00	0.00	0.01	0.03	0.05	0.03	0.03	0.04

* analyses given as: mean composition/standard deviation

Table 4: Plagioclase composition (SEM EDS analyses; in wt%)

	6a Site 5	**6b** Site 5
Na_2O	5.70	6.08
MgO	0.34	0.47
Al_2O_3	30.06	29.56
SiO_2	54.44	54.58
K_2O	0.12	0.13
CaO	9.55	9.24
TiO_2	0.00	0.00
Cr_2O_3	0.12	0.00
MnO	0.00	0.00
FeO	0.00	0.00
Total	100.33	100.06
Ab	0.35	0.37
An	0.65	0.63

Biotite-garnet alteration in drill core DDH 05-06

The least-altered amphibolite in drill core DDH05-06 (90.00 m down-hole depth [dhd]; sample 491136 in Fig. 13) has the mineral assemblage hornblende - plagioclase - cummingtonite - quartz with minor to trace volumes of ilmenite, pyrrhotite and chalcopyrite (App. 1). Chalcopyrite occurs as small anhedral grains within pyrrhotite, and cummingtonite very locally replaces the hornblende at the selvage of a thin quartz vein. The texture is granoblastic with relatively straight contacts between the grains (Fig. 13A). Incipient replacement of hornblende by cummingtonite is evident but is texturally important only closer to the alteration envelope, as shown at 84.00 m dhd in sample 491135 (Fig. 13B); the rock is not biotitised, nor is it completely unaltered – if the cummingtonite represents alteration as its occurrence along a quartz vein suggests.

With the weak alteration, minor volumes of cummingtonite systematically replace the hornblende at the grain boundaries (Figure 13B), making the granoblastic texture less regular. Also minor biotite appears as replacing hornblende. Rare K feldspar occurs associated with hornblende, muscovite, plagioclase, and quartz, and is present also within discontinuous granoblastic bands in the rock. Ilmenite shows a relatively high modal abundance (3–5 vol%) and pyrrhotite (<1 vol%), with traces of chalcopyrite, is the only sulphide present.

Near to the contact with the pegmatite (79.00 m dhd, sample 491134 in Fig. 13), the rock is biotitised, and comprises hornblende, cummingtonite, quartz, and plagioclase, with minor biotite (K_2O content suggest about 5 % biotite in the sample, App. 2), ilmenite, titanite, and rutile (Fig. 13C, App. 1). Chalcopyrite occurs as anhedral grains associated with pyrrhotite. The texture is granoblastic, and the contacts between the mineral phases are remarkably regular. Iso-orientation of the silicate grains defines a rough foliation.

Immediately within the visibly altered rock (54.00 m dhd, sample 491133 in Fig. 13), garnet and biotite make about 20 vol% of the rock, with hornblende, cummingtonite, quartz, and plagioclase forming the rest of the major minerals present (Figure 13D, App. 1). Minor ilmenite and pyrrhotite, with traces of chalcopyrite and arsenopyrite, are present with a cumulative modal abundance of about 5-6 vol%. The texture is essentially granoblastic, with all minerals appearing in equilibrium. In addition, garnet is porphyroblastic and contains inclusions of biotite, hornblende, quartz and ilmenite. Biotite-garnet-quartz intergrowth is common and may reflect replacement of plagioclase and biotite by the former three minerals.

The central parts of the altered domain in drill core DDH05-06, as exemplified by samples from 44.05 m, 45.00 m, and 52.00 m dhd (samples 491129, 491130, 491132 ; Figs. 13E, 13F, App. 1), covers the area where the visible gold occurs in association with biotite and amphibole (Figs. 6). Together with the increase in volume of biotite, also the modal abundance of pyrrhotite increases by an order of magnitude, locally reaching to about 10 vol%, whereas the volumes of the cummingtonite and ilmenite decrease appreciably. The texture still is granoblastic, with porphyroblastic garnet; the size of garnets is one order of magnitude larger than that of the other silicates. The largest garnet grains are poikiloblastic with very irregular borders, and contain biotite, Mg-Fe-amphibole, pyrrhotite, and ilmenite inclusions.

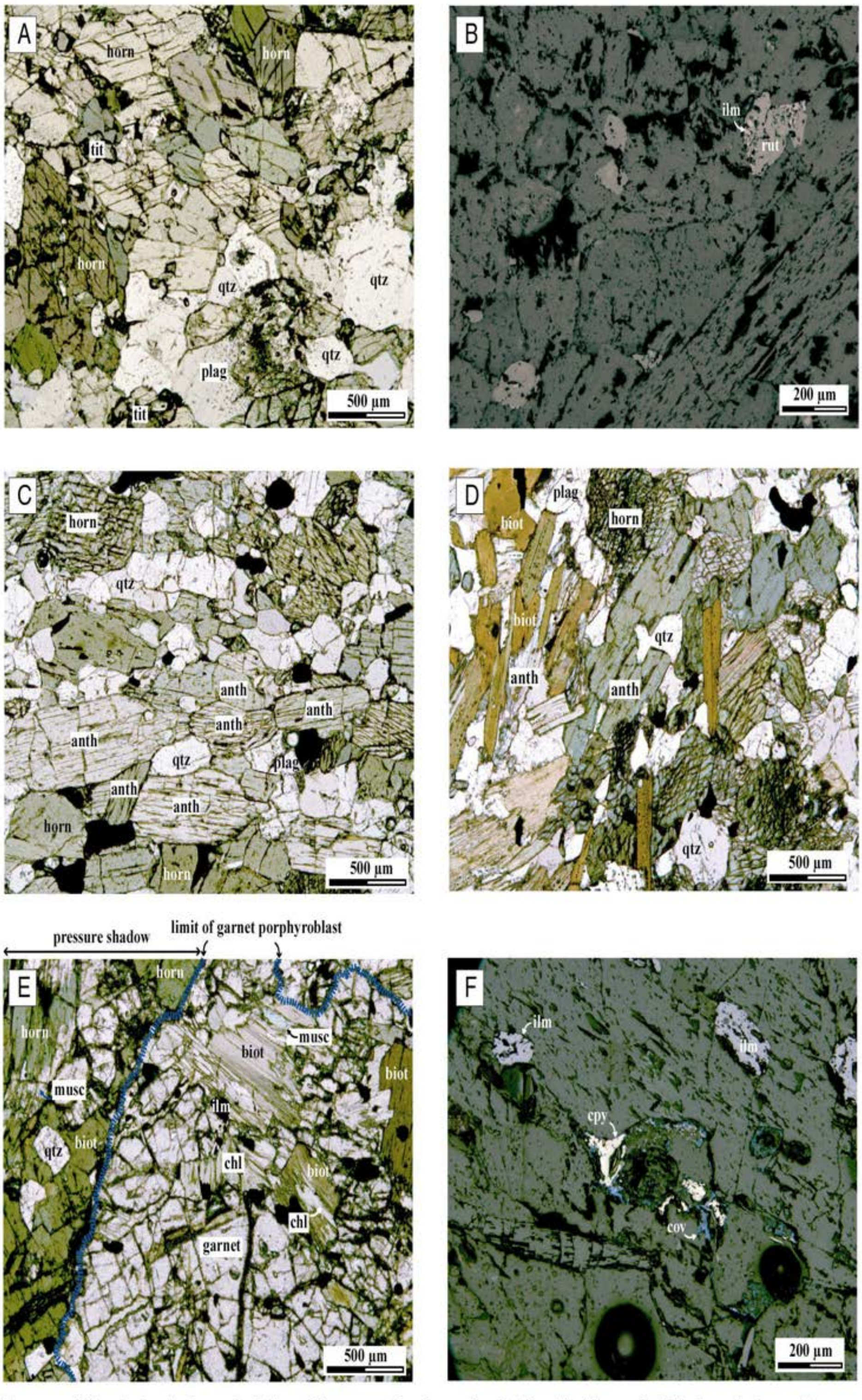

Figure 13. *Photomicrographs from samples from site 5 at Qingaaq, Storø (for sample locations, see Fig. f). All images are with plane-polarised light, except B and F which are reflected light images.*
A*: Decussate texture of least-altered amphibolite (sample 6 = 493266).*
B*: Incipient replacement of rutile by ilmenite (sample 493266).*
C*: Weak foliation defined by lepido- and granoblastic bands (sample 5 = 493265).*
D*: Biotitised amphibolite. Mineral assemblage biotite - hornblende - cummingtonite (albeit abbreviated as anth) - quartz - plagioclase (sample 4 = 493264).*

***E**: Porphyroblastic garnet with inclusions of biotite, muscovite, chlorite, and ilmenite which all also occur in the pressure shadows of the garnets. Muscovite also replaces biotite (sample 1 = 493267).*

***F**: Anhedral covellite partially replacing chalcopyrite (sample 1). Abbreviations: anth = cummingtonite, biot = biotite, chl = chlorite, cov = covellite, cpy = chalcopyrite, gar = garnet, horn = hornblende, ilm = ilmenite, musc = muscovite, plag = plagioclase, po = pyrrhotite, qtz = quartz, rut = rutile, tit = titanite.*

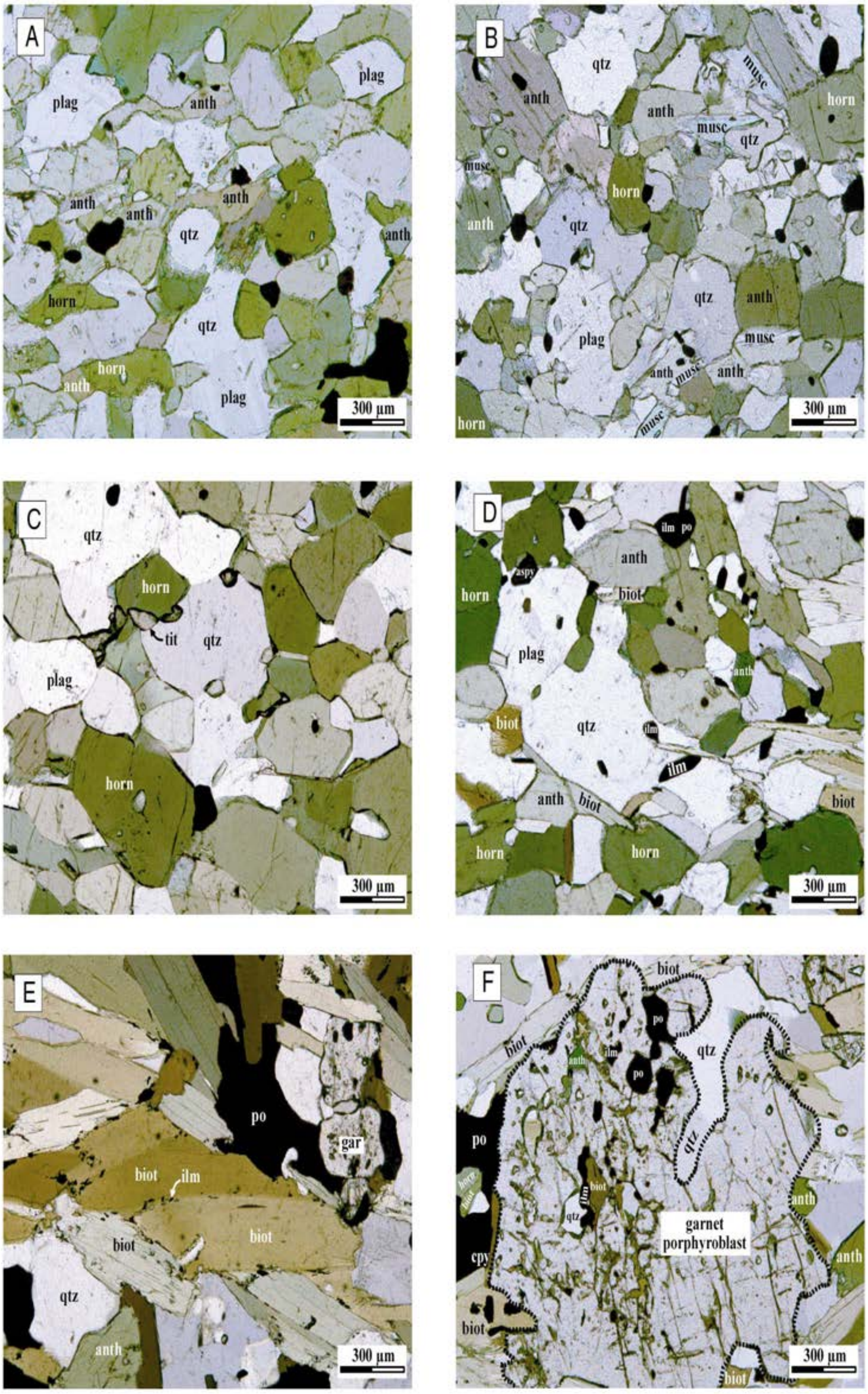

Figure 14. *Photomicrographs of samples from the drill core DDH05-06, northern slope of Qingaaq, Storø. All images are with plane-polarised transmitted light.* ***A****: Granoblastic least-altered amphibolite (sample 7 = 90.00 m dhd, GEUS no. 491136); hornblende possibly partially replaced by cummingtonite.* ***B****: Hornblende partially replaced by cummingtonite (sample 6 = 84.00 m dhd, GEUS no. 491135).* ***C****: Granoblastic texture in sample 5 (= dhd 79.00 m dhd, GEUS no. 491134).* ***D****: Weakly biotitised amphibolite (sample 4 = 54.00 m dhd, GEUS no. 491133).* ***E****: Intensely biotitised amphibolite: biotite associated with garnet, cummingtonite (= anth), quartz and pyrrhotite. Ilmenite at the biotite grain boundaries (sample 1 = 44.05 m dhd, GEUS no. 491129).* ***F****: A garnet porphyroblast with biotite, pyrrhotite, cummingtonite (= anth), and quartz inclusions (GEUS no. 491129). Abbreviations: anth = cummingtonite, biot = biotite, gar = garnet, horn = hornblende, ilm = ilmenite, plag = plagioclase, po = pyrrhotite, qtz = quartz.*

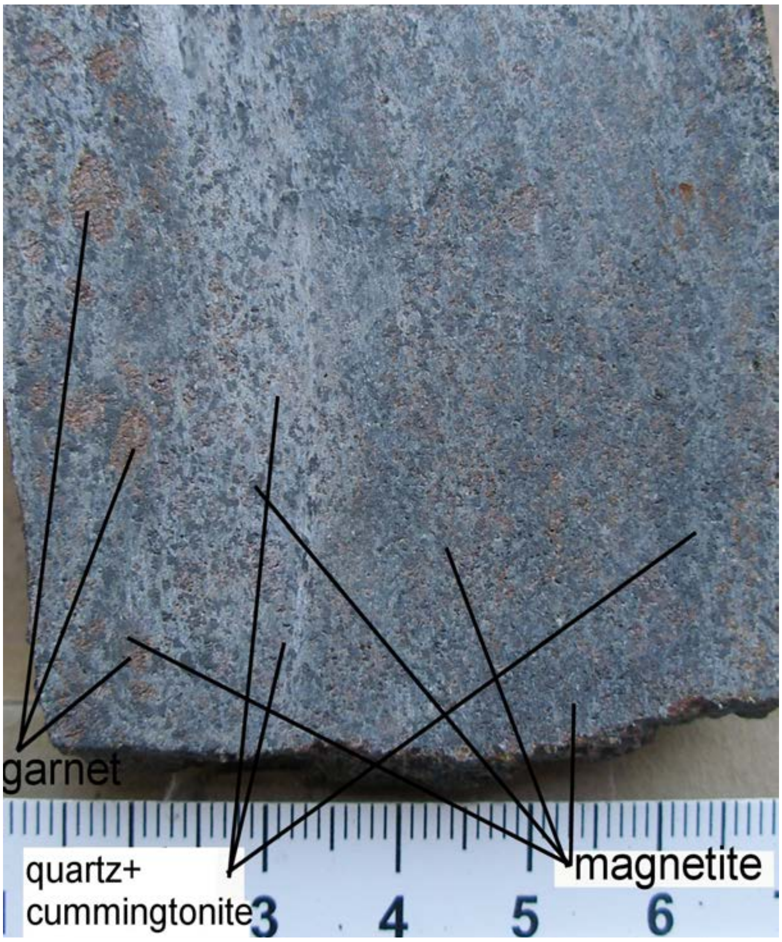

Figure 15. *Close-up of a typical garnet-magnetite rock at Qingaaq. Sample 493243.*

Figure 16. *Fold nose defined by biotite-garnet ('non-magnetic ironstone') and garnet-magnetite ('magnetic ironstone') rocks (both very dark) enveloped by pale grey garnet-sillimanite mica gneiss. Pegmatite in upper left part of the photo. View to the NE. Site 2. Qingaaq. 64°24.440', 051°05.622'.*

Figure 17. *Hinge of an isoclinal mesoscale fold: dark garnet-magnetite rock and felsic gneiss. Site 3, location at about 13.00 m of the profile; Qingaaq.*

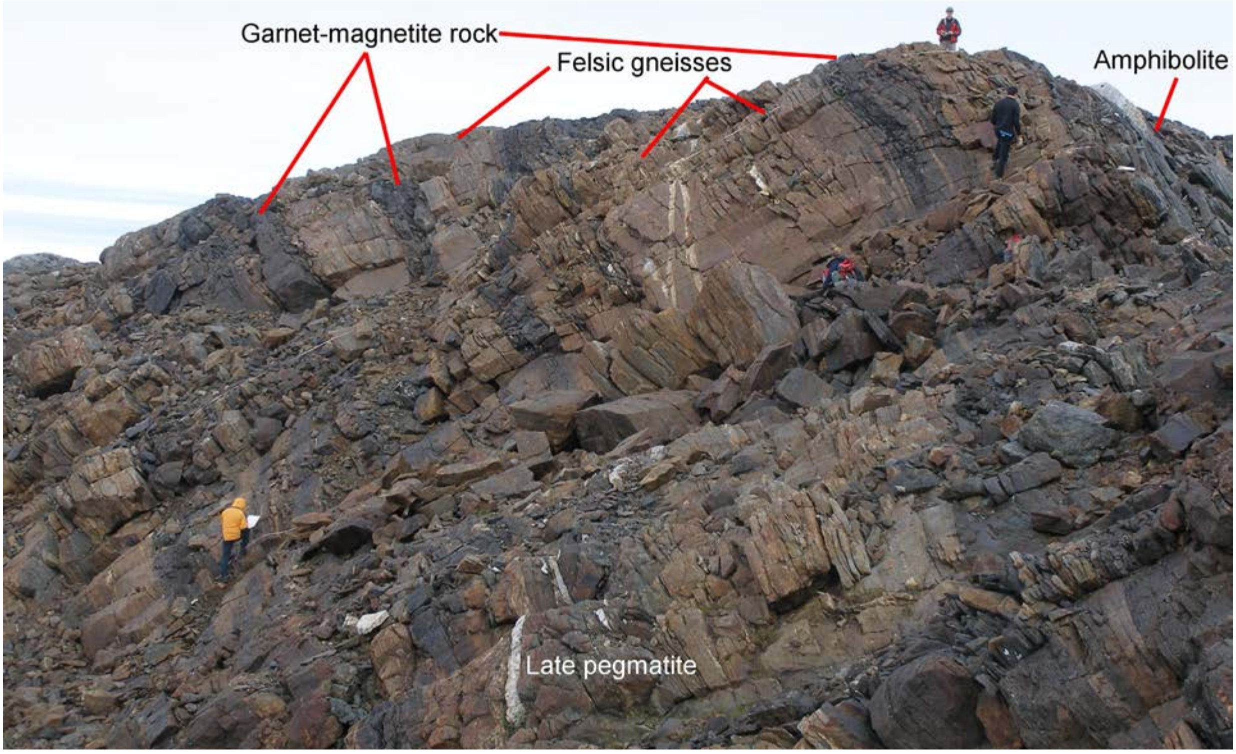

Figure 18. *Site 3 and its immediate surroundings: mostly felsic gneisses and garnet-magnetite rocks. View to the WNW. Qingaaq. 64°24.444', 051°05.700'.*

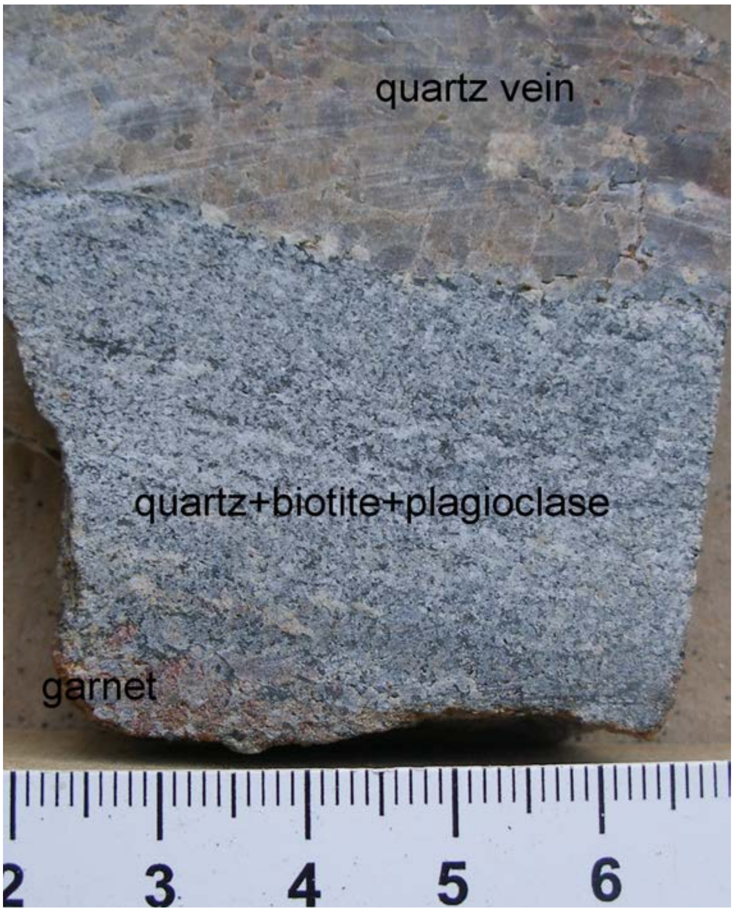

Figure 19. *Felsic mica gneiss, some garnet, and a quartz vein. Sample 493238.*

Figure 20. *Felsic mica gneiss, early, deformed quartz veins. Partially brownish due to weathering. Sample 493245.*

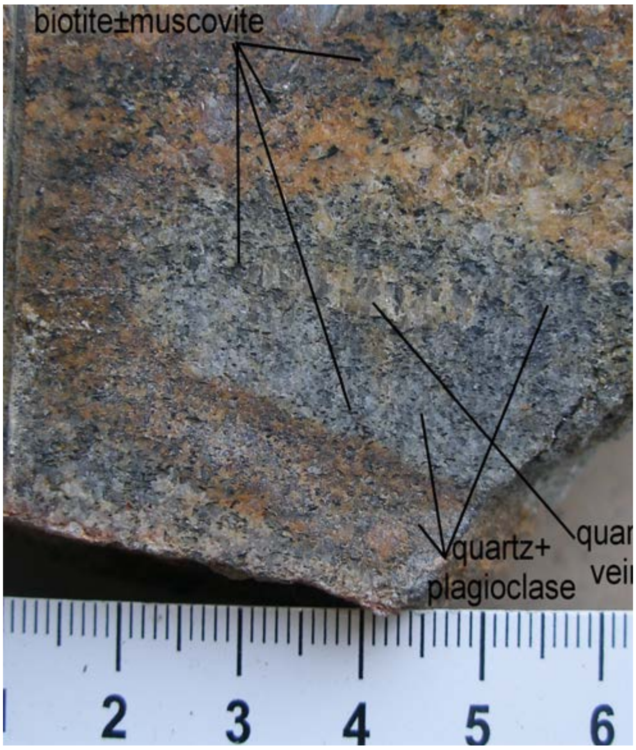

Figure 21. *Felsic mica gneiss, early, deformed quartz veins. Partially brownish due to weathering. Sample 493247.*

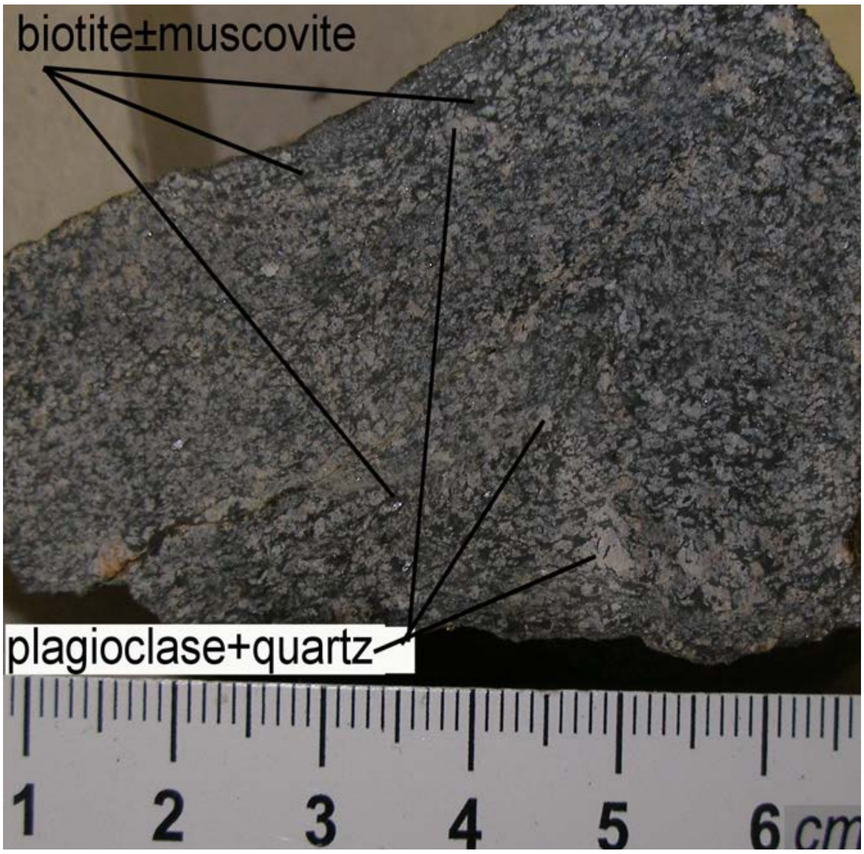

Figure 22. *Mafic mica gneiss. Zr-Ti ratios and the Jensen plot shows that this is not derived from the typical amphibolite at Qingaaq. Sample 439248.*

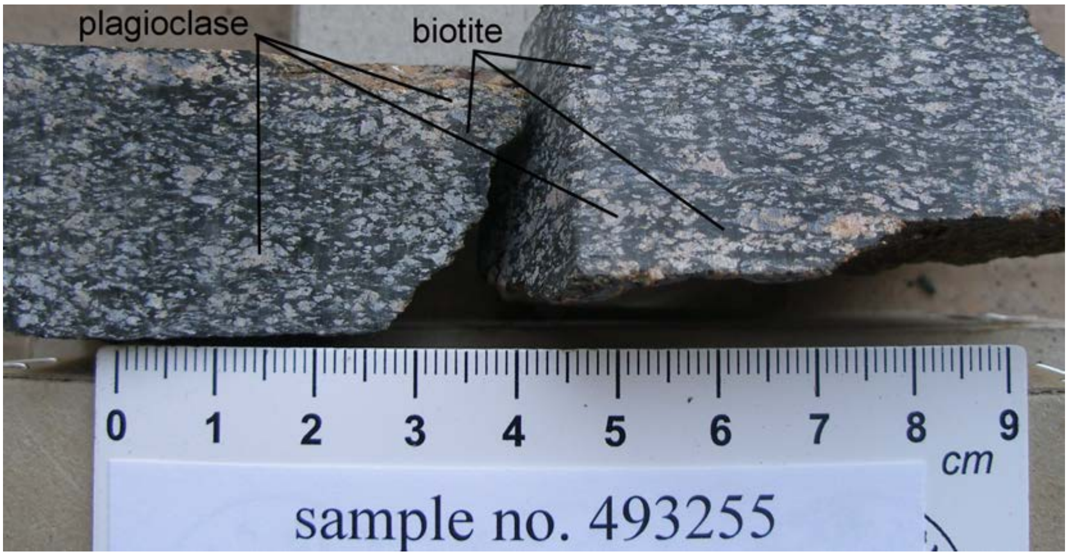

Figure 23. *Mafic mica gneiss. Zr-Ti ratios and the Jensen plot shows that this is not derived from the typical amphibolite at Qingaaq. Sample 439255.*

Figure 24. *Isoclinal fold of garnet-quartz gneiss in sillimanite-garnet mica gneiss. Site 1. Site 1. Qingaaq. 64°24'24.9''N, 051°05'36.4''W.*

Figure 25. *Boudinaged garnet-quartz gneiss, with some quartz veins, in sillimanite-garnet gneiss. Site 1. Qingaaq. 64°24'24.9''N, 051°05'36.4''W.*

Figure 26. *Sillimanite-garnet gneiss. NE slope of Qingaaq, 64°24'44.2"N, 051°04'58.1"W.*

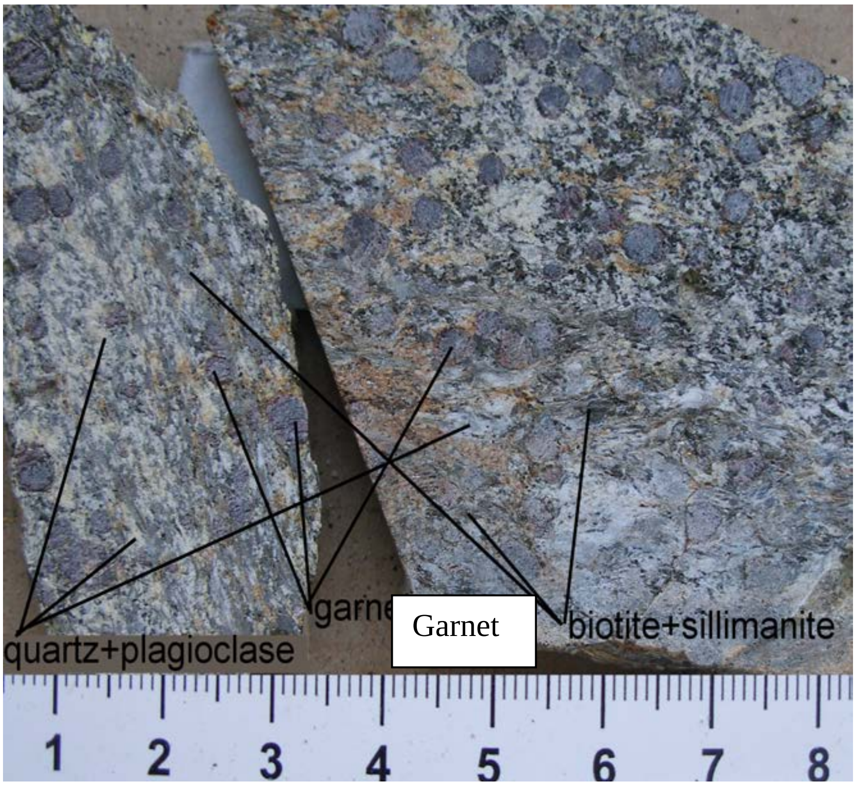

Figure 27. *Typical sillimanite-garnet gneiss. Note the large and abundant garnet porphyroblasts. Sample 493256, site 4, 64°24.474'N, 051°05.656'W.*

Figure 28. *Calc-silicate alteration, ie. deformed and metamorphosed spilitic-altered amphibolite, northern slope of Qingaaq. The dark bands are hornblende-rich and the light bands rich in diopside, plagioclase, and epidote. The white bands are early-kinematic pegmatite dykes. Location: 64°24.830'N, 051°05.155'W.*

Figure 29. *Calc-silicate alteration, ie. deformed and metamorphosed spilitic-altered amphibolite, northern slope of Qingaaq. Weakly deformed with indications of a primary breccia structure. Garnet porphyroblasts common in the diopside-plagioclase matrix. Location: 64°24.830'N, 051°05.155'W.*

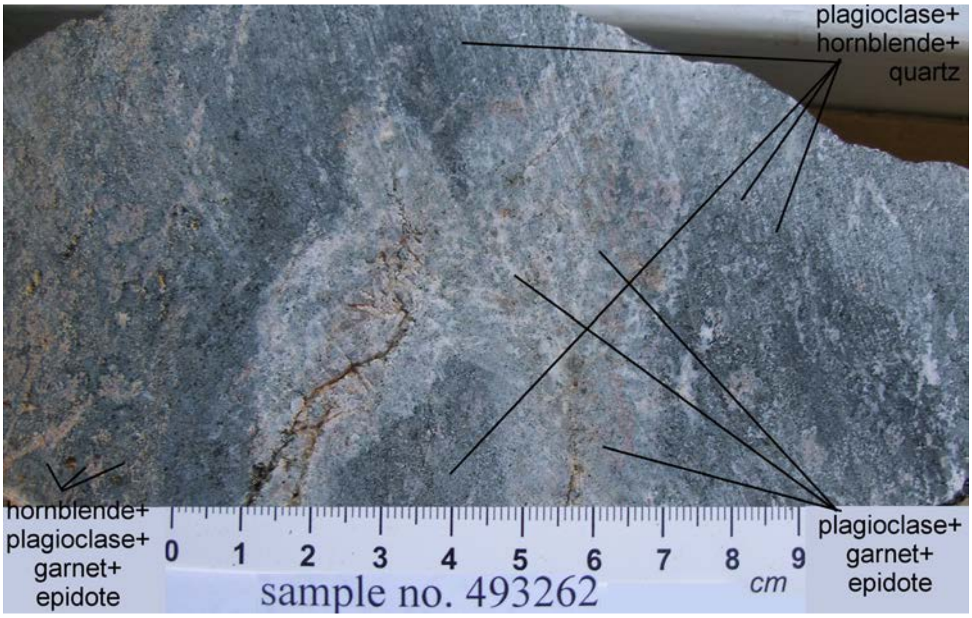

Figure 30. *Metamorphosed spilite. Hornblende-plagioclase- and diopside-epidote-dominated sub-domains. Sample 493262.*

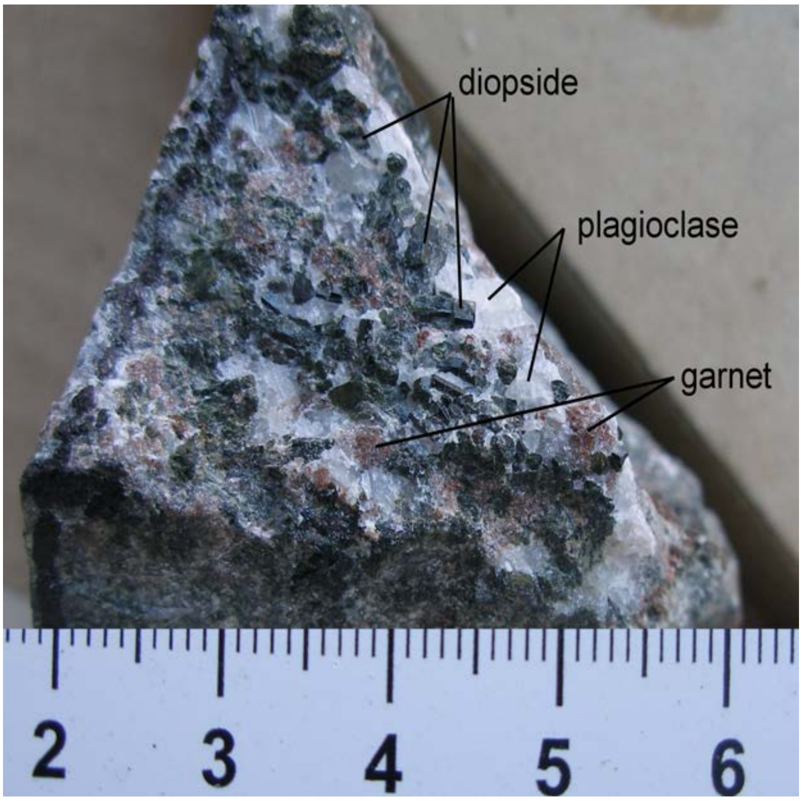

Figure 31. *Metamorphosed spilite. A coarse-grained diopside-plagioclase-garnet domain in a close view. This sample still contains some carbonate, too, possibly remains from the early spilitic calcite. Sample 493270.*

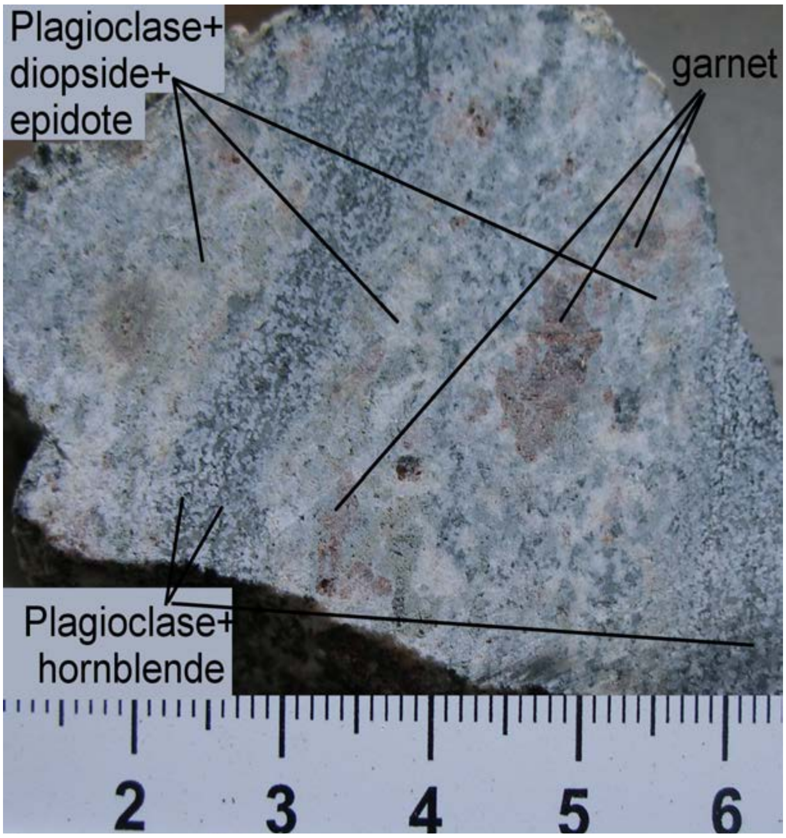

Figure 32. *Metamorphosed spilite. Hornblende-plagioclase and diopside-plagioclase-epidote-garnet subdomains. Sample 493271.*

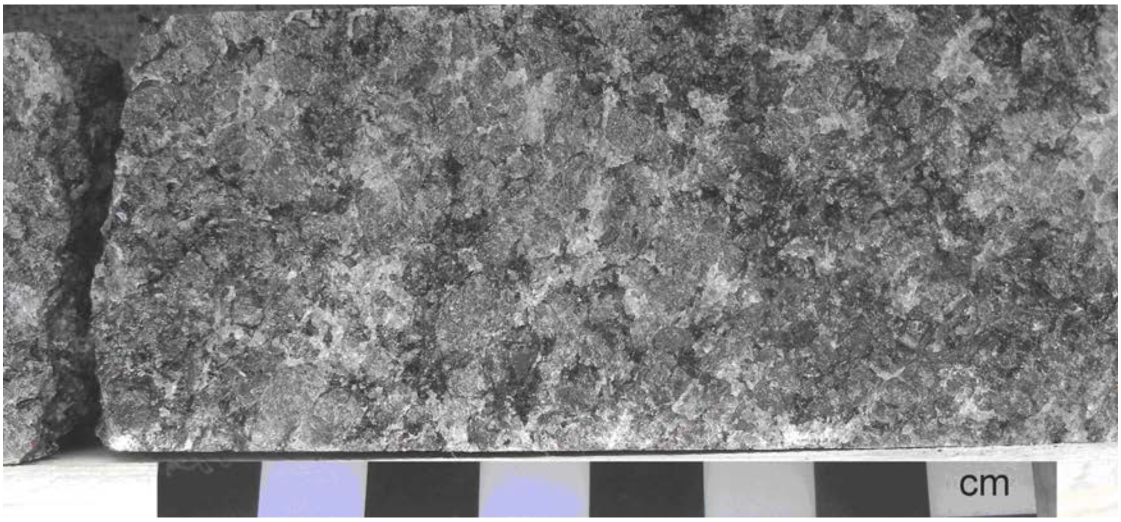

Figure 33. *Coarse biotite-garnet-altered amphibolite. DDH05-05, 141.70 m down-hole depth.*

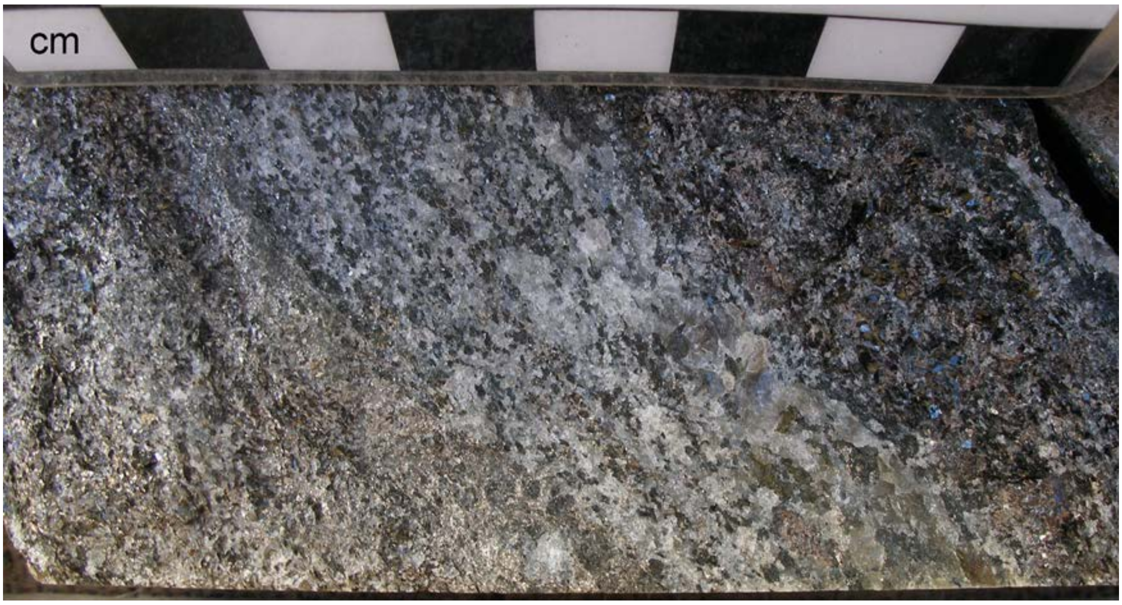

Figure 34. *Quartz, pyrrhotite, biotite-garnet alteration in amphibolite. DDH05-01, 14.50 m down-hole depth (sample 491104).*

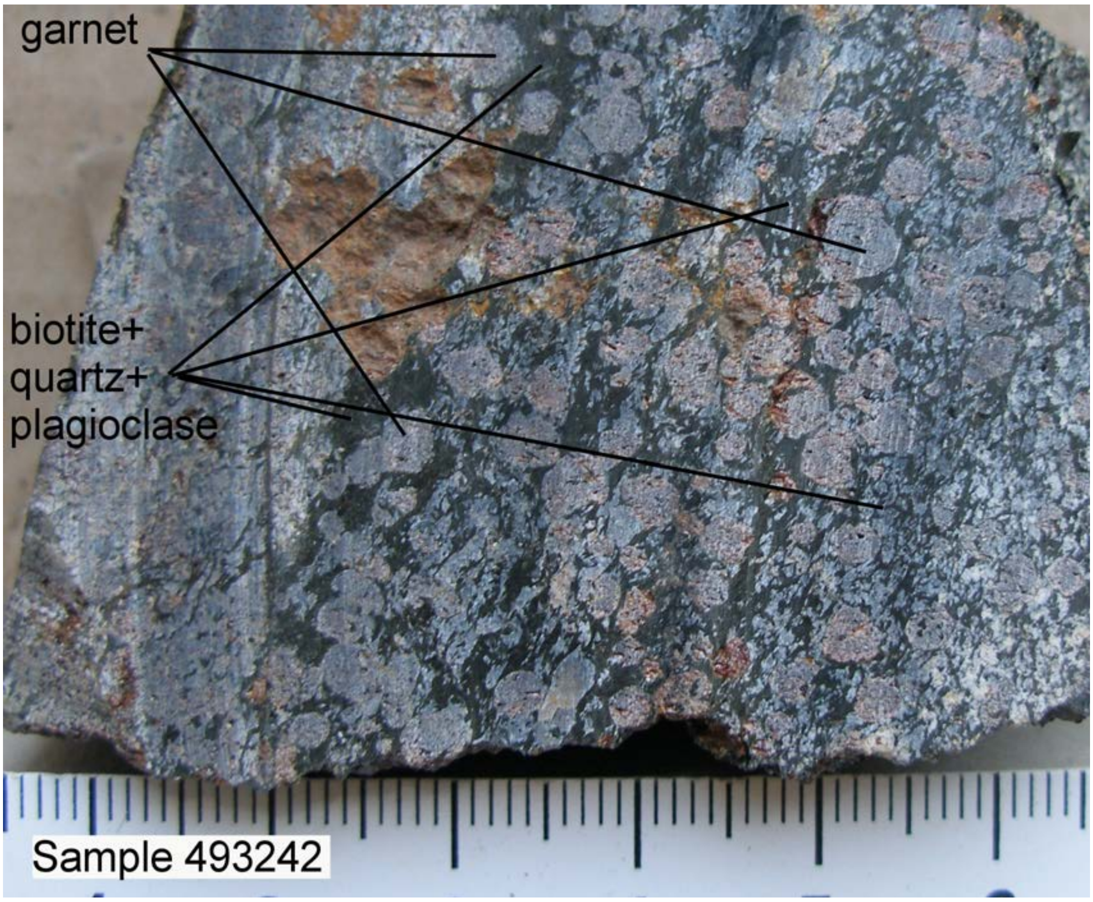

Figure 35. *Coarse biotite-garnet-altered amphibolite. Sample 439242, site 3, 64°24.458'N, 051°05.683'W.*

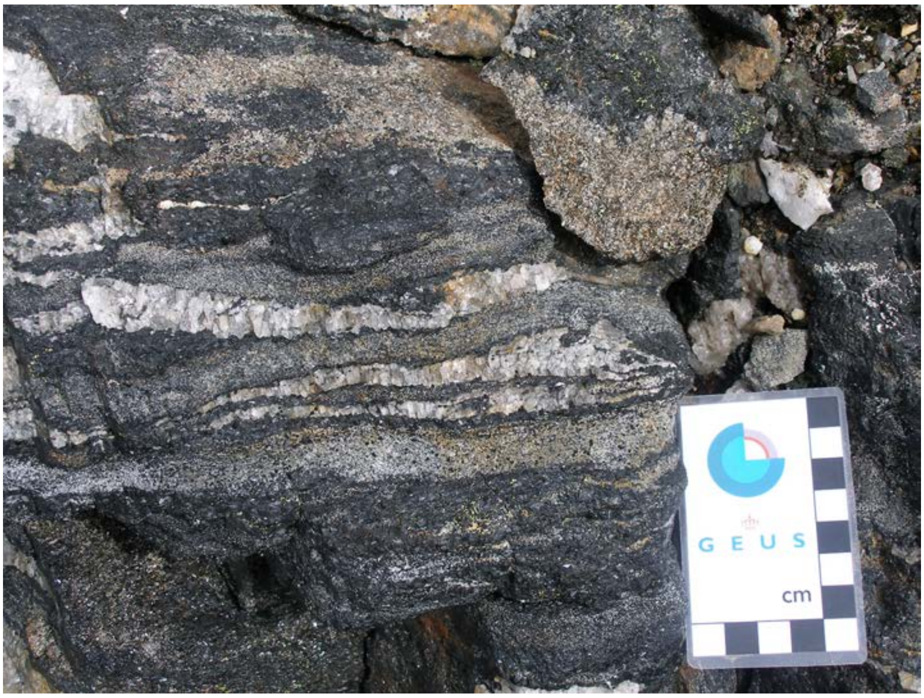

Figure 36. *Quartz veins with hornblende selvages, biotite ± garnet alteration around the veins, too. Amphibolite, site 4, Qingaaq. 64°24.479'N, 051°05.656'W.*

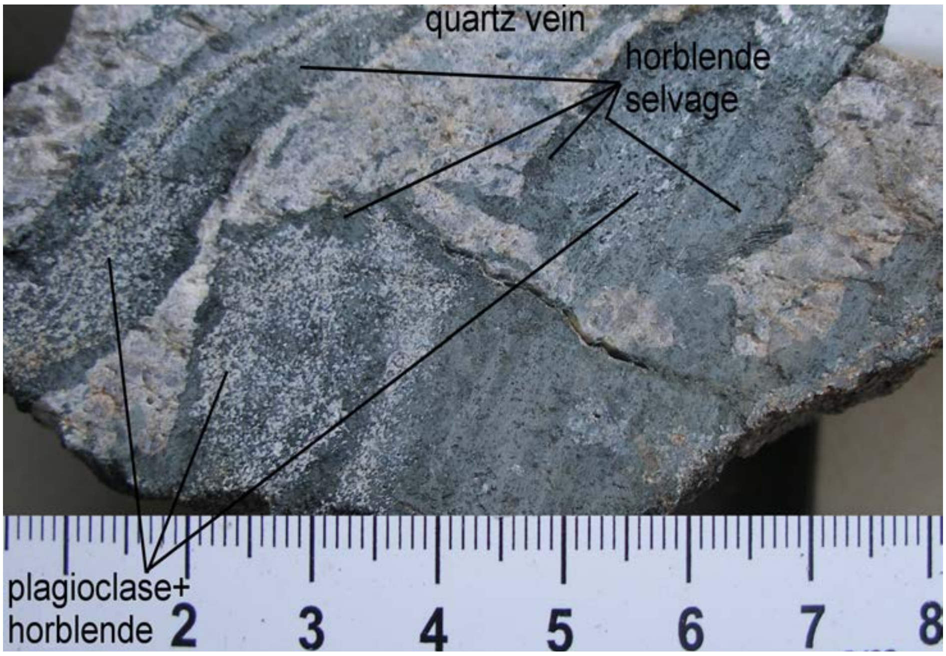

Figure 37. *Quartz veins with hornblende selvages, amphibolite. Sample 439259, site 4, 64°24.474'N, 051°05.656'W.*

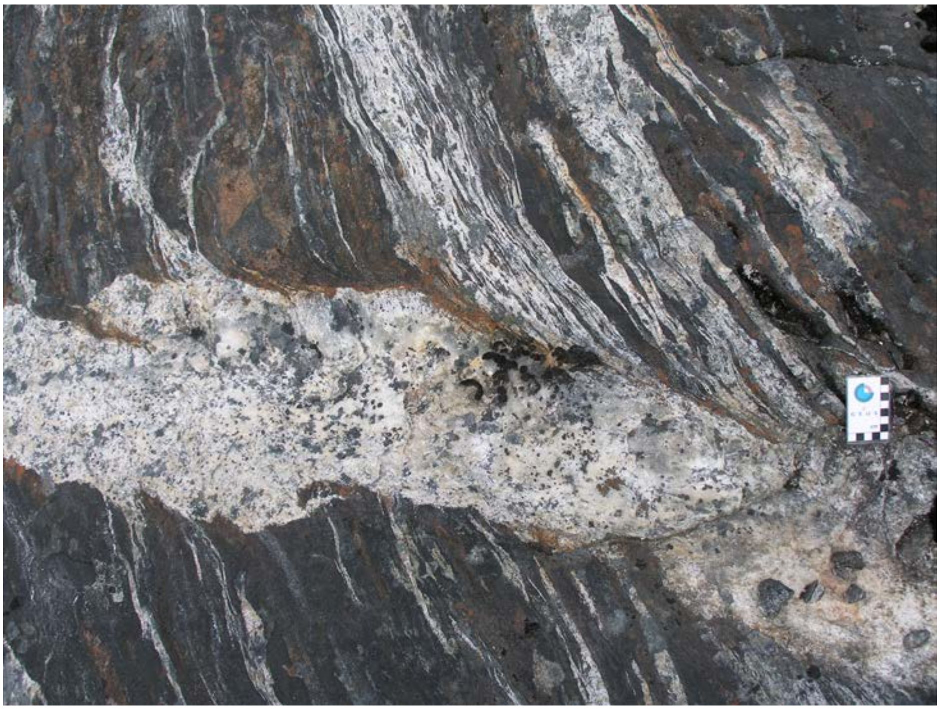

Figure 38. *Au-bearing(?), conformable quartz veins with hornblende selvages, biotite-garnet alteration beyond the selvages. These are cut across by a deformed pegmatite related to sinistral shearing. Storø Shear Zone, NNE of Qingaaq. 64°25.062'N, 051°05.019'W.*

Figure 39. *Arsenopyrite in auriferous (?) quartz vein with hornblende selvages; amphibolite. DDH05-05, 185.15 m down-hole depth.*

Figure 40. *Visible gold in quartz vein with hornblende selvages; amphibolite. DDH05-05, 50.50 m down-hole depth.*

Figure 41. *Central parts of site 5. The rusty, sulphidised zone is inside the biotite-garnet zone in amphibolite. Qingaaq. 64°24.528'E, 051°05.599'W.*

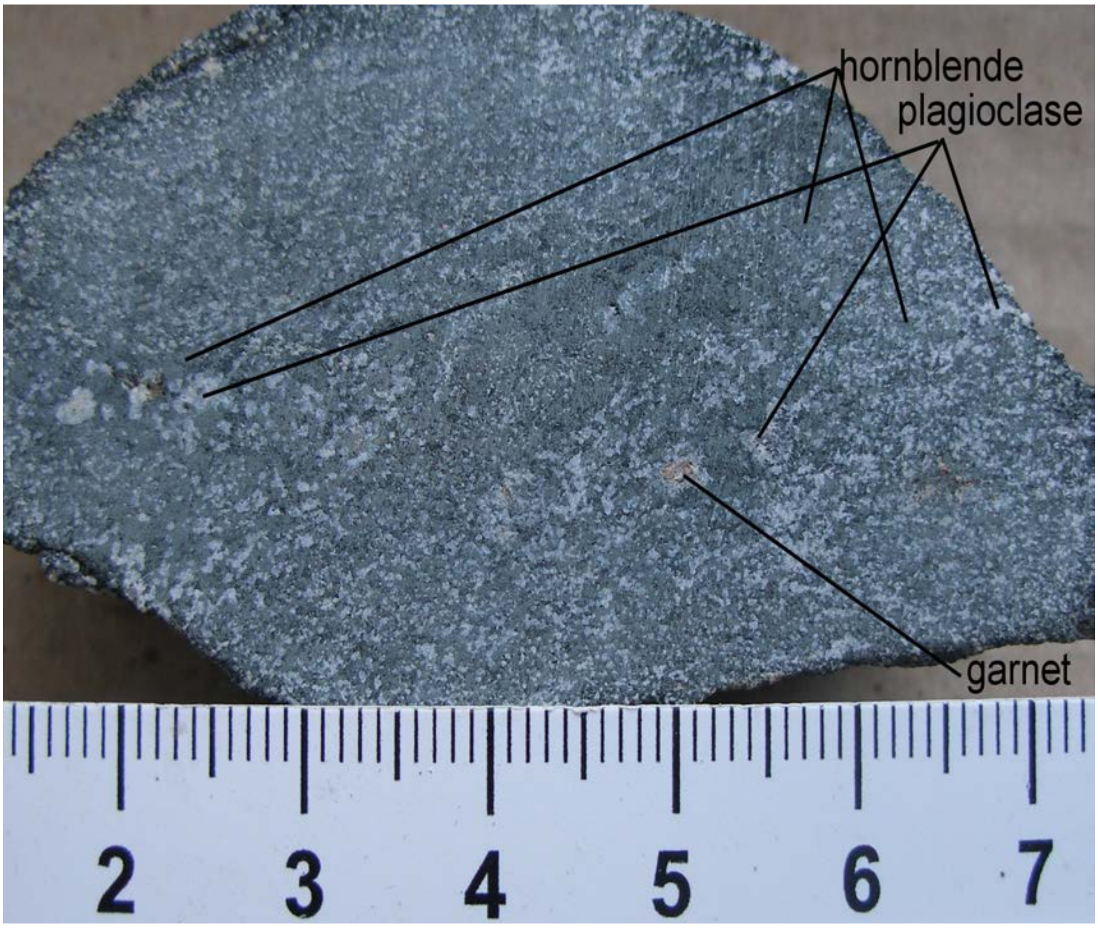

Figure 42. *Unaltered (least-altered) amphibolite. The single grain of garnet indicates that even this rock is not completely unaltered. Sample 439266, site 5.*

Mass-transfer in the Qingaaq alteration zones

Mass transfer related to alteration, and the relationship between these metasomatic changes and changes in mineral assemblages of the amphibolite at Qingaaq are described in this section.

The conceptual approach onto which a simple mass transfer examination is based on is summarised in Plot 7 which shows the concept of 'immobile trends'. This method is similar to those used elsewhere in modelling mass transfer (Gresens 1967, Grant 1986 and 2005, MacLean & Barrett 1993, Eilu & Mikucki 1998, Garofalo 2004b), and is easy to use for altered domains from all kinds of hydrothermal environments. A mass transfer evaluation starts from checking the primary variation in the composition of the rock type considered (e.g., MacLean & Kranidiotis 1987, MacLean & Barrett 1993). As discussed above, the amphibolite is a relatively homogeneous lithological unit in its primary composition (Figs. Plot 1, Plot 2a, Plot 3) and can, hence, potentially be handled by mass transfer evaluation methods. However, some bivariate plots based on the potentially least-mobile elements, for example the Ti-Al, Zr-Al, Ti-Cr, Zr-Cr ratios (exemplified by Plot 2b) clearly show that there also is primary compositional variation within the amphibolite of Qingaaq. Also, the variation in the relative contents of hornblende and plagioclase, the two dominant minerals of the least-altered amphibolite, suggest variation in the primary chemical composition. Such a variation in a tholeiite can easily be explained by fractionation of plagioclase, olivine and clinopyroxene. As the rocks under investigation are metamorphosed and multiply deformed, it may not necessarily be easy to petrographically detect the effects of fractionation.

The post-mineralisation, post-alteration regional metamorphism could also have caused variation in the rock composition. However, there are no signs of such a metamorphic effect being significant: no post-mineral, post-garnet-biotite alteration changes related to the later structures have been detected in the study area.

Consequently, we can consider most of the variation shown by the least-altered samples resulting from the primary variation which is significant for, for example, aluminium. Hence, the method presented in Plot 7 cannot straightforwardly be applied into all data form the amphibolite. Unfortunately, we cannot go into extensive evaluation of the primary compositional variation (*sensu* MacLean & Barrett 1993), because not enough data from the least-altered amphibolite is available to properly model the primary variation. On the other hand, we can select sample pairs with enough mutual compositional similarity to construct isocons for comparing individual alteration zones with each other and with the least-altered rock.

Isocon diagrams (Grant 1986) describing the trends in mass transfer during alteration in amphibolite, related to the formation of different alteration zones, are presented in Plots 8-11. In these figures, each alteration type is treated separately by plotting data from a less-altered sample against data from a sample representing the next more intensely altered rock. In most cases, a sample pair is used for an isocon plot. The samples for the pair are in each case selected so that they have as similar as possible ratios for the probable immobile elements. The regression lines (isocons) marked in these plots are fitted through the elements probably the least mobile in hydrothermal systems. When viewing the isocon plots, keep in mind that they present relative chemical trends; absolute values for mass balance calculations should not be derived from them, especially for elements with poorer analytical precision (e.g., base metals, some of the REE).

Trends of chemical change related to each alteration zone or type are summarised in Table 5. The isocon plots (Plots 8-11) indicate that:

1. Net mass changes have been minimal for the biotite-garnet alteration, as suggested by the slope of the isocons (Plots 8-11) being close to unity. The isocons do only suggest a minor net mass loss, which is also supported by the Ti-Zr plot (Plot 2a, cf. Plot 7). Only with spilitisation, a distinct net mass gain took place (Plot 8) – this trend is also supported by Plot 2a.
2. Elements immobile during all alteration were Cr, Ti, and Zr. Aluminium was only mobilised with the spilitic, not with the biotite-garnet alteration: in the latter system, Al is immobile even in the most intensely altered hornblende selvages. Also, vanadium was immobile in biotite- and biotite-garnet zones; only in the hornblende selvages it was enriched.
3. The REE, Co, Sc, and Y show immobility or weak enrichment to depletion in the gold system. In spilite, the REE and Y are immobile, and Co and Sc enriched; for the REE, this is also supported by Plot 3 Note however, that for Ce, Y and Yb, the analytical precision is not very good, and the information derived on their mobility hence not as reliable as for Eu, La, Lu, Sc, and Sm.
4. The relative mass transfer for silica generally was minor. Only in those areas where there are abundant quartz veins, has significant silica enrichment taken place and in the hornblende selvages, a significant depletion is obvious. Because in all samples, the Si concentrations are significantly higher than those for any other element, even a large absolute Si transfer can be difficult to statistically detect by the isocon.
5. Alkali and alkaline-earth elements and Mn were strongly mobilised during alteration. Barium, Cs, K, and Rb were consistently enriched and Na depleted where ever biotitisation took place, and all four are depleted with the hornblende selvage formation. The Mn was immobile with the incipient biotitisation but enriched with biotite-garnet and depleted with hornblende alteration. Strontium is depleted throughout the alteration sequence. Ca and Mg were mobilised, depleted, with biotite-garnet alteration, but enriched by the formation of the hornblende selvages.
6. Also iron was immobile with the incipient biotitisation (similar to Mn), but enriched in biotite-garnet zones and depleted in the hornblende selvages.
7. Gold and arsenic appear to follow each other in the biotite-garnet and hornblende zones, but not elsewhere. With sulphur, they show the strongest enrichment for any element; this takes place in the biotite-garnet zone. The Au-As relationship and the fact that Cu, and in the other zones also S, seem not to follow Au and As may be partially due to pre-gold mineralisation variations in Cu and S contents, possibly reflecting a weak spilitisation-related mineralisation at site. Part of the problems in any case arises from a poor precision on As values below 20 ppm, and poor precision for all the Au data. For the latter, it is unclear how precision (varies from ±7% to ±25 %) and concentration correlate. Hence, one cannot really be sure of the true correlation between these elements except in the biotite-garnet and hornblende zones. This is also the reason why As is not shown in the Plots 8 & 9. Despite the potentially

inaccurate data, gold is included into all isocon plots, as the concentration contrasts between the samples compared in the plots are much larger that the potential effects of the highest error in the data.

8. For Ni and Zn, there is some enrichment, except for the hornblende selvages where Zn appears as immobile. Note however, that the base-metal concentrations are low throughout the data. Hence, even a very weak mineralisation caused by spilitisation would affect these elements, even though no change was detected in other elements. Mass transfer evaluations do not give clear indications: Plot 8 shows sulphidation related to spilitisation, but the concentration levels are too low to be really certain of the trends. This means that we cannot be sure how much, if any, of the Cu, S and Zn enrichment in the biotite- and biotite-garnet zones is really related to the gold mineralisation. Another uncertainty comes from the poor precision of Pb data at levels below 20 ppm (>50 % uncertainty): hence the Pb is not even presented in the Plots 8–11.
9. The CO_2 concentrations are low to negligible throughout, and no real mass transfer evaluation can be done for it. All one can say is that, in absolute numbers, the CO_2 is neither significantly lost nor gained anywhere in the gold-related zones.

Table 5. *Calculated mass transfers in the studied profiles*

	Site 5						DDH 05-06						
	1	2	3	4	5	6	1	2	3	4	5	6	7
	493267	493262	493263	493264	493265	493266	44.1	45.0	52.0	54.0	79.0	84.0	90.0
g/100 g protolith													
SiO_2	-17.1	-14.9	0.5	-3.3	-6.1	0.0	-18.0	-9.7	-18.0	-15.0	-13.7	-11.1	0.0
Al_2O_3	-4.7	-4.4	-0.1	1.0	-1.9	0.0	-4.5	-5.4	-6.2	-3.8	-2.9	-2.9	0.0
Fe_2O_{3tot}	-3.2	-3.4	-0.3	0.5	-1.3	0.0	3.2	-2.0	-2.6	-1.1	-3.3	-2.4	0.0
MnO	-0.04	-0.03	0.00	0.00	-0.03	0.00	0.23	-0.16	-0.02	-0.03	-0.05	-0.05	0.00
MgO	-2.3	-2.6	0.9	1.1	-0.3	0.0	-4.7	-4.9	-5.6	-4.5	-2.0	-1.5	0.0
CaO	-7.1	-4.3	-1.3	-2.7	-1.8	0.0	-6.3	-8.2	-5.6	-5.1	-1.1	-2.7	0.0
Na_2O	-1.1	-1.1	0.0	0.2	-0.2	0.0	-2.4	-0.9	-1.4	-1.3	-0.9	-0.6	0.0
K_2O	0.5	0.2	0.2	0.7	0.0	0.0	1.3	1.6	0.3	0.6	0.1	0.1	0.0
TiO_2	-0.20	-0.23	0.00	-0.01	-0.03	0.00	-0.35	-1.13	-0.37	-0.34	-0.29	-0.14	0.00
P_2O_5	-0.03	-0.05	0.04	-0.01	0.03	0.00	-0.02	-0.15	-0.06	-0.04	0.01	0.07	0.00
g/1000 kg protolith													
Ba	91.2	96.0	37.0	67.9	-2.7	0.0	120.2	97.2	23.9	253.7	14.2	21.0	0.0
Sr	-84.7	-58.7	-46.0	-50.7	-40.6	0.0	-116.2	-117.6	-64.4	-77.0	-49.0	-89.5	0.0
Y	-8.0	-3.4	0.0	-1.7	-0.2	0.0	3.7	-14.6	-7.1	-7.1	-4.1	0.3	0.0
Sc	-5.5	-6.1	1.0	2.1	-1.4	0.0	-6.1	-23.8	-21.8	-17.7	-8.4	-4.7	0.0
Zr	0.0	0.0	0.0	0.0	0.0	0.0	0.0	0.0	0.0	0.0	0.0	0.0	0.0
V	-48.8	-48.4	12.0	25.5	-17.5	0.0	-53.1	-215.0	-129.4	-99.7	-65.5	-31.4	0.0
Au *	-0.7	-0.6	43.0	21.4	-0.2	0.0	1105.7	30.9	187.4	333.7	6.4	41.8	0.0
As	-1.2	-2.0	-3.4	-0.7	-0.3	0.0	197.4	7.5	1114.4	508.3	-0.4	-1.7	0.0
Cr	-76.2	-84.3	-27.0	0.4	-36.4	0.0	-120.5	-146.0	-227.2	-223.7	-81.3	-103.0	0.0
Co	-18.8	-20.2	-2.0	1.8	-6.3	0.0	-24.0	-38.9	-17.7	-23.8	-16.9	-21.6	0.0
Ce	-7.2	-1.3	-2.0	-2.3	-3.3	0.0	-4.2	5.1	2.4	5.6	-6.6	-6.9	0.0
Eu	-0.3	0.0	0.0	0.0	-0.1	0.0	-0.2	-0.5	0.0	-0.1	-0.3	0.2	0.0
Hf	-0.7	-0.6	0.0	-1.0	-0.2	0.0	-0.6	-0.6	-0.8	0.1	-0.5	-0.4	0.0
La	-2.9	0.4	0.6	-0.2	-2.2	0.0	0.5	6.3	4.4	4.9	-1.1	-0.6	0.0
Lu	-0.1	-0.1	0.0	-0.1	0.0	0.0	0.0	-0.3	-0.3	-0.3	-0.1	0.0	0.0
Nd	-3.5	-2.5	0.0	-1.2	-3.6	0.0	-5.5	-3.3	0.4	-4.8	-7.2	-7.0	0.0
Sm	-0.8	-0.3	-0.1	-0.1	-0.2	0.0	-0.2	-0.6	0.0	-0.1	-0.6	-0.3	0.0
Th	0.0	0.1	0.2	0.2	0.2	0.0	0.4	1.4	0.3	0.2	-0.4	0.2	0.0
Yb	-1.3	-0.6	-0.4	-0.5	-0.5	0.0	-0.3	-2.3	-1.9	-1.8	-1.0	-0.6	0.0
Cu	89.5	-7.0	-19.0	-2.6	-7.7	0.0	-28.2	84.7	-27.2	-96.0	-90.4	-93.4	0.0
Ni	-109.9	-89.1	-24.0	8.1	-35.4	0.0	-57.3	-52.7	-106.0	-97.6	-6.0	-65.9	0.0
Pb	0.8	0.5	1.0	4.8	1.2	0.0	2.9	13.6	1.2	2.3	1.6	2.0	0.0
Zn	-17.6	-9.6	0.0	-11.5	-18.7	0.0	19.0	43.8	9.0	16.4	-9.8	-10.2	0.0
CO_2	-12.0	-6.6	0.0	51.3	-9.9	0.0	-6.8	-24.6	-32.6	-6.2	-19.6	-16.7	0.0
S	604.0	106.9	0.0	-2.4	75.8	0.0	7559.2	18966	1112.4	261.1	-1188.1	-1293.7	0.0
Zr^{6-7}/Zr^n	0.64	0.69	1.00	0.98	0.88	1.00	0.69	0.70	0.60	0.69	0.76	0.80	1.0
Dist. (m)	3.0	2.6	2.0	1.6	0.8	0.0	46	45	38	36	11	6	0.0

Note: The mass transfer Δx of a chemical component in sample n of Site 5 is calculated using the following formula:

$\Delta x = (Zr^6/Zr^n)\, X^n - X^6$. The mass transfer Δx in DDH 05-06 is calculated using the following formula:
$\Delta x = (Zr^7/Zr^n)\, X^n - X^7$
*: referred to g/10^6 kg of protolith. The negative values occur where Au concentration is < LOD

Table 6. *Biotite-garnet geothermometry*

sample	pair	Temperatures* (°C)			
		F&S (1978)	P&L (1983)	B-HW (1992)	B-GS (1992)
472867 area 1	bt-gn	633	612	636	640
472867 area 2	bt-gn	698	645	674	678
472873	bt-gn	517	548	527	499
472895	bt-gn centre	607	599	623	602
472895	bt-gn rim	655	624	644	624
472898 area 2	bt-gn	658	625	637	626
472898 area 3	bt-gn rim	502	540	539	519
472899	light bt-gn	652	622	628	618
472899	dark bt-gn	657	622	628	618

* Temperatures calculated using geothermometer calibration of Ferry & Spear (1978), Perchuk & Lavrent'eva (1983), and Battacharya et al. (1992), with Hackler & Wood (1989) or Ganguly & Saxena (1984) data.

Fluid inclusion investigation and garnet-biotite geothermometry

Samples from garnet-biotite-quartz assemblageses have been investigated for their fluid inclusion characteristics. Workable fluid inclusions could only be found in the quartz and, in general, this mineral has little fluid inclusions and is fairly pure. Nevertheless, several different typologic types of fluid inclusions were found, isolated in the crystals, as clustered assemblages, or as trails trough the quartz crystals. The relative timing of these assemblages could be made based on crosscutting relations. The oldest fluid inclusions in quartz segregations intergrown with cm-sized garnets have small (1-10µm), gaseous inclusions, either isolated or in clusters in the crystals that contain pure CO_2. Their melting point (Tm_{CO2}) is identical to the triple point of CO_2 at -56.6°C (Roedder, 1984). They show homogenisation (Th_{CO2}) around -20±9°C (n = 51), indicating molar volumes between 41.07 to 44.54 cm^3/mol. Younger intragranular trails of inclusions also contain CO_2, but their molar volumes are much higher, between 44.54 and 293.88 cm^3/mol.

Still younger trails of inclusions contain an immiscible assemblage of either highly saline brines or pure H_2O (Tmice~0.0°C), and low-density CH_4 (homogenisation to the vapour phase). The brine inclusions are biphase, having a vapour bubble of 5-10 vol% and could not be frozen on cooling to -180°C. This indicates a high concentration of dissolved salts, but precludes exact determination of the salinity. Preliminary Laser Ablation ICP-MS analyses of these inclusions indicate that they are $CaCl_2$-NaCl rich brines. Their homogenisation temperature is around 107±9°C. Associated CH_4 inclusions homogenize to the vapour around -145°C (Vm ~ 2980 cm^3/mol). Finally, monophase aqueous or mixed aquous-CH_4 assemblages are the youngest fluid inclusions trapped. They must have formed at low temperature and pressure (<80°C and <10 bar).

Co-existing garnet and biotite were analyzed quantitatively by microprobe in a variety of samples (Table 1 and 3). The analyses were carried out at Geological Institute in Copenhagen on a Geol Superprobe 8200 with 15 Kev and 15nA using natural and synthetic standards. The analyzed garnets show a variation in composition between more almandine-rich (Xalm = 0.90; Xgr = 0.05; Xpyr = 0.03; Xsp = 0.01) and more grossular-rich (Xalm= 0.65; Xgr = 0.23; Xpyr = 0.08; Xsp = 0.03). The composition of coexisting biotite also shows a variation in its Fe content with Fe/Fe+Mg ranging between 0.585 to 0.791. Moreover, the more Fe-rich biotite is associated with the most Fe-rich garnet. Garnet-biotite geothermometry, using the calibration by Ferry & Spear (1978), Perchuk & Lavrent'eva (1983) and Bhattacharya et al. (1992), indicates temperatures ~ 630°C for all analyzed garnet-biotite pairs, except for the more Fe-rich garnet-biotite pair of sample 472873 and for the more Fe-rich garnet rim - Fe-rich biotite pair of sample 472898 (Plot 12). For the latter two, a lower temperature of ~530°C is indicated. This could indicate that there were two episodes of garnet formation.

Discussion and conclusions

Rock types present in outcrop and drill core investigated and reported here include: Fe-tholeiitic amphibolite, sillimanite-garnet gneiss, and a narrow sequence comprising garnet-magnetite rock, mafic and felsic mica gneisses, and biotite-garnet-quartz gneiss.

The amphibolites are Fe-tholeiitic in composition, probably lavas. Neither petrographic nor geochemical data have been found to indicate that any of the other rock types were derived from amphibolite. Nor have we, so far, been able to prove any other primary precursor for the gneisses. The combination of the magnetite-rich bands with the garnet-mica rock does not resemble a typical BIF sequence. It has not even a faint resemblance to a distinct banded appearance with repeated magnetite/hematite and quartz layers. The sillimanite gneisses do resemble rocks undergone advanced argillic alteration in epithermal settings then metamorphosed under amphibolite facies conditions. There are Precambrian sillimanite-rich rocks in possibly similar settings at, for example, Hemlo in Canada (Powell et al. 1999) and Enåsen in Sweden (Hallberg 1994). The Ti-Zr plot (Plot 2c) does not support the derivation of the garnet-magnetite rocks or the other gneisses directly, by any simple alteration, from the amphibolites. Note however, that we have not tested any mass balance evaluation methods for comparing the amphibolites and the gneisses. The REE plot (Plot 6) would also allow the sillimanite-garnet gneisses to be derived from the amphibolites if the LREE were enriched, but the REE plot does not support such a derivation for the mica gneisses or garnet-magnetite rocks.

The 'calc-silicate' altered domains in amphibolite clearly appear as a result of synvolcanic, pre-metamorphic, submarine spilitic alteration in the volcanic sequence (cf. Reed 1983, Barley et al. 1990). Their present mineral assemblages, characterised by abundant diopside and epidote, can very well be products of regional-metamorphic recrystallisation of the original chlorite-, epidote-, and albite-rich assemblages. The data in the Plots 1, 2b and 3 support the idea that these rocks are derived from the surrounding amphibolite.

During spilitisation (Plot 8, Table 5), REE, Ti, Zr, and Cr were immobile, Fe, Mg and P depleted, and Al, Ba, Ca, Cu, Mn, Na, Ni, S, Sc, Si, Sr, and V enriched. These chemical changes are similar to those detected for spilitisation in rocks in greenschist facies environments and in the present submarine hydrothermal systems (Reed 1983, Lesher et al. 1986, Seewald & Seyfried 1990, Elliot-Meadows & Appleyard 1991). These chemical changes are quite different, as expected, from those described below for the biotite-garnet alteration, and must be taken into account also in the mass transfer evaluations in the latter systems where these two styles of alteration overprint each other, as is the case for the sample 493262 (App. 2). The Fe depletion also suggests a potential source for the abundant iron in the garnet-magnetite rocks, if the latter are chemical precipitates.

Biotite-garnet alteration in amphibolite seems to be related to gold mineralisation. This alteration forms domains from 0.5 m to >60 m wide obviously enclosing all of the laminated, potentially auriferous quartz veins. No alteration related to gold has been detected in other rock types at Qingaaq or Aappalaartoq, even though ore-grade gold is detected in the other rock types, too (Skyseth 1998, Appel et al. 2003, Coller & Coller 2005), the genetic category of gold mineralisation still is somewhat unclear, and the enrichment of gold could even be, partially, related to pre-metamorphic processes at Storø.

Biotite-garnet alteration has several features typical for orogenic gold mineralisation formed under amphibolite-facies conditions (Witt 1993, McCuaig & Kerrich 1998, Witt & VanderHor 1998, Eilu et al. 1999, Ridley et al. 2000, Eilu & Groves 2001): 1) laterally, alteration is restricted to the local shear zones which is typical for orogenic gold deposits formed under ductile deformation; 2) the degree of alteration does not gradually increase towards the main garnet-biotite zone and potentially auriferous quartz veins within a profile across an altered shear zone, but shows oscillation; 3) the brownish alteration haloes are narrow and comprise the distal biotite and the proximal biotite-garnet zones and, as the most proximal expression, 1–5 cm wide hornblende selvages next to the quartz veins; 4) biotite-garnet alteration at Storø took place within shear zones, during deformation.

Regarding petrography and mineral assemblages, the relationship between hornblende and cummingtonite remains unclear. The latter has been detected in both the least-altered and more intensely altered amphibolite, both next to narrow quartz veins and pervasively in the rock. Either the presence of cummingtonite reflects weak alteration or it just is a partial regional-metamorphic replacement of hornblende. The cummingtonite may even reflect both, also being a peak-regional metamorphic replacement of an amphibole formed during alteration which had a composition slightly different from that of the hornblende.

In the biotite zone, biotite and quartz partially replace hornblende and, apparently, ilmenite and quartz replace the titanite. Biotitisation explains the enrichment of Ba, Cs, K, Ni, and Rb and the depletion of Ca, Co, and Sr (Plot 9, Table 5). Destruction of titanite would explain at least some of the depletion of Ca, Ce, La, Lu, Nd, Sm, Sr, and Yb, but possibly also other reactions related to accessory minerals are needed for. In addition, data on Au, Cu, S and Zn suggests that minor sulphide mobility extends to the biotite zone, too.

The biotite-garnet zone is characterised by the replacement of hornblende-plagioclase-titanite assemblage by biotite-garnet-quartz-ilmenite with minor pyrrhotite and traces of chalcopyrite, sphalerite, arsenopyrite and gold. This replacement explains nearly all chemical changes shown in Plot 10. The depletion of phosphorus also suggests (partial?) destruction of apatite which would easily explain at least part of the REE mobility in the zone.

Nearly all elements were mobilised with the formation of the hornblende selvages (Plot 11, Table 5). This is explained by the fact that these zones also show the most intense mineralogical changes in the amphibolite of Qingaaq. The product of alteration is a nearly monomineralic rock; hence, most of the elements are depleted compared to the less intensely altered rocks. Only those elements which are the least mobile in any environment remained immobile (Al, Cr, Ti, Zr), and those are enriched which were easily accommodated into the amphibole (Ca, Mg, Ni, Sc, V) and the minor titanite (e.g., Ca, La, Lu, Sc, V, Y, Yb).

The mineral assemblage of the biotite-garnet zone is made by more phases than the least-altered amphibolite itself, which indicates a low thermodynamic variance within the altered domains. The present mineral assemblage is a probable consequence of formation in a closed chemical system characterised by a relatively low volume of fluid, which is typical of metamorphic environments. In contrast, high-variance assemblages (i.e., those characterised by fewer minerals than the country rock) form in open chemical systems where the interaction is fluid-dominated. Such assemblages are found in both greenschist- and amphibolite-facies orogenic gold deposits which have not been metamorphosed after mineralisation (McCuaig & Kerrich 1998, Ridley et al. 2000). Structural relations in the field indicate that gold mineralisation and garnet-biotite alteration was associated with ductile shear of the D1-deformation event predating deformation associated with the development of the Storø Shear Zone (Coller & Coller, 2005). The latter event produces a fabric which reworks the earlier garnet porphyroblasts. Garnet-biotite geothermometry indicates metamorphic temperatures between 530 and 630°C. Using the molar volume of the isolated and clustered CO_2 inclusions found in coexisting quartz (possibly primary inclusions), this would further indicate pressures between 4 and 6 kbars (Plot 13). Later fluid inclusions indicate also CO_2-rich fluids at lower temperatures and pressures and finally the circulation of highly saline brines and pure water in association with low-density methane fluids through the supracrustal sequence. However, the latter were present at late retrograde conditions at relatively low temperature and pressure ($T < 120°C$ and $P < 10$ bar).

Open questions at this stage, recommendations for further work

1. The exact relationship between major stages of deformation and biotite-garnet alteration: this still has to be shown by structural analysis at Qingaaq and/or Aappalaartoq. Together with spatial interpretation of the drillcore data this would also improve knowledge of the overall structure and dimension of the mineralised zones.
2. The sequence containing the garnet-magnetite rocks should be investigated by comparing it to BIF-bearing sequences metamorphosed to amphibolite facies elsewhere. They should also be compared to Fe-rich precipitates from the modern sea floor and from ophiolitic settings in low-metamorphic grade areas, especially because such precipitates can be Au-rich, too.
3. For more robust mass balance evaluations, more data (= more samples) from the unaltered (or least-altered) amphibolite should be employed, either more samples analysed or data also taken from previous works. This is needed to get a more comprehensive model of the primary compositional variation of the amphibolite, if such a mass transfer evaluation is seen useful.
4. Mass balance evaluation should be tested for comparison between the amphibolites and the various gneisses of Qingaaq.
5. All gneisses should also be compared to altered rocks from various hydrothermal settings elsewhere, e.g. with epithermal and VMS settings. Could from there emerge any relationship to gold enrichment at Storø? Did pre-gold mineralisation processes prepare ground for mineralisation at Storø, and if so what were these processes?
6. Radiometric age dating is recommended for all the rock, alteration, vein and dyke types at Qingaaq. Not just zircon, but also monazite and xenotime could occur in suitable positions. Hornblende and biotite could also give useful dates by the Ar-Ar method.
7. Further fluid inclusions studies should be directed towards identifying the gold-mineralizing fluid and should involve characterisation of the fluid associated with the different metamorphic and magmatic events in the area (e.g. pegmatites, Qôrqut granite).

8. Also ultramafic rocks should be checked for gold mineralisation. Alteration-wise, signs of orogenic gold mineralisation in ultramafic rocks at high metamorphic-grade rocks typical are phlogopite, diopside and garnet (± talc, calcite, tremolite, olivine) with thin quartz and quartz-diopside veins.

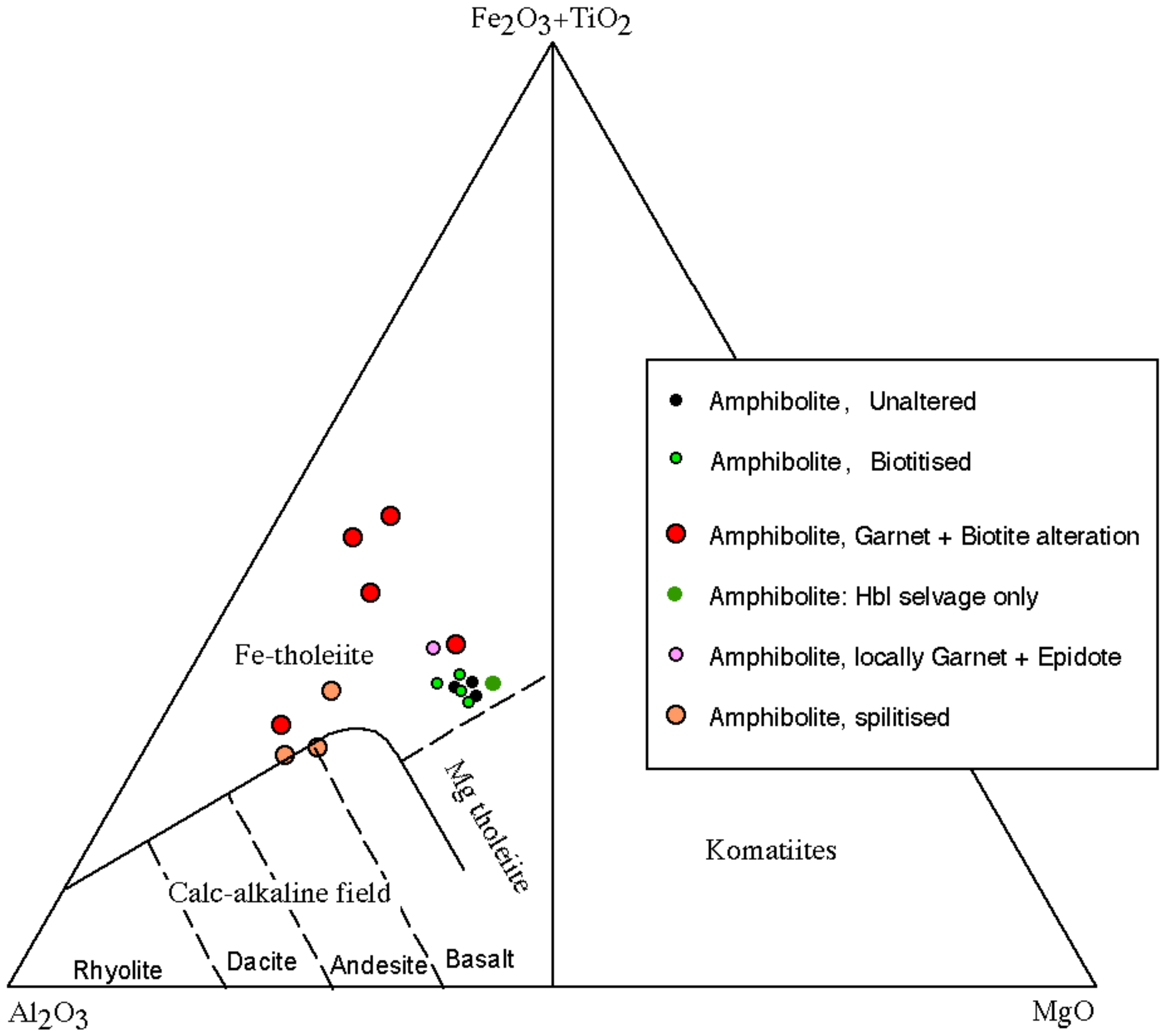

Plot 1. Jensen cat ion plot (Jensen 1976) for all amphibolite samples analysed from Qingaaq. Note that biotitisation has a minor (if any) effect on the elements relevant for the plot, whereas biotite-garnet alteration and spilitisation clearly affect on the sitting of the samples in the plot. 'Unaltered' refers to the least-altered amphibolite detected at Qingaaq.

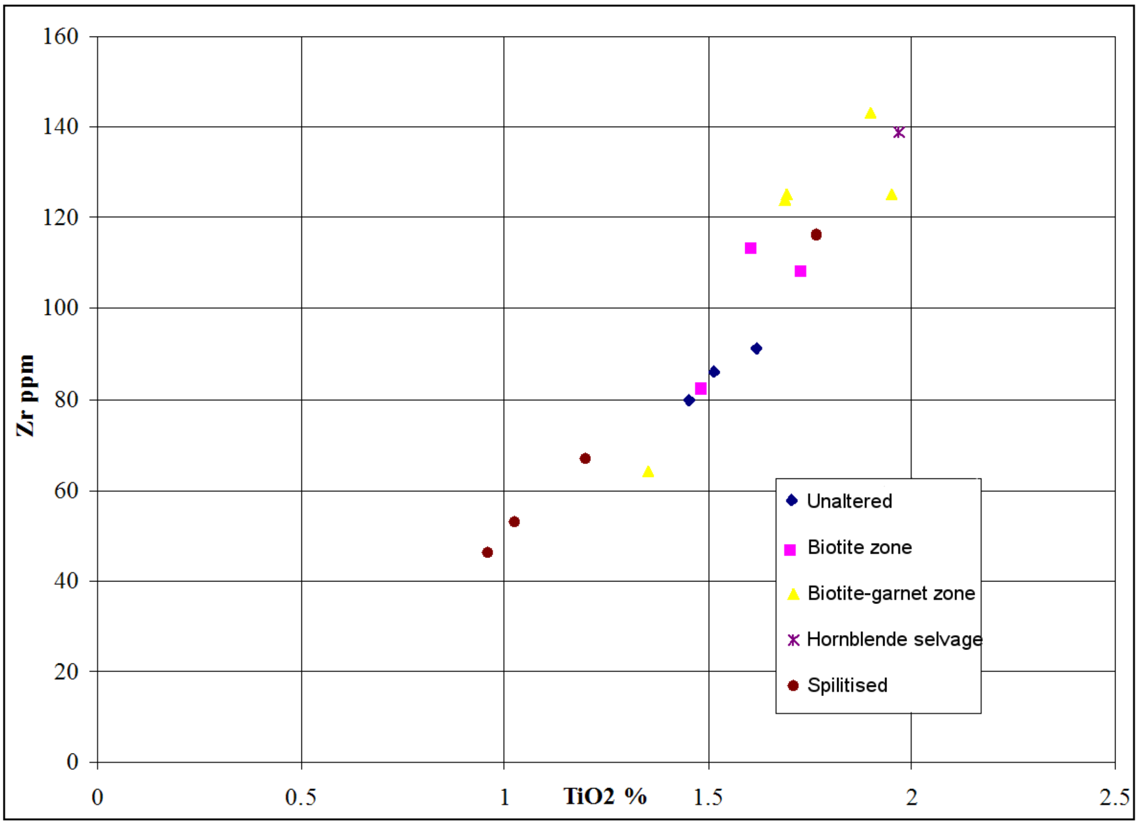

Plot 2a. TiO_2 vs. Zr plot for all analysed amphibolites indicating just one precursor for all amphibolite types mapped at Qingaaq: all samples plot along a diagonal trend that crosses at or near the origin of the plot. 'Unaltered' refers to the least-altered amphibolite detected at Qingaaq.

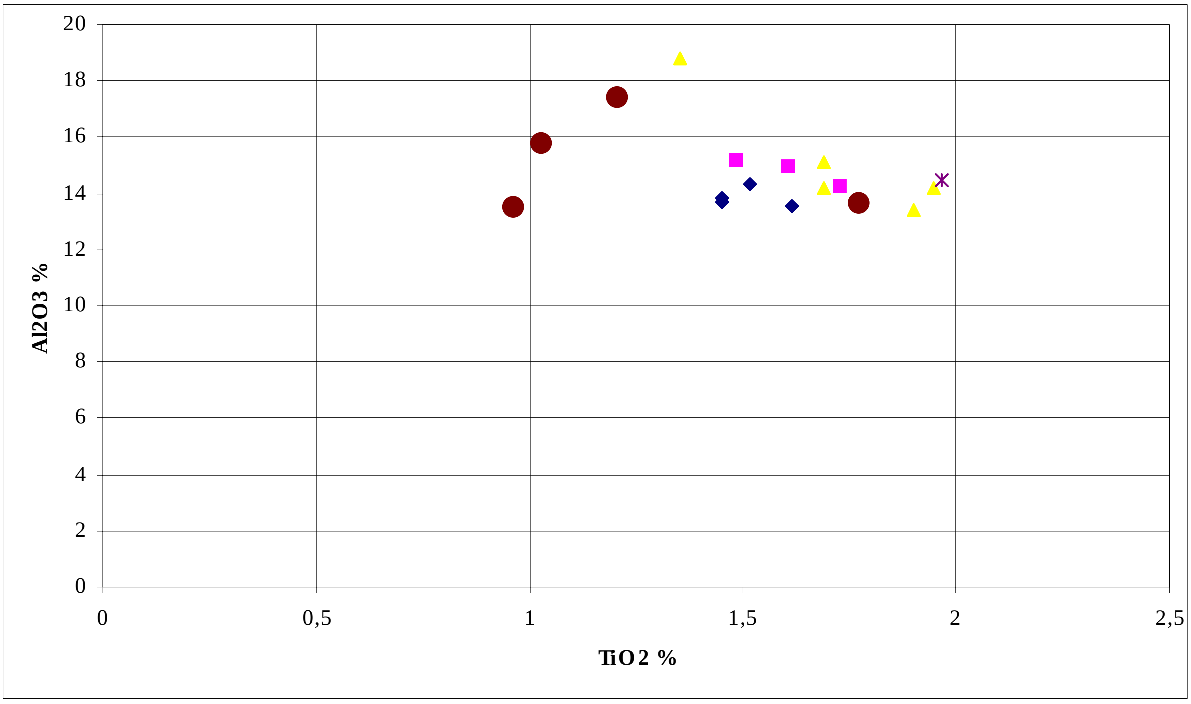

Plot 2b. TiO_2 vs. Al_2O_3 plot for all analysed amphibolites suggesting primary variation in the chemical composition of the lithological unit at Qingaaq: the least-altered samples define a trend that does not go anywhere close to the origin of the plot. For legend, see Plot 2a.

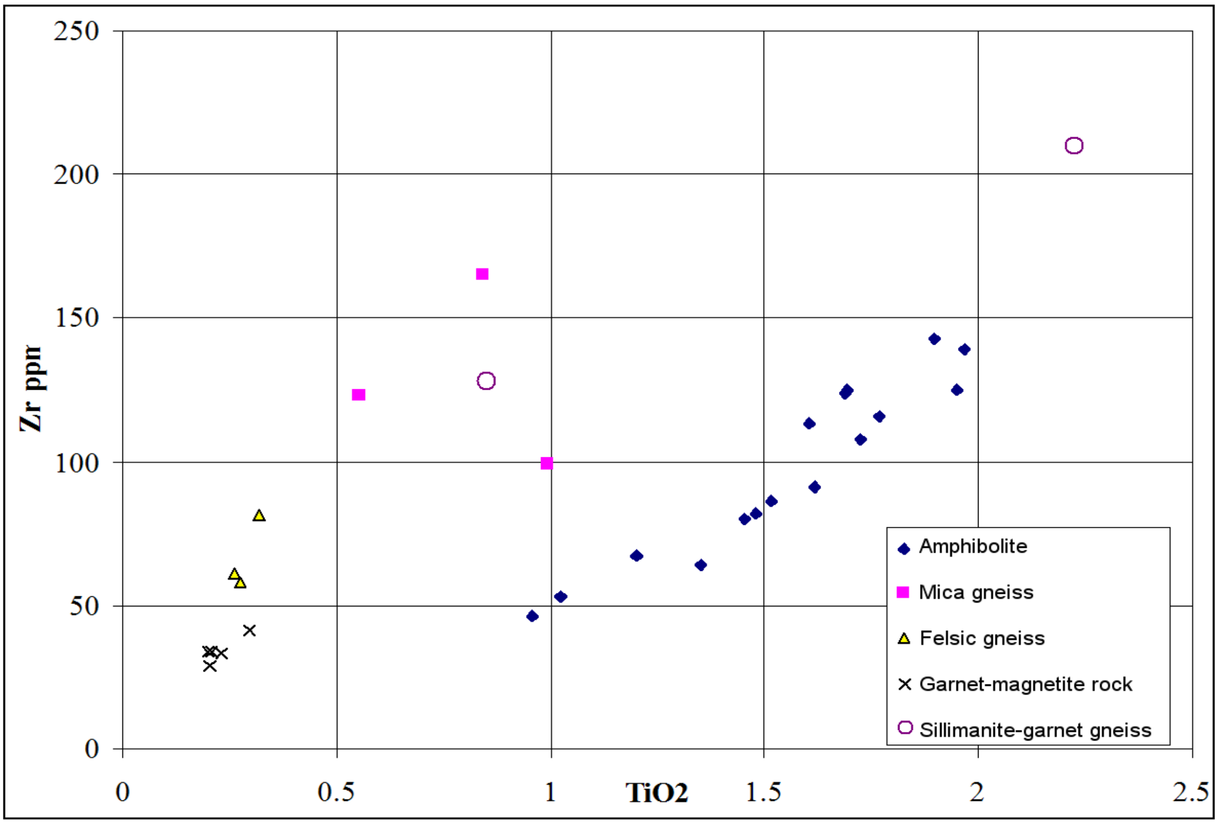

Plot 2c. TiO_2 vs. Zr plot for all samples analysed from Qingaaq.

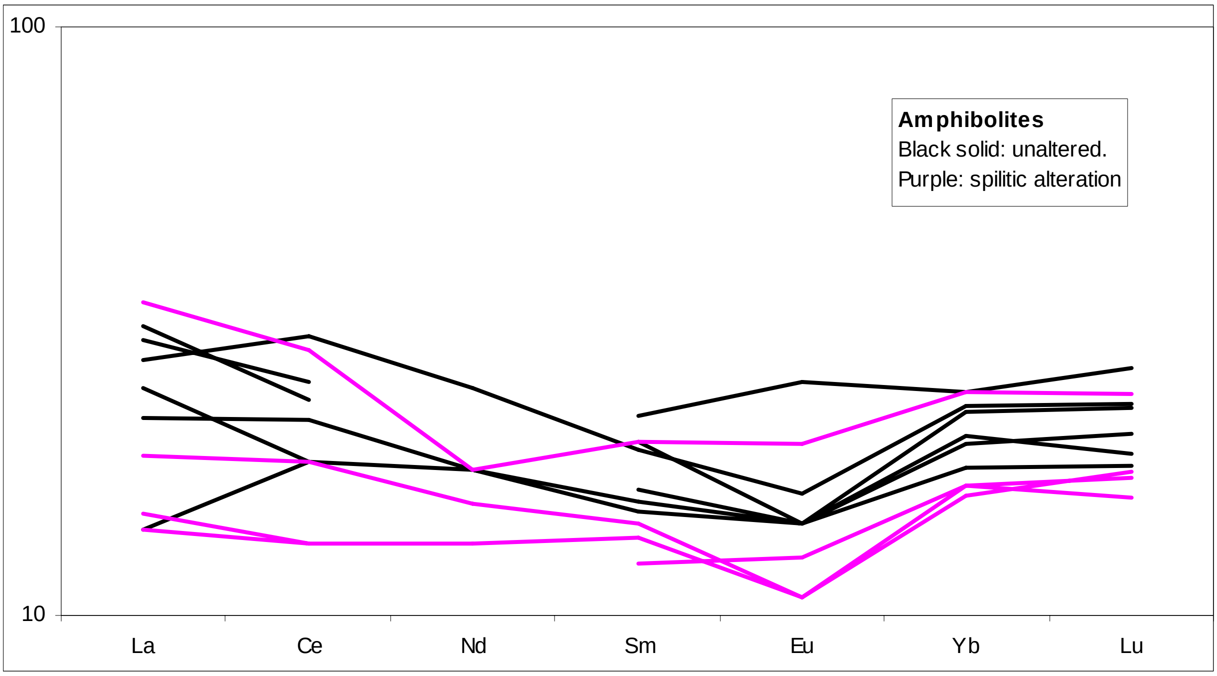

Plot 3. Chondrite-normalised REE plot for both the least-altered and the spilitised amphibolites from Qingaaq. Normalisation values from Kerrich and Wyman (1996).

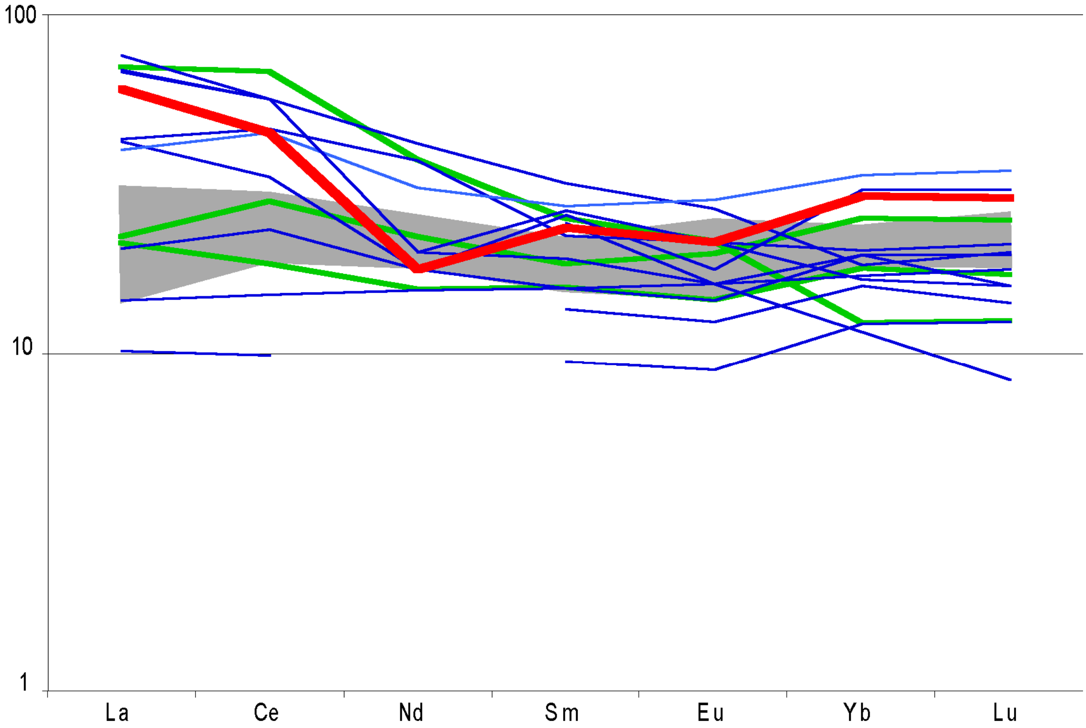

Plot 4. Chondrite-normalised REE plot for amphibolites from Qingaaq. Grey area = least altered; green = biotite zone; blue = biotite-garnet zone; red = hornblende selvage of a quartz vein. Normalisation values from Kerrich and Wyman (1996).

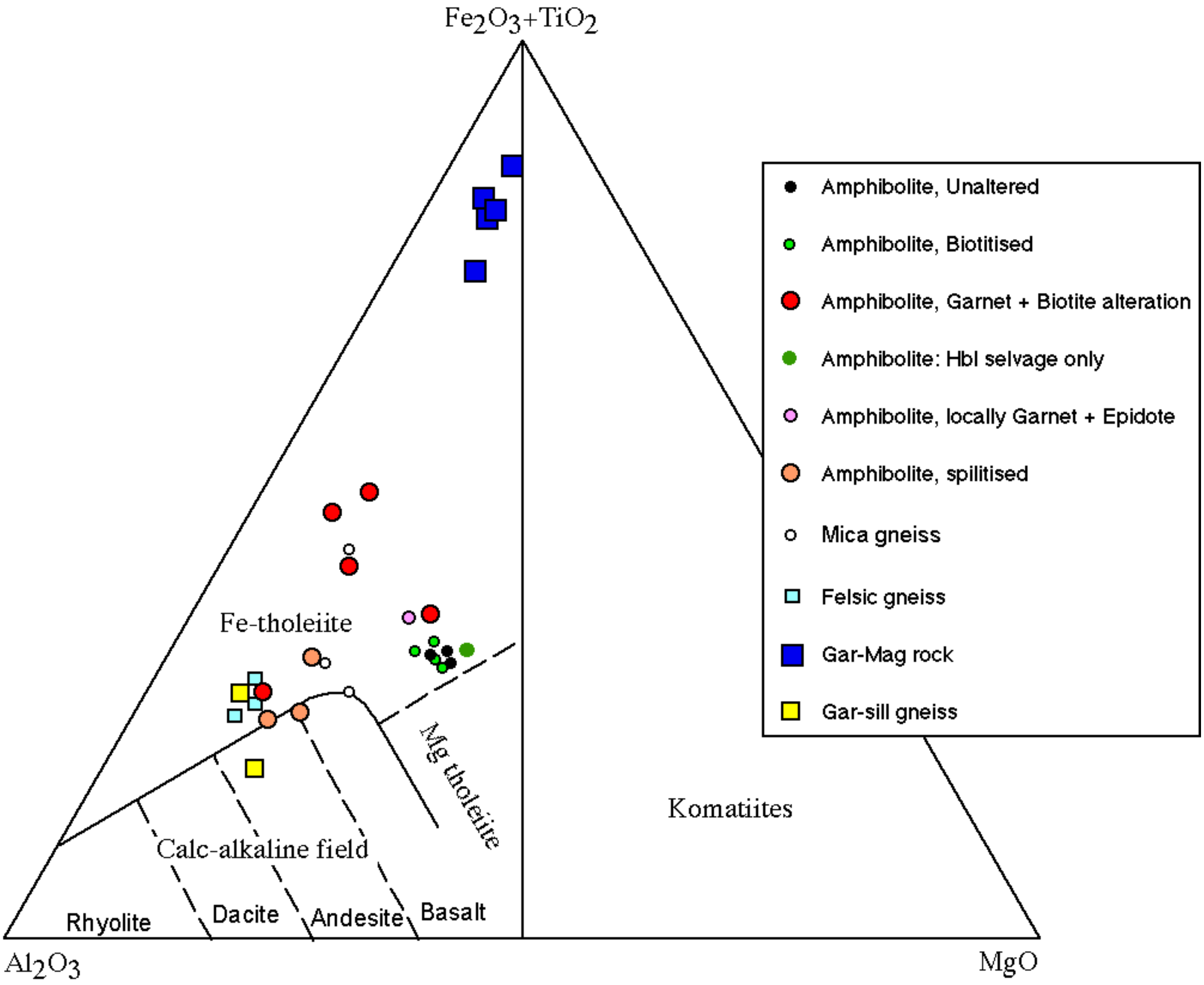

Plot 5. Jensen cation plot (Jensen 1976) for all samples analysed from Qingaaq. Felsic, mica and sillimanite-garnet gneisses plot quite close to the most altered amphibolites and, as expected, the garnet-magnetite rocks plot close to the Fe corner of the diagram. 'Unaltered' refers to the least-altered amphibolite detected at Qingaaq.

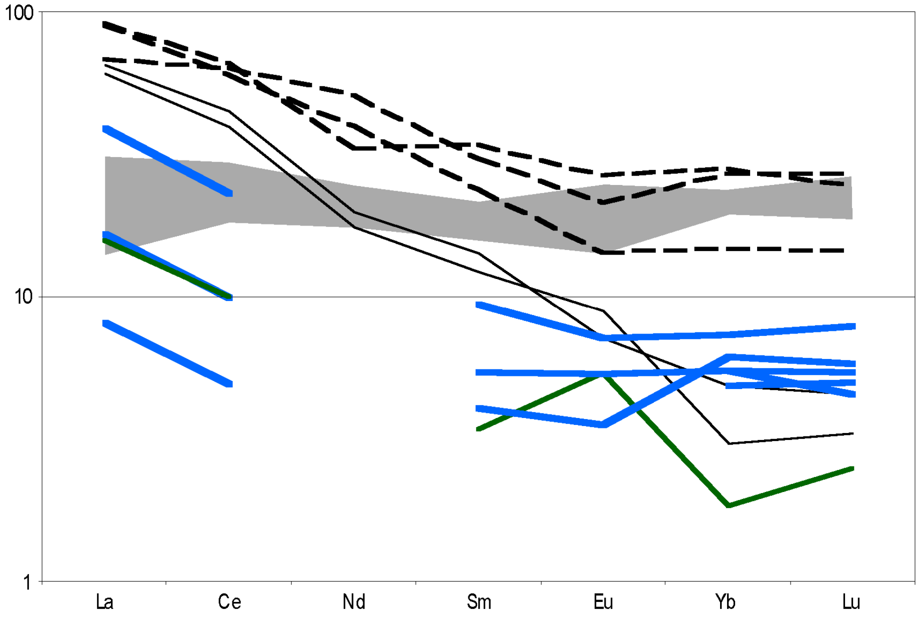

Plot 6. Chondrite-normalised REE plot for the least-altered amphibolites and various gneisses from Qingaaq. Grey area = least-altered; black solid = felsic mica gneiss; black dashed = sillimanite-garnet gneiss; green = felsic garnet-mica gneiss; blue = garnet-magnetite rock. Normalisation values from Kerrich and Wyman (1996).

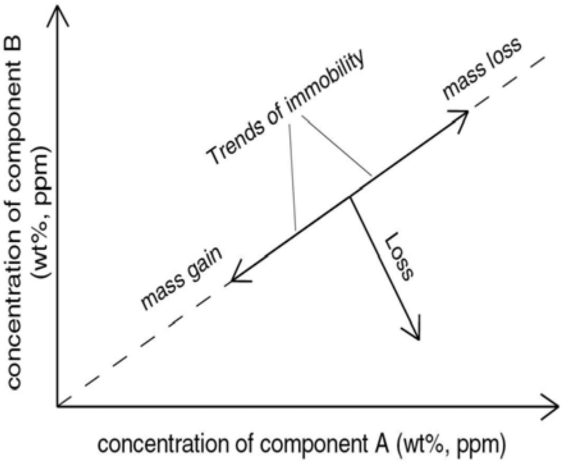

Plot 7. Possible trends defined by a pair of immobile and/or mobile elements in a hydrothermally altered rock sequence (from MacLean & Kranidiotis 1987, Garofalo 2004). By definition (MacLean & Kranidiotis 1987, MacLean & Barrett 1993), two component, here A and B, are immobile if their concentration ratio, measured from several samples, remains constant. This is graphically shown in a bivariate plot where the concentrations of A and B define a coherent diagonal line. If alteration causes a net mass gain in the rock, the concentration ratios from altered rock will lie along the line but plot closer to the origin than the unaltered samples; this is caused by dilution of the immobile elements by material added into the rock. In the case of net mass loss, the altered rocks will plot along the line further away from the origin than the unaltered samples of the same rock. Any distinct deviation from the line either indicates that the elements considered show primary

compositional variation of the rock, or indicate mass transfer during alteration. If all unaltered samples plot along the line, all deviation by the altered samples suggest mass transfer of one or both of the elements considered. When one element used for the plot is immobile and the other mobile, deviation downwards from the diagonal line suggest depletion and deviation upwards enrichment.

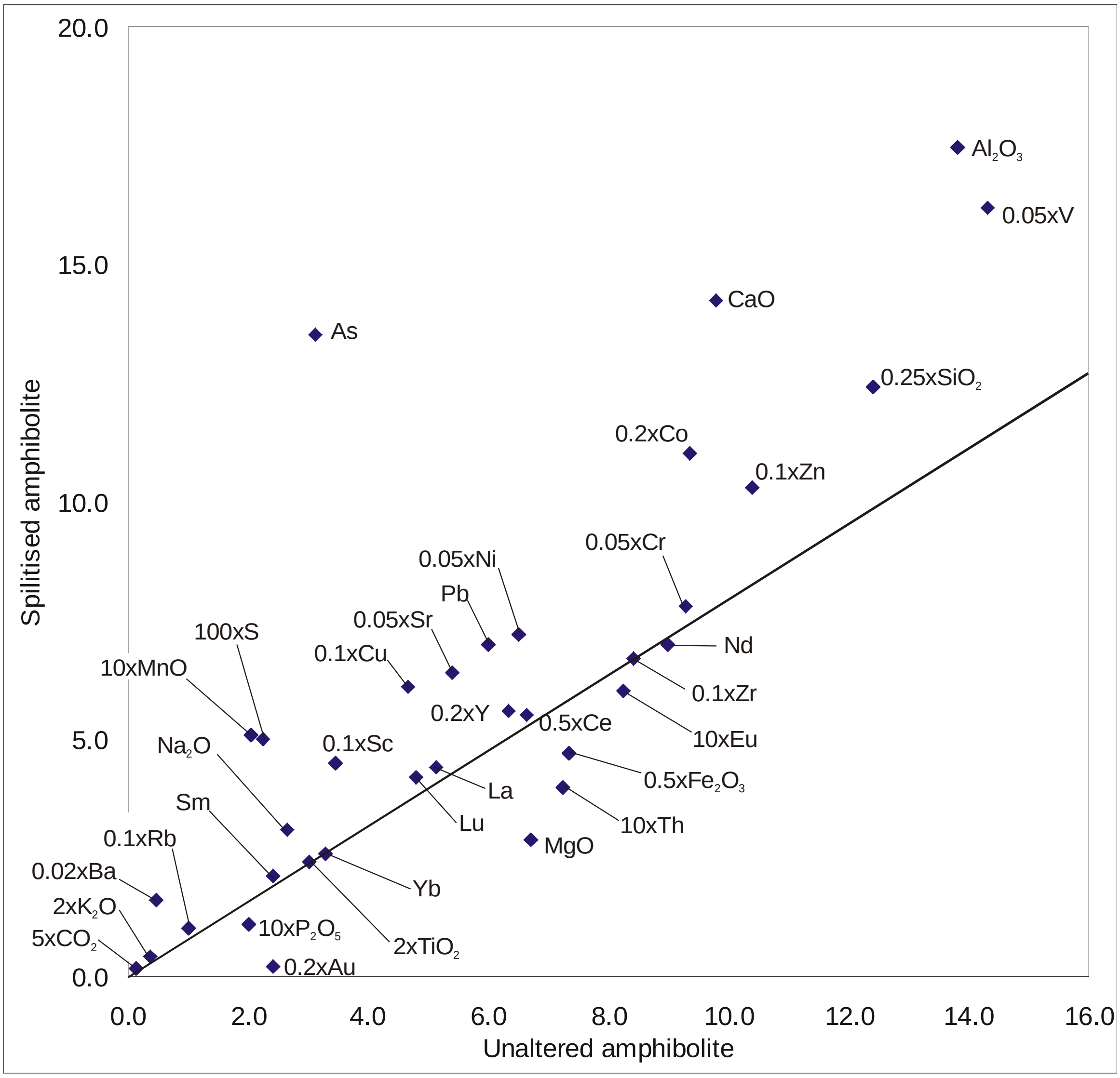

Plot 8. Isocon describing mass transfer during spilitisation ('calc-silicate alteration') in amphibolite. Multiplied concentrations plotted as per cent for the major elements, S and CO_2, as ppb for Au, and as ppm for the rest of the trace elements. Note that some elements analysed are not plotted, because their concentrations consistently are below or only very slightly above detection limit in the data available for this plot resulting in potential error too large for any mass transfer consideration. The diagonal regression line (isocon) is fitted trough Ti, Zr and REE. When viewing the isocon plot, keep in mind that it shows relative chemical trends, not absolute values of mass balance.

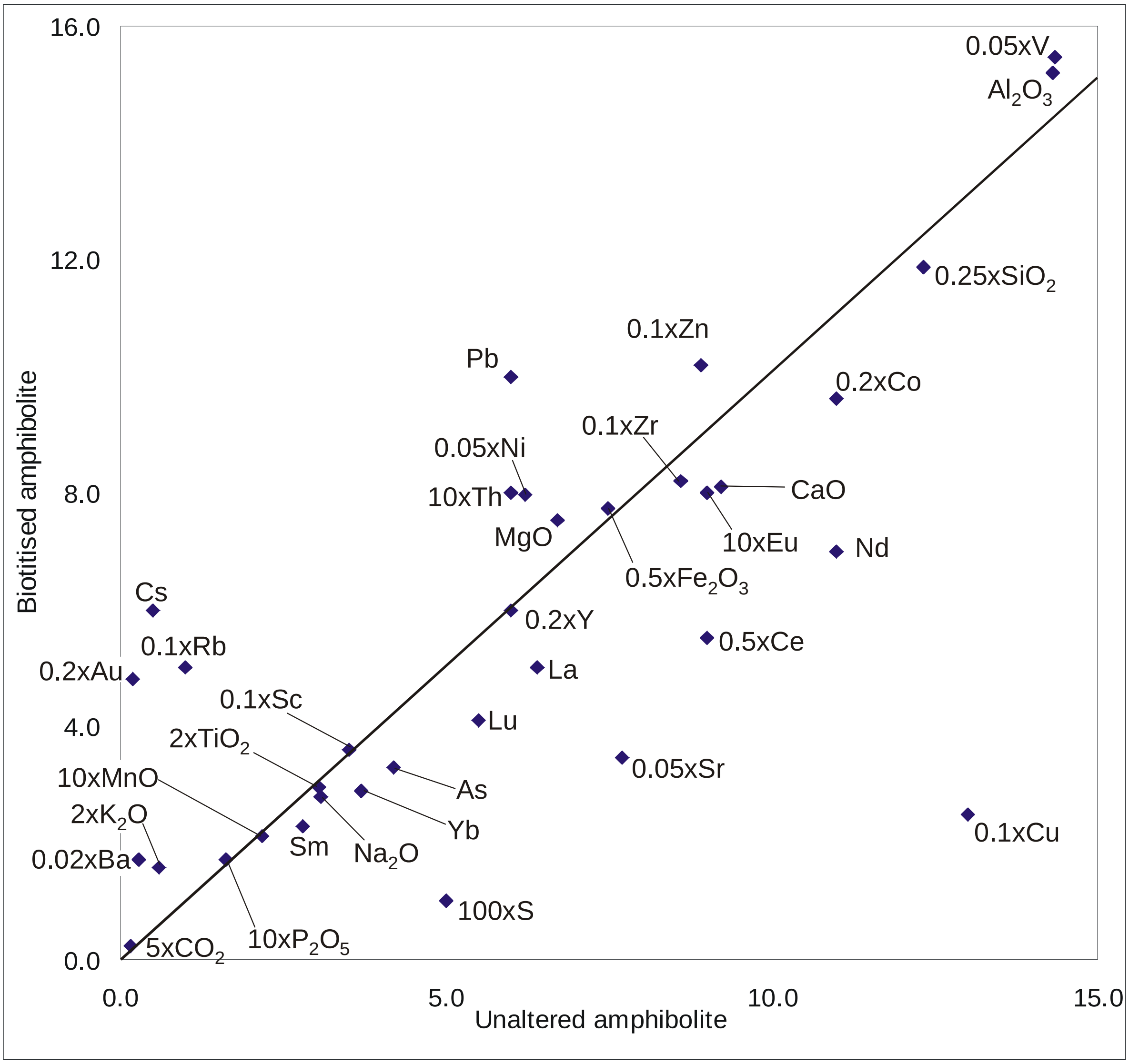

Plot 9**.** Isocon describing mass transfer during biotitisation (distal alteration potentially related to gold mineralization) in amphibolite. Multiplied concentrations plotted as per cent for the major elements, S and CO_2, as ppb for Au, and as ppm for the rest of the trace elements. Note that some elements analysed are not plotted, because their concentrations consistently are below or only very slightly above detection limit in the data available for this plot resulting in potential error too large for any mass transfer consideration. The diagonal regression line (isocon) is fitted trough Al, P, Sc, Ti and Zr. When viewing the isocon plot, keep in mind that it shows relative chemical trends, not absolute values of mass balance.

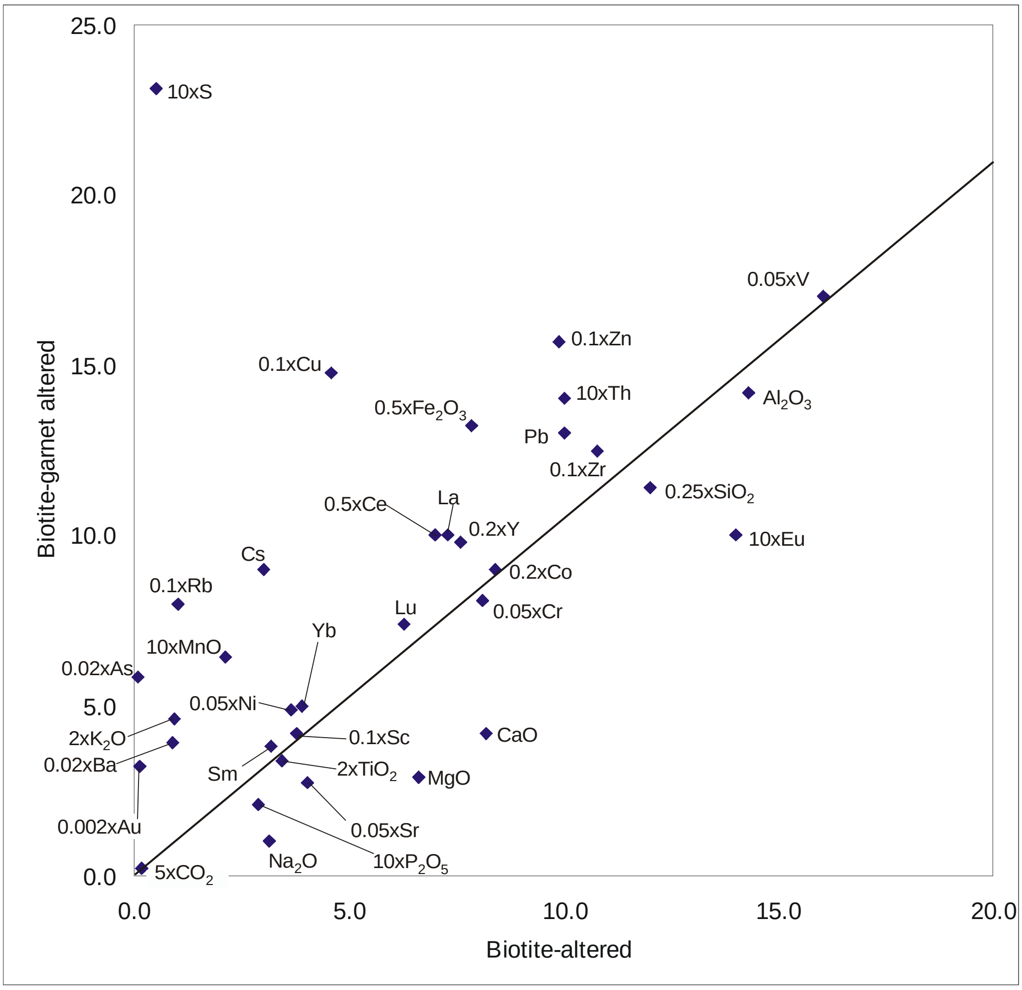

Plot 10**.** Isocon describing mass transfer during biotite-garnet alteration (proximal alteration potentially related to gold mineralization) in amphibolite. Multiplied concentrations plotted as per cent for the major elements, S and CO_2, as ppb for Au, and as ppm for the rest of the trace elements. Note that some elements analysed are not plotted, because their concentrations consistently are below or only very slightly above detection limit in the data available for this plot resulting in potential error too large for any mass transfer consideration. The diagonal regression line (isocon) is fitted trough the elements shown above to be the least mobile. The diagonal regression line (isocon) is fitted trough Al, Sc, Ti, V and Zr. When viewing the isocon plot, keep in mind that it shows relative chemical trends, not absolute values of mass balance.

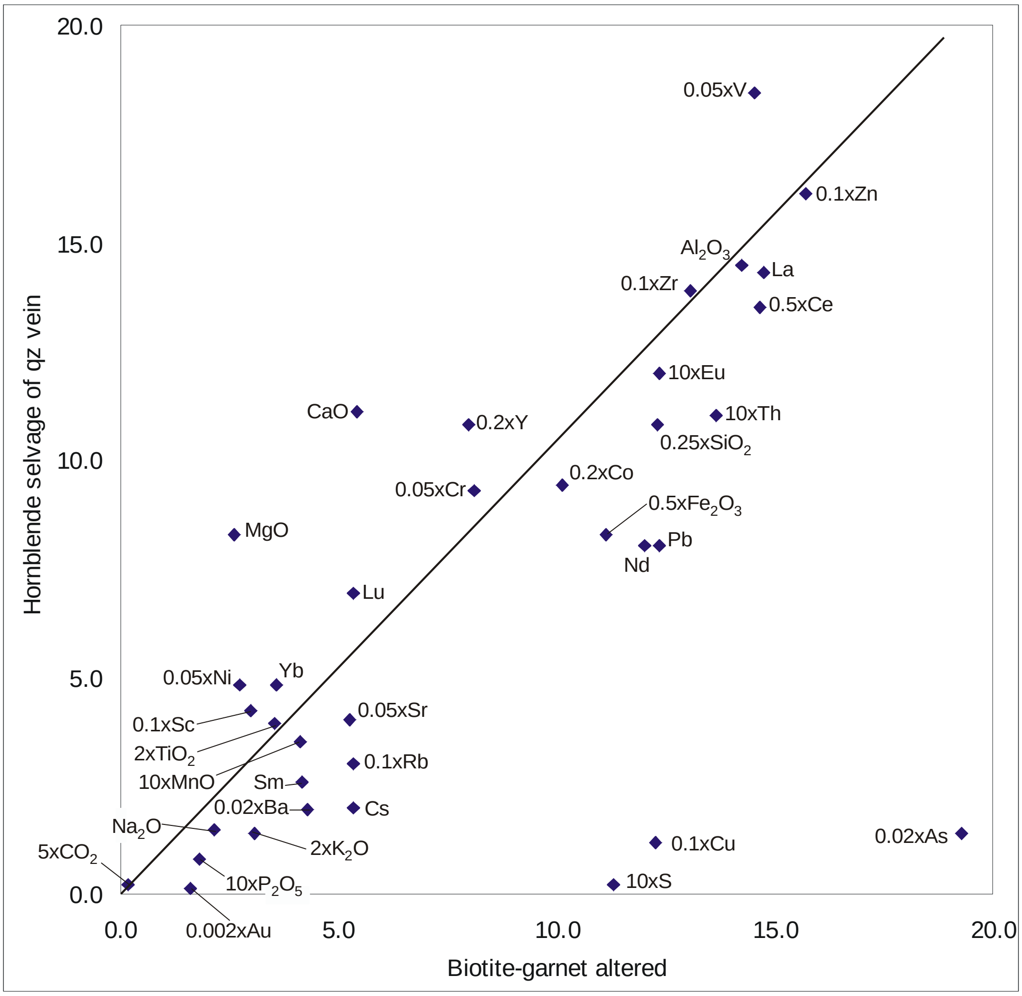

Plot 11**.** Isocon describing mass transfer during formation of the hornblende selvages of potentially auriferous quartz veins in amphibolite. Multiplied concentrations plotted as per cent for the major elements, S and CO_2, as ppb for Au, and as ppm for the rest of the trace elements. Note that some elements analysed are not plotted, because their concentrations consistently are below or only very slightly above detection limit in the data available for this plot resulting in potential error too large for any mass transfer consideration. The diagonal regression line (isocon) is fitted trough the elements shown above to be the least mobile. The diagonal regression line (isocon) is fitted trough Al, Ti, and Zr. When viewing the isocon plot, keep in mind that it shows relative chemical trends, not absolute values of mass balance.

References

Appel, P.W.U., Garde, A.A., Jørgenssen, M.S., Moberg, E.D., Rasmussen, T.M., Raith, J., Schjøth, F & Steenfeldt, A. 2003: Preliminary evaluation of the potential of the greenstone belts in the Nuuk region. General geology and evaluation of compiled geophysical, geochemical and ore geological data. GEUS Report 2003/94. 147 p.

Appel, P.W.U., Coller, D., Coller, V., Heijlen, W., Moberg, E.D., Polat, A., Raith, J., Schjøth, F, Stendal, H. & Thomassen, B. 2005: Is there a gold province in the Nuuk region? Report from field work carried out in 2004. GEUS Report 2005/27. 79 p.

Barley, M.E., Cassidy, K.F., Golding, S.D., Groves, D.I. & McNaughton, N.J. 1990. Assessment of mineralized zones: Alteration haloes. In: Ho, S.E., Groves, D.I. & Bennett, J.M.: Gold deposits of the Archaean Yilgarn Block, Western Australia: nature, genesis and exploration guides. Geology Department (Key Centre) & University Extension, The University of Western Australia, Publ. 20, 317-327.

Battacharya, A., Mohanty, L., Maji, A., Sen, S.K., & Raith, M. 1992: Non-ideal mixing in the phlogopite-annite boundary: Constraints from experimental data on Mg-Fe partitioning and a reformulation of the biotite-garnet geothermometer. Contributions to Mineralogy and Petrology, 111, 87-93.

Coller, D. & Coller, V. 2005: Field Report on Structural Mapping of the Auriferous Greenstones on Central Storø, Nuuk Fjord, West Greenland. In *The 2004 GEUS Field Program*. GEUS Report 2005/09. 84p.

Eilu, P., Mathison, C.I., Groves, D.I. & Allardyce, W. 1999: Atlas of Alteration Assemblages, Styles and Zoning in Orogenic Lode-Gold Deposits in a Variety of Host Rock and Metamorphic Settings. Geology and Geophysics Department (Centre for Strategic Mineral Deposits) & UWA Extension, The University of Western Australia, Publ. 30. 64 p.

Eilu, P, & Groves, D.I. 2001: Primary alteration and geochemical dispersion haloes of Archean orogenic gold deposits in the Yilgarn Craton: the pre-weathering. Geochemistry: Exploration, Environment, Analysis, 1, 183-200.

Eilu, P. & Mikucki, E.J. 1998: Alteration and primary geochemical dispersion associated with the Bulletin lode-gold deposit, Wiluna, Western Australia. Journal of Geochemical Exploration, 63(2), 73-103.

Eilu P., Mikucki, E.J. & Dugdale, A.L. 2001: Primary geochemical dispersion related to the Bronzewing lode-gold deposit, Western Australia. Mineralium Deposita 36, 13-31.

Elliot-Meadows, S.R. & Appleyard, E.C. 1991: The alteration geochemistry and petrology of the Lar Cu-Zn deposit, Lynn Lake Area, Manitoba, Canada. Economic Geology, 86, 486-505.

Era Maptec. 1995: Structural analysis of the Qingat gold prospect, Storo, Nuuk fjord, West Greenland. In Field report for Nunaoil. Report GEUS File No. 21452. pp. 1-58.

Ferry, J.M. & Spear, F.S. 1978: Experimental calibration of the partitioning of Fe and Mg between biotite and garnet. Contributions to Mineralogy and Petrology, 66, 113-117.

Friend, C.R.L. & Nutman, A.P. 2005: New pieces to the Archaean terrane jigsaw puzzle in the Nuuk region, southern West Greenland; steps in transforming a simple insight into a complex regional tectonothermal model. Journal Geological Society of London, 162, 147-162.

Ganguly, J. & Saxena, S.K. 1984: Mising properties of aluminosilicate garnets: constraints from natural and experimental data, and application to geothermo-barometry. American Mineralogist 69, 88-97.

Garofalo, P.S. 2004a: Mass transfer during gold precipitation within a vertically extensive vein network (Sigma deposit - Abitibi greenstone belt - Canada). Part I. Geometry of hydrothermal alteration haloes. European Journal of Mineralogy, 16(5), 753-60.

Garofalo, P.S. 2004b: Mass transfer during gold precipitation within a vertically extensive vein network (Sigma deposit - Abitibi greenstone belt - Canada). Part II. Mass transfer calculations. European Journal of Mineralogy, 16(5), 761-76.

Grant, J.A. 1986: The isocon diagram - a simple solution to Gresens' equation for metasomatic alteration. Economic Geology 81, 1976-1982.

Grant, J.A. 2005: Isocon analysis: A brief review of the method and applications. Physics and Chemistry of the Earth, Parts A/B/C, 30(17-18), 997-1004.

Gresens, R.L. 1967: Composition-volume relationships of metasomatism. Chemical Geology, 2, 47-65.

Hackler, R.T. & Wood, B.J. 1989: Experimental determination of Fe and Mg exchange between garnet and olivine and estimation of Fe-Mg garnet mixing properties. American Mineralogist 74, 994-999.

Hallberg, A. 1994: The Enåsen gold deposit, central Sweden. 1. A Palaeoproterozoic high-sulphidation epithermal gold mineralization. Mineralium Deposita 29, 150-162.

Hollis, J.A., van Gool, J.A.M., Steenfelt, A. & Garde, A.A.: Greenstone belts in the central Godthåbsfjord region, southern West Greenland. GEUS Report 2004/110. 110 p.

Jensen, L.S. 1976: A new cation plot for classifying subalkalic volcanic rocks. Ontario Div. Mines, Misc. Paper 66. 22 p.

Juul-Pedersen, A. 2005: Et borekerne-baseret petrografisk og isotopgeokemisk studie af Storø Au forekomsten, Vestgrønland. Unpublished M. Sc. Project. University of Copenhagen, Denmark, 70 p + Appendices.

Kerrich, R. & Wyman, D.A. 1996: The Trace Element Systematics of Igneous Rocks in Mineral Exploration: An Overview. In: Wyman, D.A.: Trace Element Geochemistry of Volcanic Rocks: Applications for Massive Sulphide Exploration. Geological Association of Canada, Short Course Notes Volume 12.

Lecuyer, C., Gruau, G., Anheusser, C.R. & Fourcade, S. 1994: The origin of fluids and effects of metamorphism on the primary chemical compositions of Barberton komatiites: New evidence from geochemical (REE) and isotopic (Nd, O, H, $^{39}Ar/^{40}Ar$) data. Geochimica Cosmochimica Acta 58, 969–984.

Lesher, C.M., Gibson, H.L. & Campbell, I.H. 1986: Composition-volume changes during alteration of andesite at Buttercup Hill, Noranda District, Quebec. Geochimica Cosmochimica Acta 50, 2693-2705.

Lottermoser, B.G. 1992: Rare earth elements and hydrothermal ore formation processes. Ore Geology Revievs 7, 25–41.

MacLean, W.H. & Kranidiotis, P. 1987: Immobile elements as monitors of mass transfer in hydrothermal alteration: Phelps Dodge massive sulphide deposit, Matagami, Quebec. Economic Geology, 82 (951-962).

MacLean, W.H. & Barrett, T.J. 1993: Lithogeochemical techniques using immobile elements. Journal Geochemical Exploration 48. 109-133.

McCuaig, T.C. & Kerrich, R. 1998: P-T-t-deformation-fluid characteristics of lode gold deposits: evidence from alteration systematics. Ore Geology Reviews, 12, 381-453.

Mountain, B.W. & Williams-Jones, A.E. 1995: Mass transfer and the path of metasomatic reactions in mesothermal gold deposits: an example of Flambeau Lake, Ontario. Economic Geology, 91, 302-21.

Pedersen, N.H. 1998: A peak metamorphic timing for gold mineralization at Storø, SW Greenland. In: J.R. Wilson & S. Plesner: Abstract volume, Nordiske Geologiske Vintermøde. Århus, 13-16 January 1998. Dept. Earth Sci. Århus Univ. Denmark.

Perchuk, L.L. & Lavrent'eva IV 1983: Experimental investigation of exchange equilibria in the system cordierite-garnet-biotite. In: Saxena, S.K. (Ed.) Kinetics and Equilibrium in Mineral Reactions, Advances in Physical Geochemistry 3, pp. 199-239. Springer, NY.

Polat, A. 2005: Geochemical and petrographic characteristics of the Ivisaartoq and Storø greenstone belts, southern West Greenland: progress report. In: Hollis, J.A.: Greenstone belts in the central Godthåbsfjord region, southern West Greenland, pp. 80-112. GEUS Report 2005/42.

Powell, W.G., Pattison, D.R.M. & Johnston, P. 1999: Metamorphic history of the Hemlo gold deposit from Al_2SiO_5 mineral assemblages, with implications for the timing of mineralization. Canadian Journal Earth Sciences 36, 33-46.

Reed, M.H. 1983: Seawater-basalt reaction and the origin of greenstones and related ore deposits. Economic Geology 78, 466-485.

Ridley, J.R., Groves, D.I. & Knight, J.T. 2000: Gold deposits in amphibolite and granulite facies terranes of the Archean Yilgarn Craton, Western Australia: evidence and implications of synmetamorphic mineralization. Metamorphosed and Metamorphogenic Ore Deposits. 11, pp. 265-90.

Roedder, E. 1984: Fluid Inclusions. Mineralogical Society of America. Reviews in Mineralogy 12, 644 p.

Skyseth, T. 1997: Gold exploration on Storø 1996 South West Greenland. Exploration License 13/97. Nunaoil A/S, Nuuk. 14 p.

Skyseth, T. 1998: Gold exploration on Storø 1997 south west Greenland. Exploration License 13/97. Nunaoil A/S, Nuuk. 25 p.

Seewald, J.S. & Seyfried, W.E. 1990: The effect of temperature on metal mobility in subseafloor hydrothermal systems: constrains from basalt alteration experiments. Earth Planetary Science Letters 101, 388-403.

Tindle & Webb 1990: European Journal of Mineralogy, 2, 595-610.

Tomkins, A.G., Pattison, D.R.M. & Zaleski, E. 2004: The Hemlo gold deposit, Ontario: an example of melting and mobilization of a precious metal-sulfosalt assemblage during amphibolite facies metamorphism and deformation. Economic Geology 99, 1063–1084.

Tomkins, A.G. & Mavrogenes, J.A. 2002: mobilization of gold as a polymetallic melt during pelite anatexis at the Challenger deposit, South Australia: a metamorphosed Archean gold deposit. Economic Geology. 97, 1249–1271.

Trepka-Bloch, C. 1995: Gold exploration, Storø 1995, License 02/92, Nunaoil A/S, 19pp.

Witt, W.K. 1993: Lithological and structural control on gold mineralization in the Archaean Menzies-Kambalda region, Western Australia. Australian Journal Earth Sciences 40, 65–86.

Witt, W.K. & VanderHor, F. 1998: Diversity within a unified model for Archaean gold mineralization in the Yilgarn Craton of Western Australia: An overview of the late-orogenic, structurally-controlled gold deposits. Ore Geology Reviews 13, 29-64.